Doctoral Thesis

Kinetics and oligomerization of the F-BAR domain protein Growth Arrest Specific Protein 7 dependent on the receptor, Cdc42, Src, and the multicomplex adaptors protein at the membrane

受容体の下流における Cdc42、Src、およびアダプタータンパク質群に依存する F-BAR ドメインタンパク質 GAS7 分子集合機構の解析

Wan Nurul Izzati Binti Wan Mohamad Noor
Nara Institute of Science and Technology
Division of Biological Sciences
Molecular Medicine and Cell Biology
Professor Dr Shiro Suetsugu

22 February 2021

Table of Contents

Laboratory (Supervisor)	Molecular Medicine and Cell Biology (Professor Dr Shiro Suetsugu)		
Name	Wan Nurul Izzati Binti Wan Mohamad Noor	Date	February 22, 2021
Title	Kinetics and oligomerization of the F-BAR domain protein Growth Arrest Specific Protein 7 dependent on the receptor, Cdc42, Src, and the multicomplex adaptors protein at the membrane		

Phagocytosis is a subcellular structure that is made with membrane remodeling to uptake micron-sized particles. This process is mediated by the signaling cascades that are initiated by the phagocytic receptors, including FcγRII. The activation of the Src family kinases and of the Rho-family GTPase, cell division control protein 42 (Cdc42), and the accumulation of the signaling phosphoinositides including phosphatidylinositol-4,5-bisphosphate (PIP_2) play important roles in the phagocytic signaling. The signals are thought to be transmitted through multi-scaffolding proteins via the SH3 domains, which include Nck, WISH/NCKIPSD/DIP/SPIN90, N-WASP, and so on. The Bin-Amphiphysin-Rvs167 (BAR) domain proteins, especially Growth Arrest-Specific protein 7b (GAS7b), is an essential member of the FCH (F)-BAR subfamilies that assemble to shape the membrane of the phagocytic cups. However, the regulation of the assembly of GAS7b dependent on Cdc42 and Src kinases downstream of FcγRII had been unclear. Moreover, the kinetics of the assembly of the BAR domains, including that of the GAS7b F-BAR domain, on the lipid membrane downstream of these signaling cascades had not been clarified. Here, I show that the kinetics and quantitative measurement of the assembly of GAS7b on the reconstituted liposomes by fluorescent resonance energy transfer (FRET). The time-dependent increase in the FRET between CFP-GAS7b and YFP-GAS7b indicated the rapid oligomerization of GAS7b on the membrane. The maximums of the FRET were increased in the presence of the molecular scaffolds, including N-WASP, Nck, and WISH, and it was enhanced by the presence of an active form of Cdc42. Moreover, Src kinase and the cytoplasmic region of FcγRIIa that were attached to the membrane further increased the FRET, reaching approximately 50% FRET efficiency. The half-time of the assembly quantitatively showed the enhancement of the assembly rate by the presence of these N-WASP, Nck, WISH, Cdc42, Src, and FcγRIIa. In contrast, the presence of the membrane-binding deficient mutant of GAS7b, as well as the SH3 domain mutant of WISH, reduced the maximum FRET,

suggesting the defect in this multicomplex assembly. In phagocytotic macrophage RAW264.7 cells, the FRET of GAS7b was reduced with the presence of Cdc42 inhibitor (ML141) and the Src inhibitor PP2 as examined by the FLIM-FRET analysis. These results indicate that the assembly mechanism of the F-BAR domain protein GAS7 is dependent on the Cdc42, Src kinase, and the molecular scaffolds.

1.0 Introduction

1.1 Phagocytosis is mediated by FcγRII, receptor, and kinase

The process of phagocytosis involves subcellular structures that correlate with membrane remodeling to uptake micron-sized particles. This process is mediated by the signaling cascades that are initiated by the phagocytic receptors, including Fc-gamma receptor II (FcγRII), which is an immunoreceptor having a tyrosine-based activation motif (ITAM) for intracellular signaling. FcγRII is a glycoprotein that consists of a subunit for IgG binding and a intracellular γ subunit for dimerization to activate the intracellular signaling (1). In phagocytosis, the ITAM at the γ subunit is phosphorylated by the Src family kinases that are anchored at the plasma membrane by lipidation (2). The phosphorylated ITAM motif can recruit the protein having the Src homology 2 (SH2) domain that specifically binds to the phosphorylated tyrosine (3). Thus, the Src at the plasma membrane could activate the FcγRII-mediated signaling.

Upon receptor activation for phagocytosis, the signaling phospholipids, i.e., phosphoinositides are generated at the plasma membrane and further activate the intracellular signaling and protein assemblies (4,5). Thus, in the activation of the Src family kinases from the FcγRII receptors, the phosphoinositide kinases are activated, producing phosphoinositides. Among phosphoinositides, phosphatidylinositol-4,5-bisphosphate (PtdIns (4,5) P2, PIP_2) and phosphatidylinositol (3,4,5) trisphosphate (PtdIns (3,4,5) P3, PIP_3) play the important roles in phagocytosis (6). These are essentials phosphoinositides that play essential roles in phagocytosis (7). These phosphoinositides are not abundant at the plasma membrane in resting state, therefore, the acute production of these phosphoinositides upon the receptor activation is crucial in signaling cascade for subcellular structure formation such as phagocytosis and endocytosis. The production of PIP_2 at the plasma membrane leads to the production of PIP_3, and both PIP_2 and PIP_3 dictate the downstream actin polymerization process (Figure 1). Following, the activation of the guanine nucleotide exchange factors (GEFs) for the activation of Rho family GTPases including cell division control protein 42 (Cdc42). This further the signaling process as the recruitment and regulation of the proteins that trigger the actin uncapping and the nucleation of actin polymerization (8).

1.2 Cdc42, N-WASP, and the actin cytoskeleton by the multivalent interaction

In phagocytosis, Rho-family GTPase Cdc42 is essential in regulates the actin cytoskeletal rearrangement and engulfment process (9). Besides, Cdc42 is involved in orchestrating the cytoskeleton and cell polarization (10). Cdc42 is a key regulator in controlling the organization of the actin cytoskeleton by modulating its downstream multicomplex proteins. The activation of Cdc42 is initiated by GEF, which convert the GDP-bound form of Cdc42 (inactive Cdc42) to the active GTP-bound form (active Cdc42) of Cdc42 (11). Cdc42 is involved in the formation of the macromolecular complexes with scaffolding proteins and kinases for actin cytoskeletal reorganization (12). As previously reported, many possible target proteins can interact with Cdc42. However, the most important and established route for induction of the actin polymerization is the cooperative activation of neuronal Wiskott-Aldrich syndrome protein (N-WASP) by Cdc42 and PIP_2 (Figure 1).

1.2.1 Neuronal Wiskott-Aldrich syndrome protein (N-WASP)

Wiskott Aldrich syndrome (WAS) is a disease that arises from the dysfunction of the WAS gene (13). The WASP expression is retracted in the immune system and WAS disease is associated with an immunological deficiency, which is characterized by dermatitis, macrothrombocytopenia, and a problem with the immune system (13,14). It is also reported to be closely linked to the defects in phagocytosis (15). The orthologous of WASP that is expressed ubiquitously is N-WASP (16). WASP and N-WASP share almost 60% similarity in amino-acid sequence homology. The major difference includes that N-WASP has the two actin-binding domains Verprolin homology, cofilin homology, and acidic (VVCA) regions, whereas WASP has one Verprolin homology region, resulting in VCA (17). This extra verprolin region made N-WASP have a higher binding with actin compare with WASP, resulting in stronger induction of actin polymerization (18). WASP and N-WASP also have Cdc42/Rac-interactive binding (CRIB) motif that can bind with Cdc42 (12,17,19) (Figure 1). The binding at the CRIB domain is very important to unmask the autoinhibition of N-WASP. The binding region for PIP_2 resides in front of the CRIB, which are abundant in the positively charged amino-acid residues, resulting in the electrostatic interaction between the PIP_2 and WASP/N-WASP (20). This unmasking of the auto-inhibition allows the binding of WASP/N-WASP with Arp2/3, which triggers the nucleation of actin polymerization (21). Furthermore, N-WASP is also activated with the presence of the Cdc42, suggesting that Cdc42 might be a

key regulator in the phagocytosis process (22). Moreover, N-WASP consists of a proline-rich region that can bind to several proteins that consist of SH3 domain like WISH/NCKIPSD/DIP/SPIN90, Nck, Grb2, Src, Fyn, and so on (12). The proteins having the Bin/Amphiphysin/Rvs167 (BAR) domain (described later) also have the SH3 domains that bind to WASP and N-WASP.

1.2.2 WISH/NCKIPSD/DIP/SPIN90

WISH/NCKIPSD/DIP/SPIN90 is an N-WASP interacting SH3 protein and can bind to WASP and N-WASP through the SH3 domain (19,23). WISH proteins are essentials in endocytosis, membrane ruffling, and synaptic remodeling (24,25). Furthermore, WISH is also involved in the rearrangement of actin polymerization by directly interacting with the Arp2/3 complex (26). In COS-7 cells, SPIN90 shown to be involved in lamellipodia formation and the lamellipodia formation of the SPIN90 knockout cells were impaired (27). WISH has the SH3 domain that is similar to those of Fyn and Src, suggesting that they can interact with each other (28).

1.2.3 Nck

Nck is an adapter protein that comprises one SH2 domain and three SH3 domains. The architecture of Nck allows for multivalent protein-protein assemblies (29,30). In phagocytosis, Nck links Cdc42 to ITAM peptide through WASP or N-WASP (31). Besides, Growth factor receptor-bound protein 2 (Grb2) is known to play a similar role in actin polymerization to Nck (32). The difference between Grb2 and Nck is the number of SH3 domains (Figure 1g and f). Both Nck and Grb2 are known to be potentially involved in actin dynamics and rearrangements. In a study by Case and her group, the Nck and N-WASP interact together with specific stoichiometry to regulate actin assembly (33). Subsequently, Nck and N-WASP are also known to mediate the phagocytosis process (31).

1.2.4 The multivalent interaction

Membrane proteins are cooperatively moving together at the intracellular site of plasma membrane, will causes protein scaffolds that will function in specific subcellular structures. This protein scaffolds apparently will behave in different ways as no specific principles or regulations to impute this multivalent interaction (29). In Banjade and Rosen's reconstituted system, they have found that Nephrin receptor, Nck and N-WASP have multivalent interaction that further stimulate the actin rearrangements for the cells to interact with other cells and as well as to move. This explained how protein clustering, phase separation and protein stoichiometry (33) can affects the protein assembly and multivalent interactions of proteins.

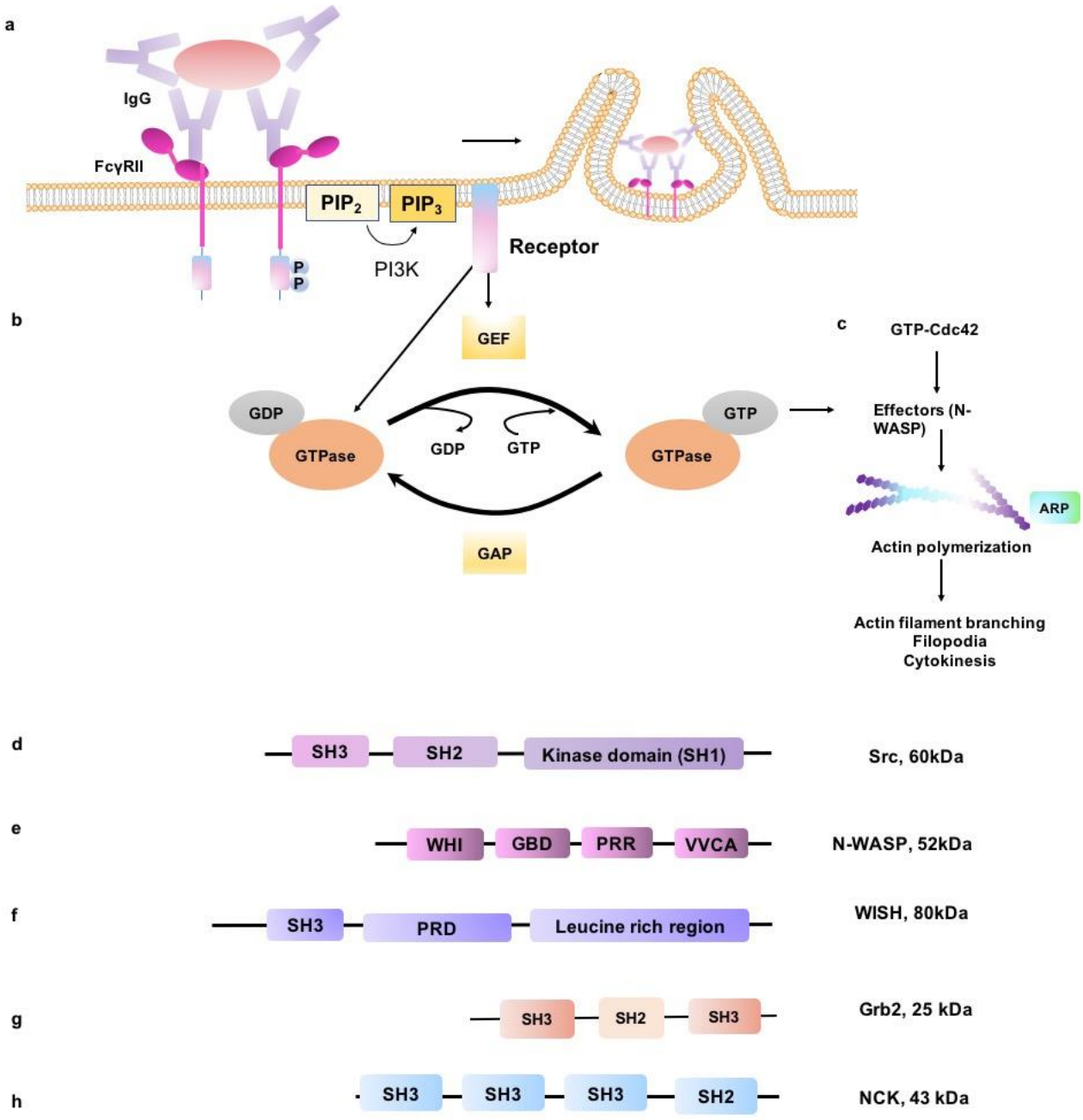

Figure 1; Illustration of FcγRII mediated phagocytosis process in the presence of ITAM receptors with schematics domain of Src, N-WASP, WISH, Grb2 and Nck**.** b) Illustration of FcγRII mediated phagocytosis process by the signaling phosphoinositides of PIP_2 and PIP_3. This interaction will be further driving the actin polymerization that has activated the Rho GTPase family in c. c) The illustration of GTP-Cdc42 that is activated by N-WASP and further cooperatively modulates actin filament branching, filopodia, and cytokinesis. The figure is adapted and reconstituted from (20,21,34). d) The domain structure of Src. Src have SH3, SH2, and SH1 domains. The SH3 domain is responsible for binding with the proline-rich domain. The SH2 domain, known as the phosphotyrosine interaction motif, interacts with phosphotyrosine residue, either with its own or other proteins. Moreover, Src also has a kinase domain that controls the enzymatic activities and regulates the substrate known as the SH1 domain. e) The schematics domain of N-WASP protein. f) The schematics domain of the WISH protein. g) The schematics domain of the Grb2 protein. h) The schematics domain of the Nck protein. Schematics not drawn to scale.

1.3 Plasma membrane curvature & BAR domain

All these assembly occurs beneath the plasma membrane. Cells are made up of plasma membranes that control the in and out movement activities of their cellular body. The phagocytotic structure is a part of the plasma membrane, by which is made by the deformation of the plasma membrane upon specific protein-protein assembly. The plasma membrane consists of a lipid bilayer that has been mainly made up of phospholipids (Figure 2a). Phospholipids have hydrophilic head groups and hydrophobic fatty acid tails. Essentially, the composition of the acyl chain was critical to determine and trigger membrane curvature, behavior, and the dynamic of the protein interaction (35-37). Besides phosphoinositides and phosphatidylserine (PS) the plasma membrane also contains sphingolipids and cholesterol (35,37-39). Commonly, in the study about membrane proteins in cell biology, the researchers have used reconstituted liposomes as model-membrane systems (Figure 2b)

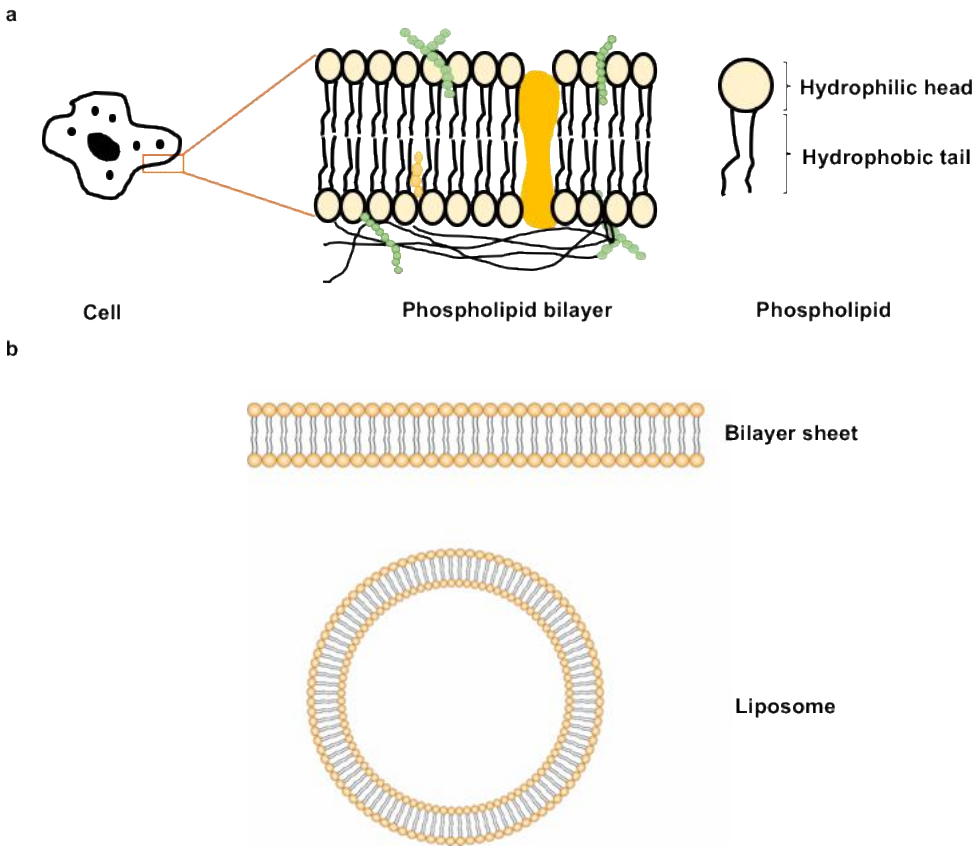

Figure 2: Plasma membrane and liposomes. a) The illustration about plasma membrane in cells. b) Illustration on bilayer sheet and liposomes that mimicking the plasma membrane. Schematics not drawn to scale.

The lipid membrane behaves passively, i.e., the protein assembly including actin cytoskeletal reorganization induced by receptor activation. After the activation of receptors, the phosphoinositide will induce the membrane deformation. Therefore, the deformation of the plasma membrane is caused by the interactions between protein-protein and clustering of protein-protein with receptors (12,29,37,40). These activities lead to the formation of membrane trafficking (41), defense mechanisms like phagocytosis (42) as well as microtubule formation for the movement of kinesin, dynein, and motor proteins (43). However, most of these proteins interact with the membrane indirectly.

How membranes identified the curvature is the most exciting insight that could be discovered, as the lipid itself contributes to the significant amount in the cell. Interestingly, solving this question will lead to revealing the protein behavior in the cellular system. Phospholipids are important building blocks of cell membranes and consist of several phospholipid classes, including PIP_2, PIP_3, phosphatidylcholine (PC), phosphatidylethanolamine (PE), and phosphatidylserine (PS) (4). In regulating the subcellular structure like phagocytosis or endocytosis, the protein acts by depending on the composition of the lipid, as different lipid modification will generate different ways of bending. The amount of PE, PC, and PS will affect protein binding (37,39). The plasma membrane also appeared to have a negative charge owing to the head group of the phospholipid that contains negatively charged ions. For example, the PS will appear naturally as a negatively charged head group as the phosphate has been attached with a serine group in the eukaryotic membrane. PS will generate a cylindrical shape of asymmetrical and appear as flat curvature (Figure 3). This type of curvature is also the same for the PC head group (35) as illustrated in (Figure 3). According to (44), PS can play a role in stimulating the immune system, as PS could distort the immune host response. PE lipid is also highly found in mammalian cells and abundantly present in the outer leaflet of the membrane (37). This PE has a conical shape of asymmetrical that can generate negative curvature as Figure 9 (36). Besides that, the presence of PE also helps in maintaining the negativity charge of the PS at the inner membrane and also controls the viscosity of the membrane by its head group. Besides**,** PE also can form hydrogen bonds with the nearest polar group, which at the same time reflects membrane structure. Physiologically, in the plasma membrane, PS could control the negativity of the plasma membrane. Remarkably, in phagocytosis cascades, the presence of PIP_2 and PIP_3 will deformed the membrane to positive curvature also contributed to the interaction of all essentials proteins to work cooperatively to initiate the process (6,20).

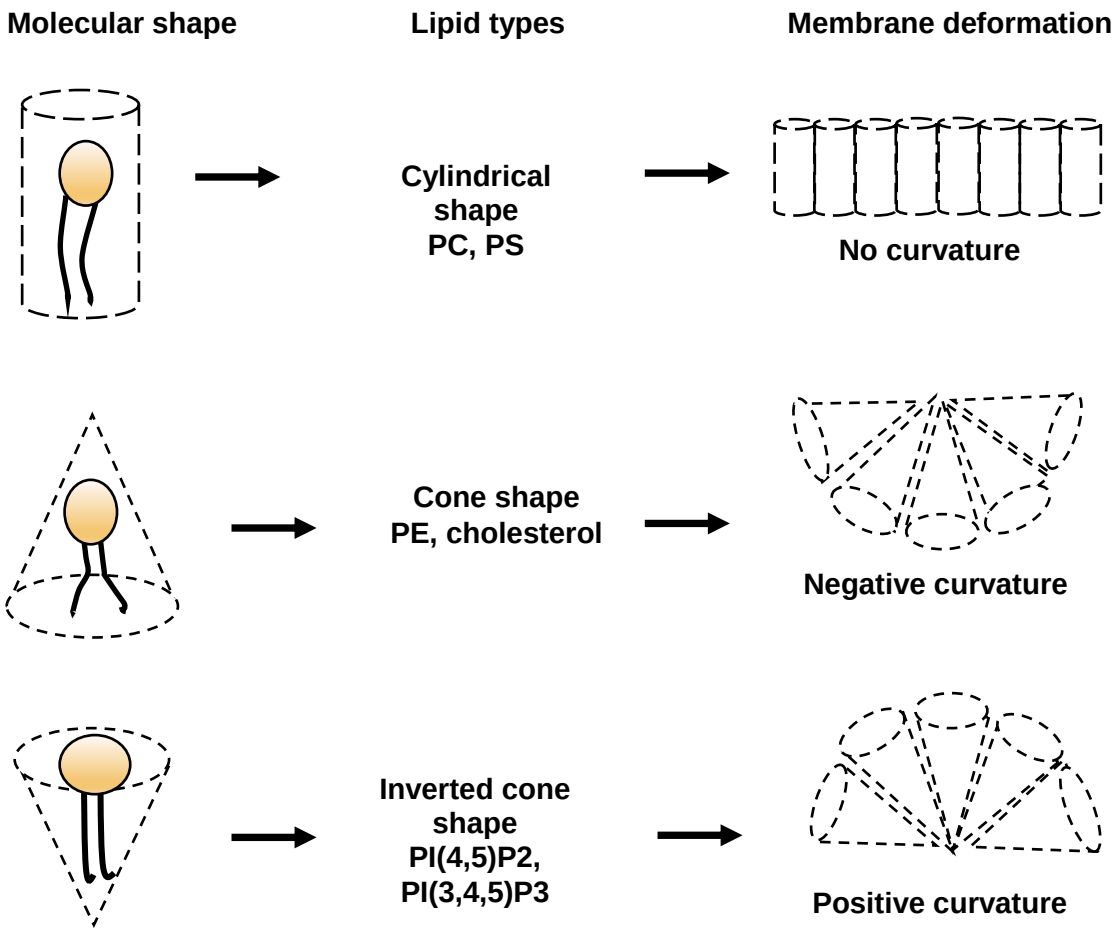

Figure 3: Illustration of the lipid head group that resulted in different deformation of membrane curvature.

The Bin/Amphiphysin/Rvs167 (BAR) domain proteins are the proteins that bind to plasma membranes. These proteins are unique in variety of the sensing and deformation of the curvature (45-48). In eukaryotes, BAR domain protein connects between the membrane deformation and actin-actin binding protein (23,49). Not only deformation of the membrane, the BAR domain proteins also are involved in membrane trafficking. In this membrane trafficking, numerous subcellular structures are generated by the ability of BAR domain to sense the membrane curvature and simultaneously to stabilize the curvature.

The membrane will have the ability to generate curves by the action of the BAR domain. Firstly, by a scaffolding of the BAR domain at the membrane. A high concentration of BAR domain will generate membrane curvature. Secondly, by insertion of the amphiphilic helix (AH) structure of the part of the BAR domain. This helix will have the ability to bind and insert between the lipid membranes. However, not all the BAR domains, but a subset of N-BAR

domains have AH. These BAR domain proteins are also the key players in actin dynamics regulation via bind and interaction with actin-binding proteins (46,47,50,51). The BAR domain, with the size of ~200 Å in length, got wide attention as to how the small protein can contribute to the movement of the membrane, cooperating with actin cytoskeleton and endocytic machineries (52-57). However, how the mechanism behind this still unclear.

1.4 BAR domain classification

The structure of the Amphiphysin BAR domain protein was first reported, and is crescent or banana shape (49,58) These BAR domains will appear as dimeric structures (49,59,60). This dimeric protein has a basic charge at the structure, reinforcing the binding with the negativity of the membrane. The BAR domain protein is divided into different subfamilies (BAR/N-BAR, F-BAR, and I-BAR), which regulate different cellular functions and bend membranes into distinctive shapes. Each BAR domain subfamilies have different shapes. The crescent shape belongs to the N-BAR, whereas the more extended the crescent shape reflected the F-BAR family. The third major BAR domain subfamily is I-BAR, which has a convex curvature shape (Figure 4).

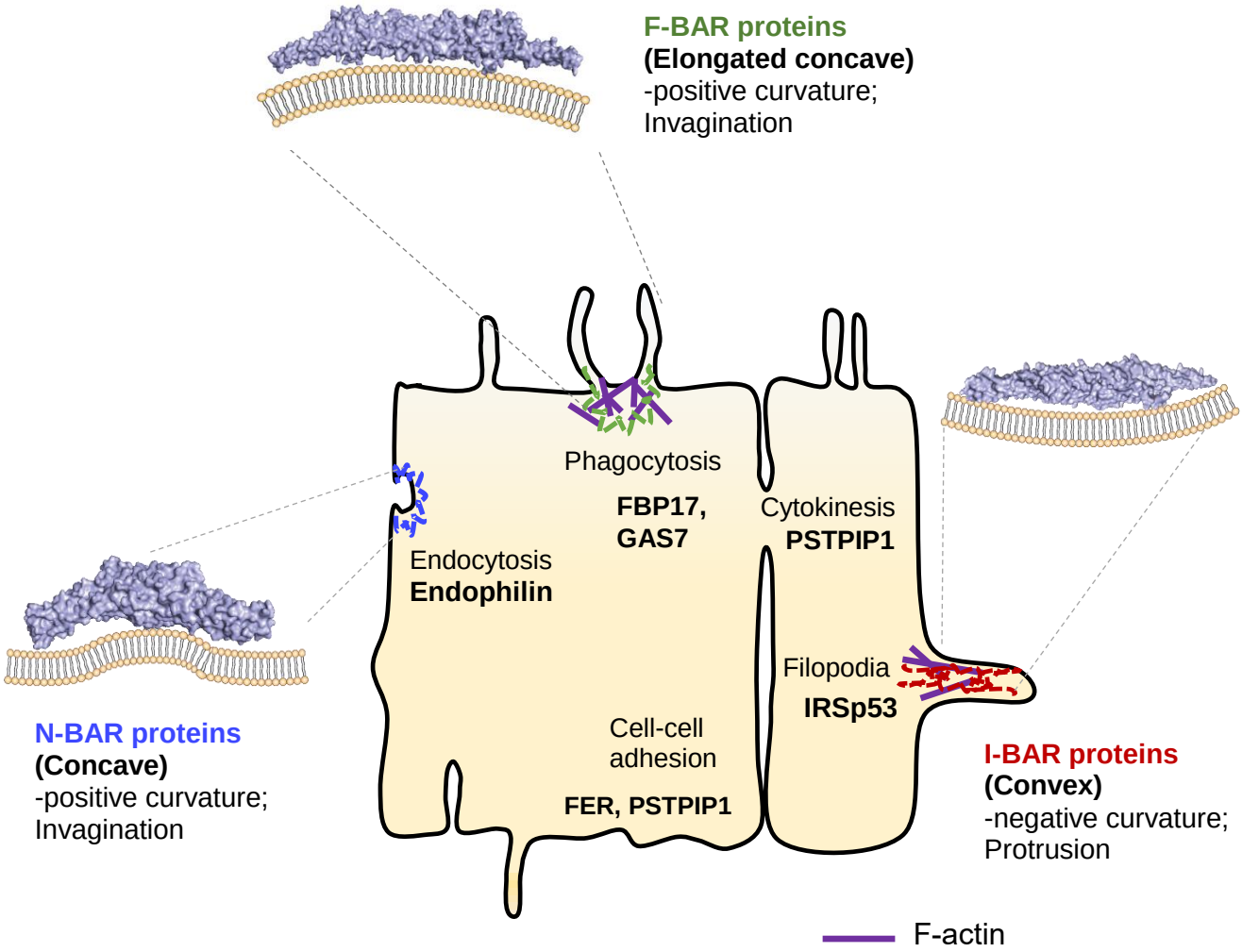

Figure 4: Curvature deformation by BAR domain protein. N-BAR (Endophilin structure-PDB ID; 2D4C) has a concave shape. F-BAR (GAS7 structure-PDB ID; 6IKN) has an elongated concave shape. I-BAR (IRSp53 structure- PDB ID; IY2O) has a convex shape. All the 3D structures of BAR domain dimers are shown as a surface from Edu-PyMOL. Schematics not drawn to scale.

Arfaptin, belonging to N-BAR subfamilies, was the first protein with structural determination (61). However, it was not recognized as the BAR domain at that time. The Arfaptin was involved in the reorganization of the cytoskeleton, by interacting with Rho family GTPases (40,62,63). Then, the BAR domains started to be recognized as a module that interacts with membrane, having unique curvatures that relates to the membrane of their actions. These BAR domains were of Amphiphysin (58), and Endophilin (64,65).

The BAR domain is being noticed for its interactions with cellular lipids in regulating the membrane curvature. Furthermore, the ability of the BAR domain to bend the membrane was because of its helix, which was harder than the membrane. Then BAR domains need to be oligomerized to shape the membrane for subcellular structure formation, because the subcellular structures are normally larger that a BAR domain. Besides that, the N-BAR domain also can bend the membrane by the N-terminal helix. This is one of the factors that this BAR domain can bend the membrane by hydrophobic interaction. The figure below the overall classification to describe these subfamilies of the BAR domain.

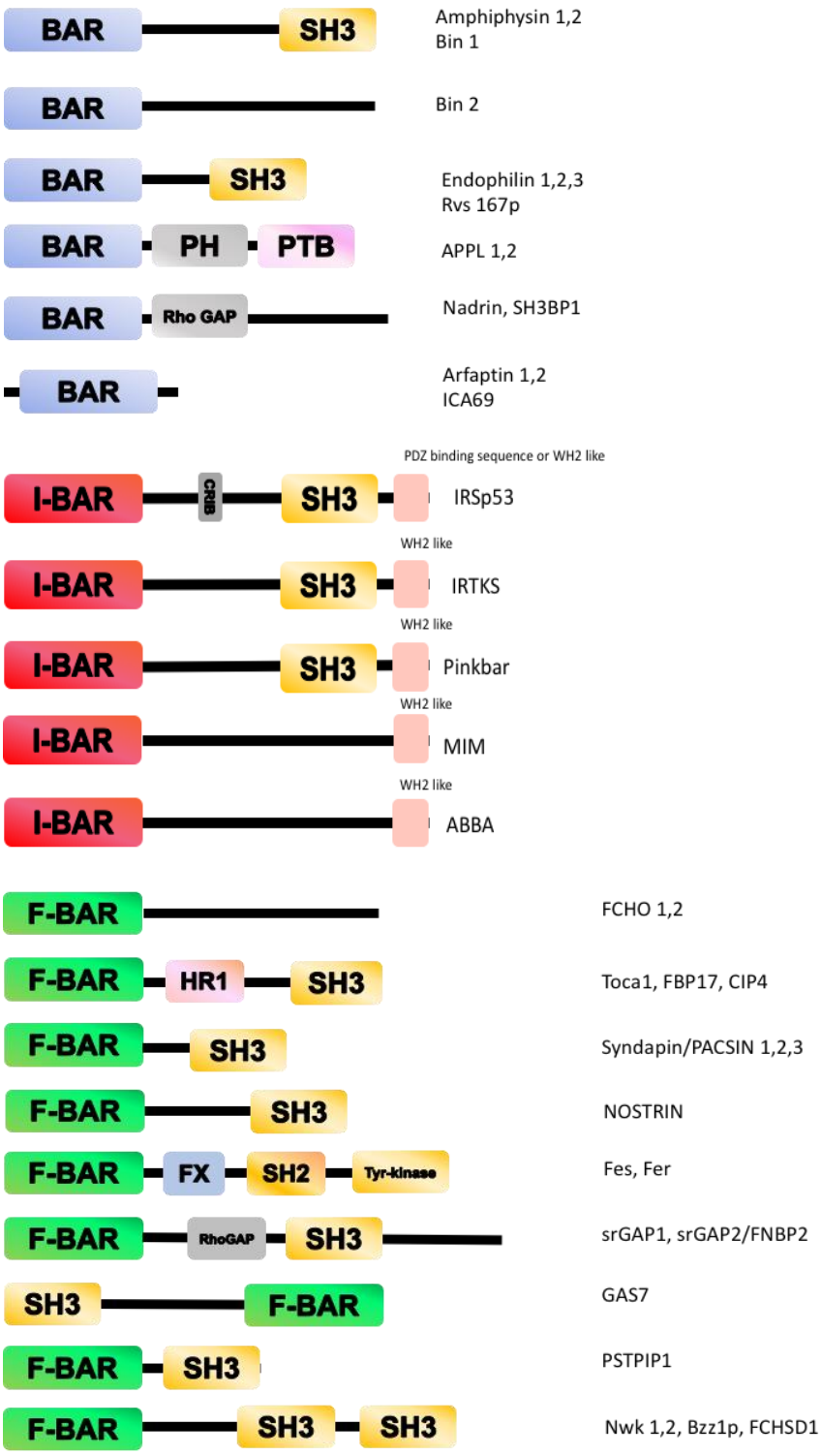

Figure 5: Classification of the BAR domain subfamilies with specific domain schematics of BAR, EFC/F-BAR, and IMD/I-BAR domain-containing proteins. Schematics not drawn to scale.

1.4.1 N-BAR

Classical BAR domain or also known as N-BAR domain, appears in a crescent shape of a dimer and has a positive concave structure (49,58,66). The N-BAR contains both the BAR domain structure and the N-terminal of the amphipathic helix. One of the examples of the N-BAR family that has a concave shape and amphiphilic helix that can cause tubulation at the membrane is Endophilin (63,64). Endophilin also can bind with dynamin that is involved in clathrin-mediated processes and prefers to bind at curved surfaces with insertion to the curved membrane (65,67).

1.4.2 I-BAR

I-BAR is the most well-known subfamilies of the BAR domain since it functions as an adaptor protein and also involves in the development of protrusion at the membrane, as well as cell migration (66,68,69). Besides, the I-BAR domain has the WH2 domain in its structure and CRIB motif (69). Insulin Receptor Substrate of 53 kDa (IRSp53) was classified under the I-BAR domain that has a different shape from N-BAR and F-BAR, which is a convex shape. IRSp53 was reported to be involved in the formation of filopodia predominantly by membrane protrusion (69-72).

1.4.3 F-BAR

F-BAR domain appeared in a crescent-shaped dimer, similar to N-BAR, but it was more elongated and generated a positive concave (40,42,47,52,54,55,57,73,74). F-BAR subfamilies are involved in membrane invagination at plasma membranes. PACSIN2 are the most well-known proteins that have been proven to have a relation with caveolae formation (51). Caveola is an uncoated pit to causes small invagination at the plasma membrane that is also related to membrane deformation. CIP4, TOCA 1, and FBP17 are the orthologous F-BAR domain proteins that can cause actin polymerization by the interaction with N-WASP-WIP (55), and are involved in clathrin-mediated endocytosis (75), as well as the tension sensing of the lamellipodia, presumably antagonizing the membrane extension by the invaginations (59). GAS7b also contains F-BAR domain that are involved in phagocytosis (42). According to the same authors, they examined that phagocytotic cup is a large membrane invagination, and GAS7 F-BAR domains assemble into relatively flat configuration. GAS7b contains the WW domain in front of the F-BAR domain. The characteristics of GAS7b F-BAR domain is described later.

1.5 Phagocytosis and GAS7 proteins

Phagocytosis is a subcellular structure that correlate with membrane remodeling to uptake micron sized particle. As previous study revealed phagocytosis is mediated by GAS7 protein, below is the illustration below shows the activity of GAS7-membrane binding, initiating the membrane deformation to generate the phagocytic cups and engulfment of the pathogens.

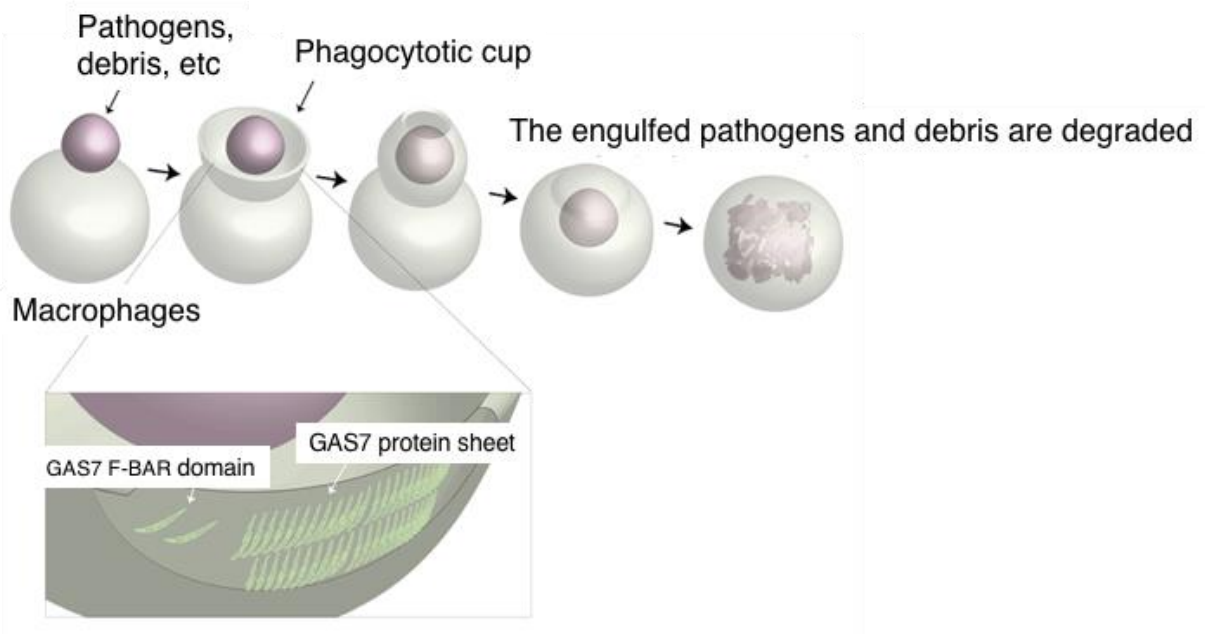

Figure 6: Illustration on how GAS7 at phagocytic cups formation in macrophages cells. The GAS7 will formed a sheet like structure at the phagocytic cup that will helps cell to eat or move. Adapted from https://bsw3.naist.jp/eng/research/index.php?id=1989

GAS7 protein with concave shape structure, belong to the F-BAR subfamily. The GAS protein was first being found from mouse fibroblast cells at cell growth arrest (G0) phase and was named due to that condition, which engaged in the function of cell cycle and also apoptosis (76). GAS7 also has been proven to play crucial roles in membrane protrusions of neurons (77,78). Recently, GAS7 have been reported to have function in preventing the fibrillogenesis of tau proteins (56), as well as act as potential pathways to cure Alzheimer's disease by altering the tau oligomerization.

There are alternative splicing isoforms of GAS7 protein, which are GAS7 F-BAR (also known as GAS7a), GAS7b, and GAS7c, as in Figure 7 (42,77,79).

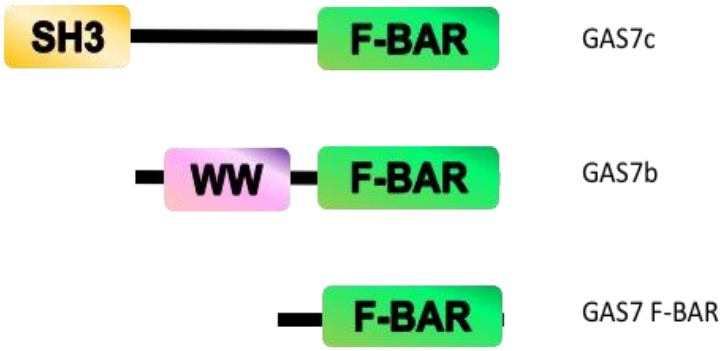

Figure 7: GAS7 isoforms.

Previous studies have reported that GAS7 have a potential as a breast cancer marker as it is able to control the transcription of p53 gene (80). Besides, GAS7 is also highly expressed in human brain tissue, testis, and lung (42,76-78,81). As this protein is primarily found in brain cells, GAS7 may have the potential to create a new pathway as well as new discovery of treatment in neurogenesis disease.

The unique characteristic of GAS7 is the presence of SH3 in front of the WW domain and F-BAR domain. According to Tseng and his groups, when they compared GAS7a, GAS7b and GAS7c isoform, they found that GAS7c which is consist of SH3 domain low expressed in lung cancer cell line that indicates, this isoform of protein might contribute to lung cancer in theirs study (79). Besides, another interesting finding about GAS7 are, in study conducted in our lab, showed that GAS7b was highly expressed in macrophage cells and colocalized with N-WASP (42) and were believed to work together in driving actin polymerization. Therefore, GAS7c also has higher binding compared to GAS7b in liposome assay that might reveal the

autoinhibition of SH3 in membrane binding (unpublished data). Yet, despite different findings and significant reasons of each study, what unifies behind the scientific facts is that GAS7 has potential in cellular effects, keenly in the immune system or neurological diseases as well as contributes the benefits to molecular cell biology.

GAS7 also consists of the two loops structures which are flat filamentous 1 (FFL1) and flat filamentous 2 (FFL2), as labeled in Figure 8a. This FFL2 is required for the sheet formation during the phagocytic cups configuration, as the deletion of these loops cause the membrane binding affinity of the GAS7 to be reduced. Besides deleting the FFL2 loop, we also have introduced the mutation at the Asp207 site, and as expected, the deleterious effect occurred in macrophage cells and also in negative staining by using a transmission electron microscope. Following this, GAS7 also shows sheet-like structure on a monolayered membrane (Figure 8c) (42).

a

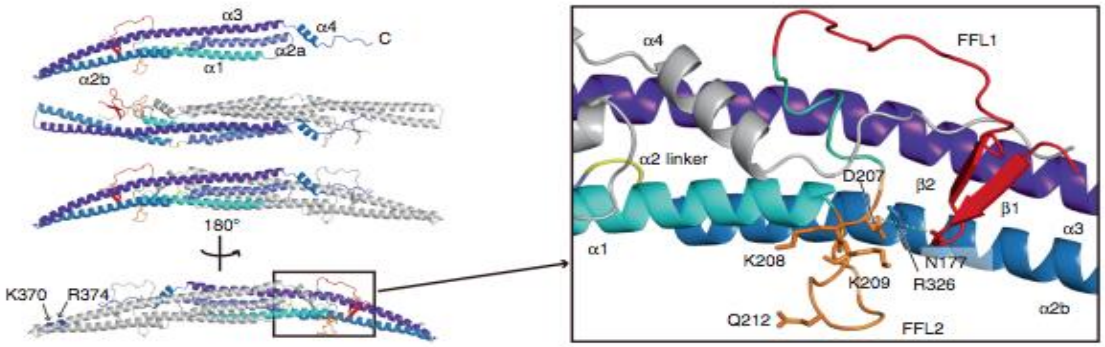

b

Suggested functions of mutation point	Point of mutation
Contact surface within dimer	N177, D207, K208, K209, R326
Contact surface with membrane	Q212, K370, R374E

c

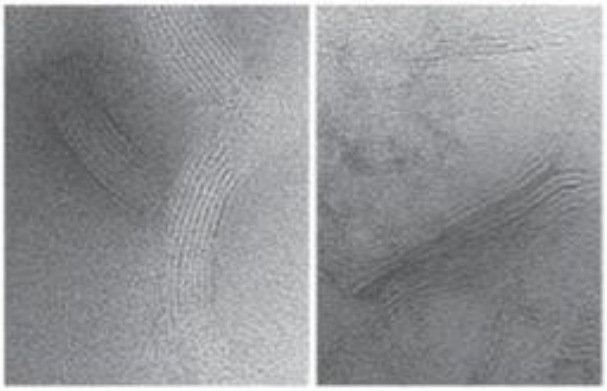

d

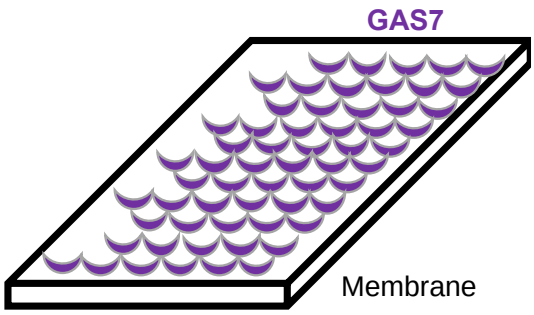

Figure 8: GAS7 structure and amino acid position. a) GAS7 structure. b) The table of summary about the mutation sites that been classified as contact surface within dimer and contact surface with membrane. c) Striation structure of GAS7 F-BAR and GAS7b on monolayered membrane. d) Cartoon illustration on how GAS7b protein assembly on membrane. Adapted and reconstituted from (42).

1.6 The mode of oligomerization of the F-BAR domains

The oligomerization of the BAR domain will help the plasma membranes to bend in specific directions and cause protrusion or invagination of the membrane. There are also more scientific perspectives (37,38,48) where these lipids activities should have spatial interaction with protein in order to generate curvature. As the bending of curvature also involved the Arp2/3 and actin polymerization. I also believed that the BAR domain somehow gave contributed to this activity. Subsequently, F-BAR have different modes of oligomerization. The mode oligomerization of the F-BAR domain is simplify in Figure 9. Likewise, The F-BAR of CIP4 and FBP17 have tips to tips mode of oligomerization that have been observed in EM (47). In other stories by Becalska and their groups, the F-BAR of Nwk can form zig-zag in the mode of the oligomer, as well as scallop like structures visualized in the negative staining (82).

In our cases, GAS7 proteins have dimer-dimer for mode of oligomer which will be resulting in the flat filamentous oligomer, in which turn the structure looks like sheet on the monolayered membrane (42) (Figure 8c). Concurrently, with *S.pombe*, Cdc15, can assembly in flat at membrane and provided platform for the binding of others protein at non concave side in order to cooperatively form architecture at membrane (83,84). This evidence showing that F-BAR can form different mode of oligomerization regardless of the how they oriented theirs structure to interact and assemble with the neighborhood dimers. However, the role of the binding proteins of the BAR domain containing proteins, that regulate actin cytoskeleton based on the oligomerization of the F-BAR domains had not been analyzed.

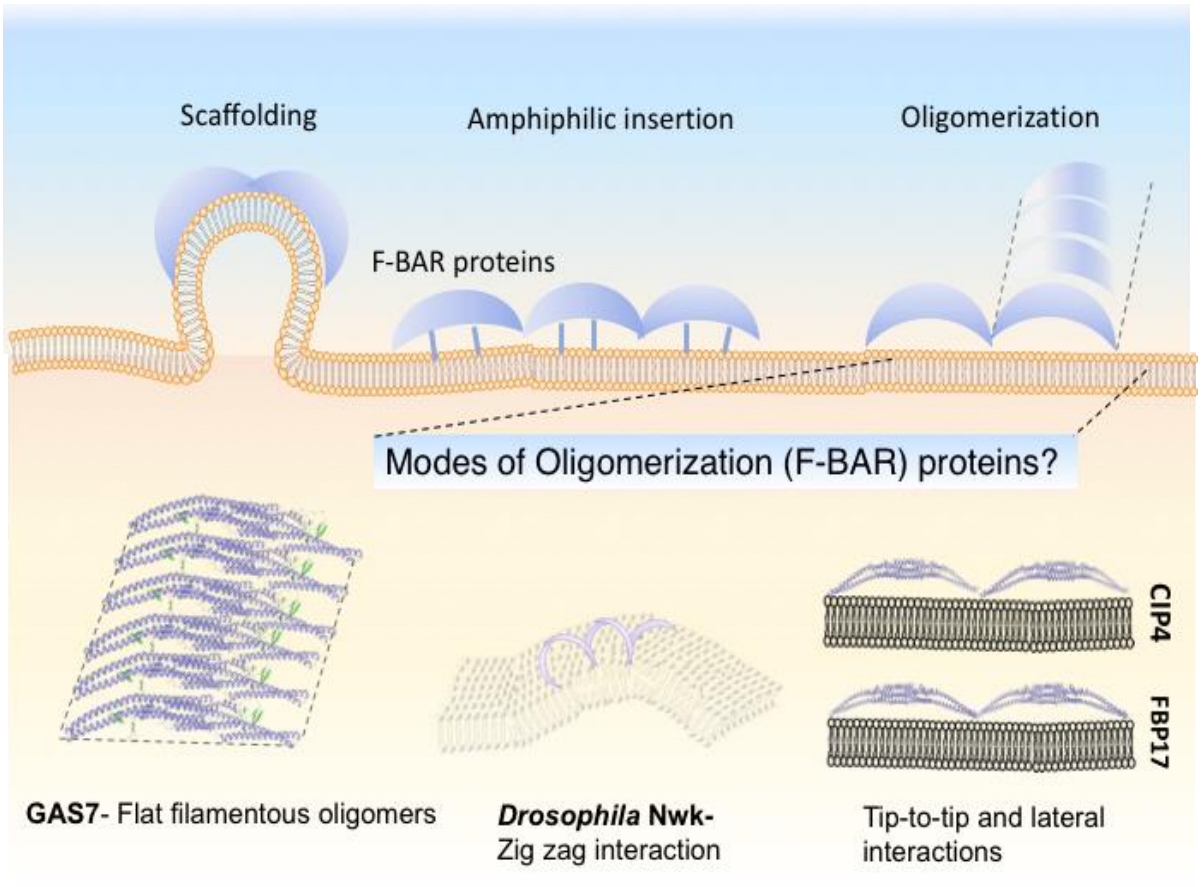

Figure 9: The mode of the F-BAR proteins oligomerized at the membrane. Upper; the different mode of the membrane deformation by binding of BAR domain protein like scaffoldings, amphiphilic insertion and oligomerization. The bottom figure is illustrated to show the different modes of the oligomerization. Bottom left; The GAS7 protein (PDB ID: 6IKN) that assembly to form flat filamentous oligomers. Bottom middle; D. melanogaster Nwk F-BAR, an orthologue of mammalian FCHSD1/2 which can form zigzag assembly. Bottom right; CIP4 protein (PDB ID: 2EFK) and FBP17 (PDB ID: 2EFL) protein that have tip to tip assembly. Schematics not drawn to scale.

1.7 The BAR domain oligomerization and possible relation to the multivalent interaction in the phagocytic cup

Cell that composed of cell membrane, able to alter their shape to reflect with surrounding environments, especially in engulfment of pathogen. In spite of that, the question still arises of how the extracellular signals regulates the cellular morphology, especially on how the oligomerization of the F-BAR domains is regulated and connected with actin cytoskeleton. As F-BAR domain typically have linked to another domain in the actin binding proteins, this multicomplex interaction, might showing the pathways from F-BAR domain to actin cytoskeleton (85). In addition, F-BAR also possess Src-homology 3 (SH3) domains that can govern the interaction with linking with the proteins that have proline-rich sequences to regulate actin and cytoskeletons arrangement (40). Despite of SH3 in F-BAR, there is growing evidence that F-BAR domains themselves can be a platform of multivalent of proteins scaffolding.

In the context of connecting with actin binding protein, FBP17 proteins and Toca-1 proteins can induce N-WASP-mediated Arp2/3-dependent polymerization in the presence of membrane (55,86). One noteworthy example is the FCHSD2 protein. FCHSD2 is known that is recruited to clathrin-mediated endocytosis by scaffold protein intersectin via SH3-SH3 interaction FCHSD2 recruited N-WASP to PIP_2 to induce actin polymerization, thus enhancing pit maturation (75). Thus, mouting evidence have discussing the role of actin binding protein, like N-WASP protein, however, in phagocytosis cascades, how this N-WASP and others adaptors proteins cooperatively working together with F-BAR to function as specific subcellular structure is still remain a question. Perhaps, this multicomplex interaction will give new in sight on how F-BAR domain binding to membrane, oligomerize and assembly together and cause subcellular structure changes in cell.

Hence, as exciting as how GAS7 can help in the formation of phagocytic cups and also appear as a sheet on the monolayered membrane, this study focused on revealing how this formation of sheet undergo oligomerization and its deformation kinetics. As reported before, the mode of the protein oligomerization has divergence of mechanism. Our group had published about mechanism binding of GAS7 in vitro and in vivo, but a cogent of assembly of this protein for how fast the GAS7 protein can move to bend the membrane is still in question. Thus, this study also will resolve the question of how fast this protein moves and cooperatively working together with other adaptors protein to help the phagocytosis process.

As the first study to resolve the kinetics of F-BAR domain proteins, this study could reveal how the nanometer-sized proteins working together with actin binding protein and ITAM receptors, together providing understanding and future perspectives in the immune system. In addition, the significant function of GAS7 in helping the phagocytosis process against the pathogen, as it has a role in the phagocytic cup formation.

Kinetics study is a challenge in protein-protein interaction study because observation of milliseconds of protein interaction is quite hard with limitation of rapid and advanced equipment. However, a fast and sensitive technique of FRET in my reconstituted liposomes have provided a great platform for study protein-protein interaction that have less than seconds of interaction. In addition, the knowledge of reaction and kinetics mechanisms, is very useful in deciding the most optimum conditions for the reaction to occur. For example, in the cell, there is no specific protein concentration as the cell always synthesizes the proteins dependent on the cell environment. Thus, in kinetics study, the specific concentration to start the reaction can be examined, as well as elucidating the reaction mechanisms. Thus, the kinetics study conducted in my research will be revealed the mechanisms of protein-protein binding and clarified a few questions in cooperatively movements of the actin binding protein in phagocytosis cascade.

1.8 Thesis rationale

This study is the first study of kinetics and oligomerization of the BAR domain. Thus, further binding mechanisms should be evaluated to elucidate how the immune system works among signals, ligands, and receptors, as well as the multivalent protein-membrane functions in foreign particle annihilation. By knowing the kinetics assembly in this study, it will help in providing the optimum condition for the protein-protein interaction works in future molecular biology research. Some proteins need to undergo oligomerization in order to function in cellular conditions, and FRET analysis is the one way to evaluate the oligomerization of protein in an easy and fast way. In couple with this, GAS7b protein is actively involved in the development of the membrane invagination in phagocytic cups. As a whole the cascade of phagocytosis also will be initiated with the activation of GTPase, kinase and several phosphatidylinositol species. Though, the regulation of the assembly of GAS7b dependent on Cdc42 and Src kinases downstream of FcγRIIa had been unclear.

In this study, I show that the kinetics and quantitative measurement of the assembly of GAS7b on the reconstituted liposomes by FRET and cellular FRET experiment by FLIM. The time-dependent increase in the FRET between CFP-GAS7b and YFP-GAS7b indicated the rapid oligomerization of GAS7b on the membrane that cooperatively working with others molecular scaffolds, including N-WASP, Nck, and WISH and active form of Cdc42. Moreover, as phagocytosis also affected by Src kinase, I have also revealed that in the presence of the Src kinase and FcγRIIa can further increased the FRET. My result correlated with cellular experiment, where the FRET of GAS7b was reduced with the presence of Cdc42 inhibitor, ML141 and the Src inhibitor, PP2.

Thus, by revealing the model of kinetic of the oligomerization of this GAS7b that can cooperatively working together with other actin binding protein like N-WASP, WISH and Nck, Src kinase and FcγRII more new insight, and complicated molecular biology machinery behind these activities can be understood in future.

2.0 Materials and Methods

2.1 Gene cloning

The pGEX6P1-CFP, pGEX6P1-YFP, pGEX6P1-CFP-GAS7b, and pGEX6P1-YFP-GAS7b were cloned using Gibson assembly and were transformed into *E. coli* (JM109). Before the transformation into JM109, the mixture of the template, the insert and the Gibson Assembly® Master Mix (New England Biolabs®), were incubated at 50°C for 1 hour. The next step was followed by colony polymerase chain reaction (PCR) by using EmeraldAmp PCR Master Mix (Takara Bio). The plasmids were subjected to sequencing by (ABI machine) for confirming the sequence. Then, the plasmids were transformed into *E. coli* (Rosetta 2) for protein expression and purification.

2.2 Preparation of GAS7b mutants and others protein

Here are the list of plasmids constructed and the primer that have been used in this study.

Plasmid name	Forward primer	Reverse primer	Notes
I. pGEX6P1-CFP	GTACAAGTAGTCC CGGGTCGACTCGA GCGGCCGCAT	ACCCGGGACTACTT GTACAGCTCCATGC CGAGAGTGATC	This study
II. pGEX6P1-YFP	GTACAAGTAGTCC CGGGTCGACTCGA GCGGCCGCAT	ACCCGGGACTACTT GTACAGCTCCATGC CGAGAGTGATC	This study
III. pGEX6P1-CFP-GAS7b	CTGTACAAGTCCG GACTCAGATCTAT GAAGCCTGGGATG GTCCCCC	GGGGGACCATCCCA GGCTTCATAGATCT GAGTCCGGACTTGT ACAG	-This study -Linker between CFP and GAS7b is ATGAAGCCTGGG
IV. pGEX6P1-YFP-GAS7b	CTGTACAAGTCCG GACTCAGATCTAT GAAGCCTGGGATG GTCCCCC	GGGGGACCATCCCA GGCTTCATAGATCT GAGTCCGGACTTGT ACAG	-This study -Linker between CFP and GAS7b is ATGAAGCCTGGG
V. pGEX6P1-CFP-GAS7bK208AK209A VI. pGEX6P1-YFP-GAS7bK208AK209A	CTGTGACTACTTT TGGGCGGACGCGG CGGACCCACAAGG CAATGGCAC	CCGTGCCATTGCCT TGTGGGTCCGCCGC GTCCGCCCAAAAGT AGTCACAG	-This study -Linker between CFP and GAS7b is ATGAAGCCTGGG

VII. VIII.	pGEX6P1-CFP-GAS7bK370/R374E pGEX6P1-YFP-GAS7bK370/R374E	GGACATCGAGAAGGCACGGGAGAAGTCCACTCAGGCCGGAGATG	GCCTGAGTGGACTTCTCCCGTGCCTTCTCGATGTCCTCCTCGGTC	-This study -Linker between CFP and GAS7b is ATGAAGCCTGGG
IX. X.	pGEX6P1-CFP-WWY65C-GAS7b pGEX6P1-YFP-WWY65C GAS7b	TCAGGGCCGCCGTTACTGTGTCAACACGACTAC	GTAGTCGTGTTGACACAGTAACGGCGGCCCTGAG	-This study -Linker between CFP and GAS7b is ATGAAGCCTGGG
XI.	pGEX6P1-WISH	TCCAGGGGCCCCTGCATGTACCGCGCGCGC	TCGAGTCGACCCGGGCTAGCTGGGAACCTCTG	Provided by Thi Nyugen Nhung
XII.	pGEX6P1-WISH (Y52A)	GTACGTGCCGCCTGCCGCACTGCATCGCCTGCAGGGCATGGAACAAGATG	CTGCAGGCGATGCAGTGCGGCAGGCGGCACGTACCCGGTCTCGCCACTGC	This study
XIII.	pGEX6P1-Nck	TCCAGGGGCCCCTGGGATCCATGGCAGAAGAAGTGGTGGTAG	TCGAGTCGACCCGGGAATTCTCATGATAAATGCTTGACAAG	Provided by Thi Nyugen Nhung
XIV.	pGEX6P1-N-WASP	TCCAGGGGCCCCTGGGATCCATGAGCTCCGGCCAGCAGCAG	TCGAGTCGACCCGGGAATTCTCAGTCTTCCCATTCATCATC	Provided by Thi Nyugen Nhung
XV.	pGEX6P1-His-FcγRIIa	TCCAGGGGCCCCTGCGGTGGCTCTTTTACT CATC	GTCGACCCGGGAATTCCGGCTAATTGTTACTATTGAACATGAT	Provided by Kayoko Oona-Yakura
XVI.	pEGFP-C1-SrcY530F -Flag	GGCAGCGATTACAAGACGACGATAAGTAAGCGGCCGCGACTC	TTATCGTCGTCATCCTTGTAATCGCTGCCCTTGTACAGCTCGATGCC	Provided by Kayoko Oona Yakura
XVII.	EF-Cdc42-Flag	Suetsugu et al., 2002 (17)		
XVIII.	pGEX6P1-GAS7b-D207R	Hanawa-Seutsugu et al., 2019 (42)		
XIX.	pGEX6P1-GAS7b-K208AK209A	Hanawa-Seutsugu et al., 2019 (42)		

2.3 Protein expression

The *E. coli* strain Rosetta 2 was transformed with the expression plasmids of CFP or YFP-GAS7b, CFP or YFP-GAS7b mutants and others examined proteins. The *E. coli* strain Rosetta 2 cells were grown in the 500 ml of LB medium containing 0.1 mg/ml of ampicillin and 0.034 mg/ml of chloramphenicol. After that, the cultured *E. coli* cells were expressed and induced with the 0.2 mM isopropyl β-D-1-thiogalactopyranoside (IPTG), when the absorbance of 600 nm (OD 600) reached 0.6-0.7. Then, the culture *E. coli* cells were incubated overnight in the shaker at 20°C. The harvested *E. coli* cells were then disrupted with sonication for 3 minutes with a sonication buffer (20 mM Tris HCl pH 7.5, 150 mM NaCl, 1 mM EDTA-Na pH 8, and 5% glycerol). After that, the supernatant were centrifuged at 150 000 r.p.m for 10 minutes. All these samples expression were subjected to sodium dodecyl sulfate-polyacrylamide gel electrophoresis (SDS-PAGE) and stained with Coomassie brilliant blue (CBB).

2.4 Protein purification by GST-PreScission Protease

The harvested cells were disrupted with sonication for 3 minutes with a sonication buffer (20 mM Tris HCl pH 7.5, 150 mM NaCl, 1 mM EDTA-Na pH 8, and 5% glycerol) and were centrifuged at 150 000 r.p.m for 15 minutes. The supernatant was incubated with the equilibrated beads for a hour in 4°C. Then, the solution was centrifuged at 500 g to separate between beads and supernatant. The beads were collected and continued in a washing step with an ice-cold wash buffer (20 mM Tris HCl pH 7.5, 150 mM NaCl and 1 mM EDTA-Na pH 8) for three times. Then, 200 µl of ice-cold wash buffer and the 2 µl of PreScission Protease was added together in 1.5 ml Eppendorf tube. PreScission Protease was added to cleavage of GST tagged. The mixture was rotated in 4°C for overnight. After overnight incubation, the supernatant was collected by centrifuge at 500 g for 10 minutes at 4°C. Finally, the proteins were subjected to SDS-PAGE and stained with CBB. The proteins concentration was measured by the intensity of each protein bands based on Image J software.

2.5 Transfection of pEGFP-SrcY530F-Flag and EF-Flag-Cdc42

The pEGFP-SrcY530F-Flag and EF-Flag-Cdc42 were transfected into HEK293 with polyethylenimine (PEI) and Opti-MEM in 30 ml culture of Free Style 293 Expression medium (Gibco). The cells were grown or 2 days before collected at 37°C. For immunoprecipitation of

the proteins, cells were lysed on ice for 20 minutes with lysis buffer (20 mM Tris HCl pH 7.5, 150 mM NaCl, 5 mM EDTA-Na pH 8 and 1 mM PMSF) and then centrifuged at 12,000*g* for 10 minutes at 4°C. The supernatant was incubated with 15 µl of agarose flags beads at 4°C overnight. The beads were washed three times with ice-cold wash buffer (20 mM Tris HCl pH 7.5, 150 mM NaCl and 1 mM EDTA-Na pH 8). After that, the flag beads were incubated in 100 µg/ul flag peptide for 30 minutes at 4°C with rotation before elution. The eluate was collected and heated at 95°C for 2 minutes before subjected to SDS–PAGE then stained with CBB and western blot analysis. For FRET analysis, the eluted proteins were further used based on the concentration needed.

2.6 Preparation of POPC: POPE: POPS-GUVs

The Giant unilamellar vesicles were made from the mixing of PO lipids which consist of 20% POPC (850475C-Sigma-Aldrich), 20% POPE (850757C-Sigma-Aldrich,) and 60% POPS (840034C-Sigma-Aldrich). In addition, 5% PIP_2 (P9763-Sigma-Aldrich), 5% PIP_3 (130719-Elchon), and 10% DGS-NTA (790404C-Avanti) for liposomes that used this phosphoinositides. Lipids in chloroform were dried under nitrogen gas and subsequently incubated under vacuum for >20 minutes. The dried lipids were resuspended in 50 µl buffer containing 10 mM Tris-HCl pH 7.5, 1 mM EDTA-Na pH 8, and 300 mM sucrose for 10 minutes at 45°C for pre-hydration and then incubated for 1 hours at 37°C to form GUV. Subsequently, 0.5 µM protein and 0.5 mg/ml GUVs were incubated in the same respective buffers (or stated otherwise) for 20 minutes at room temperature.

2.7 Liposome co-sedimentation assay

The in vitro liposome-binding analysis was performed using liposomes that were prepared by natural swelling as above. The liposomes were then precipitated by centrifugation at 50,000 r.p.m for 20 minutes in a TLA100 rotor (Beckman Coulter). The pellet and supernatant were fractionated by SDS-PAGE and stained with CBB. Each proteins band intensities were measured-by Image J software.

2.8 Spectroscopy

The spectra were measured using 2 ml cuvette in a JASCO FP-6500 spectrofluorometric with proteins concentration of 0.5 μM (or stated otherwise) for CFP or YFP-GAS7b and their mutants, in buffer containing 10 mM Tris pH 7.5, 150 mM NaCl, and 1 mM EDTA-Na pH 8. The concentration of protein is dependent on each the experimental design. The samples were excited at 433 nm, and emission spectra were recorded at a 5 nm with a scan speed of 2000 nm/min. The liposomes were added during the 45 seconds of measurement. In the presence of Src and FcγRII, the liposomes were incubated in the cuvette. The proteins complex was injected at 45 seconds of measurements. The wavelength was set at 450 nm to 550 nm for detection of CFP and YFP wavelength.

All normalized average different change in YFP/CFP ratio was calculated using the formula:

$$= (527\ \text{nm} / 475\ \text{nm}) - n$$

n = first reading of each measurement.

2.9 in vitro kinase assay

Phosphorylation of pEGFP-SrcY530F with FcγRIIa was performed as described in Suetsugu et al.,(17). 25 nM pEGFP-SrcY530F and 50 nM His- FcγRIIa, were mixed in solution containing 20 mM HEPES-Na (pH 7.2), 10 mM $MgCl_2$, 3 mM $MnCl_2$, 150 mM KCl, and 1 mM ATP with or ADP. The mixture was incubated at 37°C for 10 minutes, continued for western blot with anti-phosphotyrosine (4G10).

2.10 Knockout and retrovirus-mediated gene transfer

This method was used as described previously in Hanawa-Suetsugu et al (42). The CRISPR/Cas9 system was used. The guide RNA targeting the first exon of GAS7b (GGCGGAGGGGGGACCATTCC) was designed using the server http://crispr.mit.edu and inserted into the pX330 vector. After transfection, the cells were cloned by monitoring the CFP/YFP fluorescence from the reporter plasmid pCAG-ExxFP with the GAS7 genome fragment, using a fluorescence-activated cell sorter (FACSAria (BD)). CFP-GAS7, and YFP-GAS7b-IRES-CFP-GAS7b expressed in GAS7-knockout cells, using a retrovirus. The cells were then cloned and isolated using a cell sorter. Clones with GAS7 expression similar to that of the parental cells were selected, and examined for their FRET activity. The RAW264.7

knockout GAS7b, expressing CFP-GAS7b and YFP-GAS7b-IRES-CFP-GAS7b was cultured in DMEM supplemented with 10% fetal bovine serum (FBS), 1% penicillin-streptomycin solutions in a humidified incubator, where containing 5% CO_2 and maintaining at 37 °C.

2.11 Frustrated phagocytosis

For frustrated phagocytosis, The RAW264.7 knockout GAS7b, expressing CFP-GAS7b and YFP-GAS7b-IRES-CFP-GAS7b were seeded in 35 mm dishes with a density of 5 × 10^5 cells/ml. The glass dishes were firstly coated with 1 mg/ml human IgG for 40 minutes at room temperature. After that, the excess antibodies were removed by rinsing with DMEM for three times. The cells were treated with ML141 and PP2 at 10 μM in 500 μl cell suspension. Then, the cells were incubated for 20 minutes at 5% CO_2 and 37°C. For the fixation before observation, the cells were fixed with 3% of PFA for 20 minutes. Then, the PBS-NaBH4 was added for 5 minutes, and the fixed cells were stored with PBS, 1% PVA and 10 mM MAE.

2.12 FLIM and phasor analysis

The fixed and mounted cells were subjected to FLIM measurements that were performed using a Leica TCS SP8 confocal microscope (Leica Microsystems). The microscope was implemented with a FLIM 433 WLL laser (PicoQuant). Images were acquired using a 63X water-immersion objective. For excitation and emission of fluorescence proteins, CFP excitation is 433 nm and emission is 475 nm, while YFP at excitation 514 nm and emission 520 nm. The fluorescence intensity was recorded in each pixel of a FLIM image was quantified by the phasor approach, that subjected to the lifetime analysis. Each pixel from the FLIM image gives rise to a single point (phasor) in the phasor plot. The interpretation of phasor FLIM distributions is a straightforward dot at the universal circle as reported before (87,88).

2.13 Western blotting

All the western blot detection used the primary antibody at 1:10000 by mouse anti-GAS7 (Origene, 2F6, TA501756), followed by anti-mouse or rabbit IgG alkaline phosphatase conjugate (Promega) in PBS-T with 1:10000 dilution for secondary antibody. The detection on the membrane (Immobilon P, IPVH00010, Merck Millipore) after incubation with antibodies were detected by 5-bromo-4-chloro-3-indoryl phosphate/nitro blue tetrazolium (Roche).

2.14 Statistical analyses

All data are expressed as the mean ± S.D., as indicated in the legends. Statistical analyses were performed using Microsoft Excel, for Solver Software and Student's t-test. For half-time and lifetime, Graphpad Prism (t-test) was used for statistical analyses. Value of $P < 0.05$ are considered significant.

3.0 Results

3.1 Purification of GAS7b, GAS7b mutants and other proteins

To purify the proteins, I transformed the plasmid into *E. coli* strain Rosetta 2, induced the protein expression with 0.2 mM IPTG concentration, and cultured at 20°C for overnight. Then, the bacterial pellets were harvested and were subjected to disruption with ultrasonic homogenizer. After that, the supernatant was rotated with 0.1 ml of Glutathione Sepharose 4B (GE Healthcare) at 4°C for 1 hour. The beads were collected and washed with the wash buffer (20 mM Tris-HCl pH 7.5, 150 mM NaCl, 1 mM EDTA-Na pH 8.0). This step was repeated for three times. The bound protein was cleaved by 2 µl of GST Presisson Protease in 0.3 ml the wash buffer, and was incubated for 16 hours at 4°C. The eluted proteins were carefully separated from the beads and collected. Finally, the protein concentration was measured by sodium dodecyl sulfate polyacrylamide gel electrophoresis (SDS-PAGE) that stained with CBB.

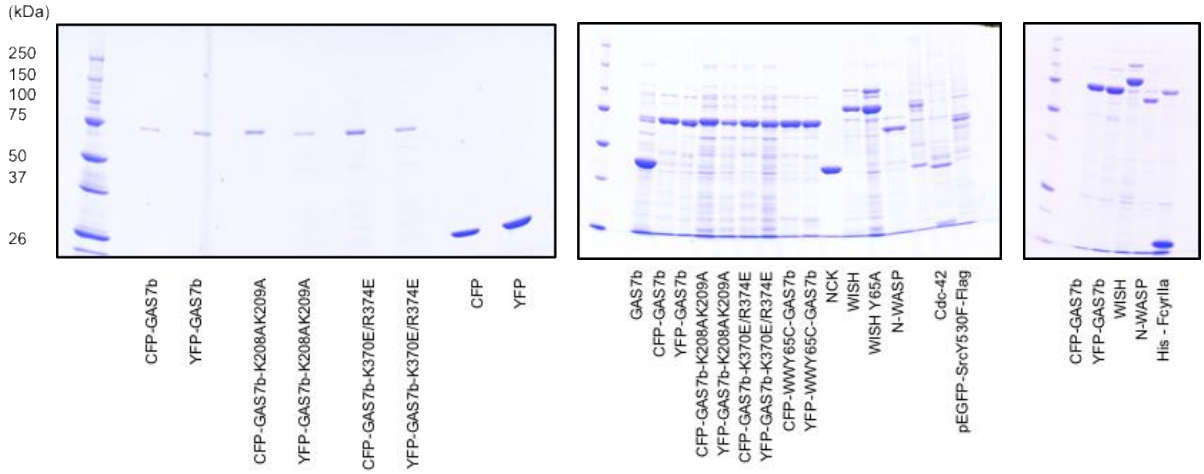

Figure 10: SDS-PAGE of protein purification of desired protein by GST-PreSission Protease. The protein concentration was determine using Image J software.

The protein was successfully purified at the expected molecular weight (Figure 10). The protein concentration was calculated by using image J according to the band intensity in each lane based on 50 kDa maker and each protein molecular weight. The protein has been collected in the wash buffer (20 mM Tris-HCl pH 7.5, 150 mM NaCl, 1 mM EDTA-Na pH 8.0) that was used throughout in this research.

3.2 Liposome co-sedimentation assay

In order to evaluate the binding of GAS7b proteins to the liposomes, I have performed liposome co-sedimentation assay. Subsequently, the protein at 0.5 μM was incubated with the liposomes having 0.5 mg/ml lipids subjected to centrifugation for 20 minutes. This technique has been used to observe the binding of the protein and lipid. GAS7b, GAS7b-D207R, GAS7b-K208AK209A have been used in this assay (42). The D207R mutation was selected to increase the basic amino acid residues and was expected to result in increased ability to bind to membrane than WT did. The K208AK209A mutation was expected to decrease the membrane binding affinity by reducing the number of the basic amino-acid residues. The liposomes consisted of the 20% of 1-palmitoyl-2-oleoyl-glycero-3-phosphocholine (POPC), 20% of 1-palmitoyl-2-oleoyl-sn-glycero-3-phosphoethanolamine (POPE), and 60% of 1-palmitoyl-2-oleoyl-sn-glycero-3-phospho-L-serine (POPS). This composition contained more negative charge than the cytoplasmic surface of the plasma membrane but was thought to ensure the binding of GAS7b to the membrane. Figure 11b show the representative gel images of SDS-PAGE of the results of the liposome co-sedimentation assay and Figure 11c shows the quantification of the proteins in the pellet. The thicker band in the pellet lane indicated the higher binding of that protein, and in this experiment the proteins without liposome acted as a control. The D207R mutant have shown an increase in binding with liposome, shown by the 60% of the proteins in the pellet while GAS7b protein in the pellet contained the 50% of the protein (Figure 11c). However, the K208AK209A mutant had decreased binding to the liposomes, as shown by the 35% proteins in the pellet (Figure 11d).

I also have determined the Kd of GAS7b to these liposomes by this binding assay using the liposomes of the concentration 0.001 μM to 0.5 μM. Then, the Kd was 0.02 μM (Figure 12).

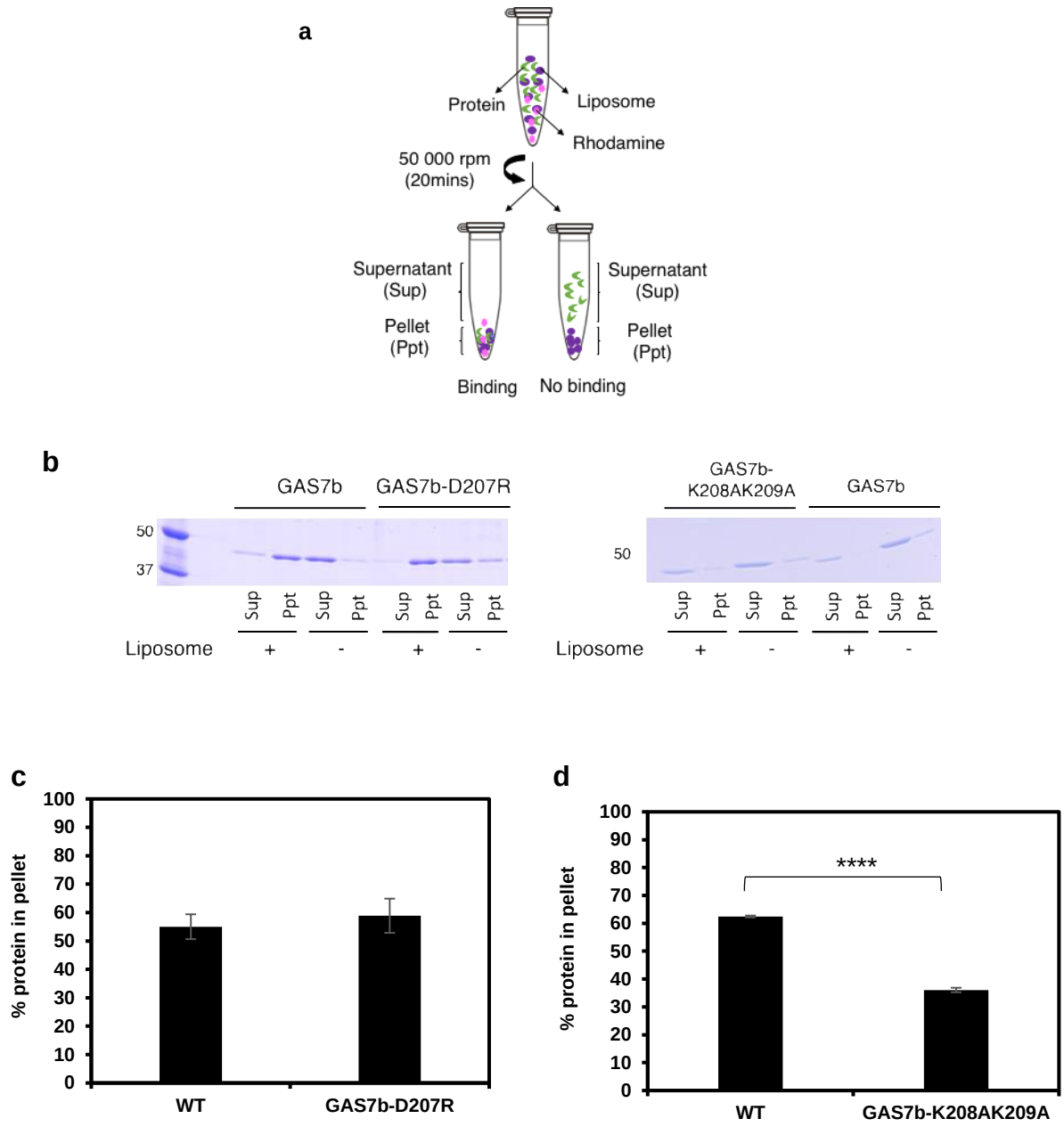

Figure 11: Liposome co-sedimentation assay. a) Illustration of liposome co-sedimentation assay method to determine the binding ability of protein and liposome. b) The result was visualized by SDS-PAGE that stained with CBB. c and d) Quantitative analysis of the binding ability of the non-tagged GAS7b and its mutants, D207R and K208AK209A in a, Error bars: SD. The concentration of GAS7b, GAS7b-D207R and GAS7b-K208AK209A are 0.5 µM with 0.4 mg/ml of liposomes. The P-values were obtained by two-tailed Student's t-test. GAS7b-K208AK209A are significant, ****p<0.0001, against the positive control.

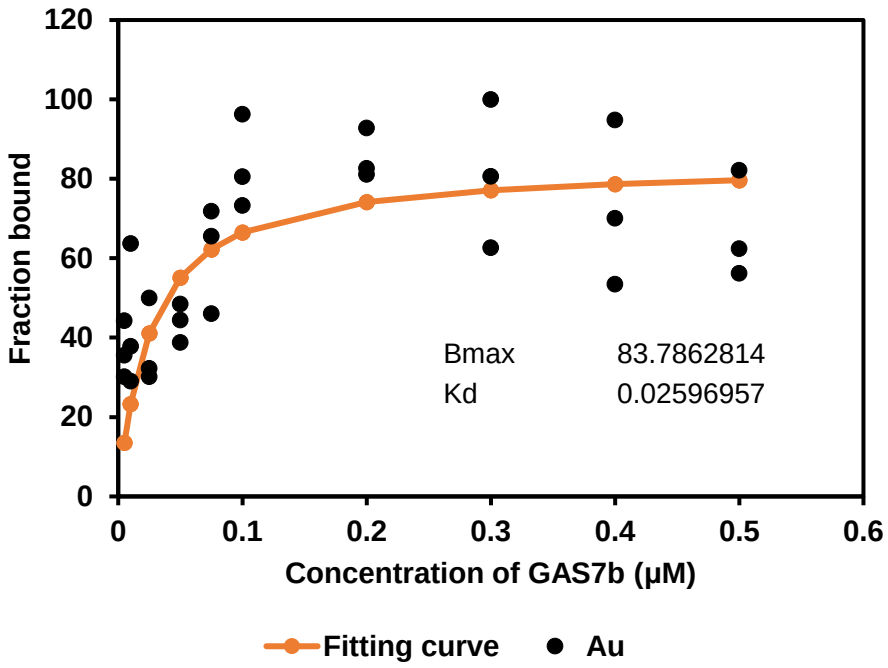

Figure 12: Binding percentage of the non-tagged GAS7b. The graph showed the binding curves GAS7b-WT. Percentage of binding was calculated percentage of (pellet/pellet and supernatant) using Image J and is plotted as function of protein concentration. The saturated of binding (Kd)= 0.02 μM was calculated by fitting using the in Excel (Solver) and is given for each binding experiment together with the calculated maximum binding (Bmax)= 83.786. The liposomes concentration is 0.2 mg/ml. Au is auxiliary unit.

Because GFP/YFP/CFP tagged GAS7b was used in FRET experiments, I have further investigated the effect of tag to GAS7b, i.e., GFP/YFP/CFP for the liposomes binding. The purpose of this experiment is to examine whether the CFP and YFP tag affected the membrane binding. Hence, I have examined the tagged-GAS7b. The K370ER374E mutant with these tags, of which mutations to the acidic residues, reduced the membrane binding. The K208AK209A mutant with the FFL2 mutation also exhibited reduced membrane binding. The D207R mutant had a tendency to bind to the membrane more strongly than GAS7b-WT. Therefore, the tagged GAS7b was found to bind to the membrane as well as GAS7b did with 60% PS (Figure 13b).

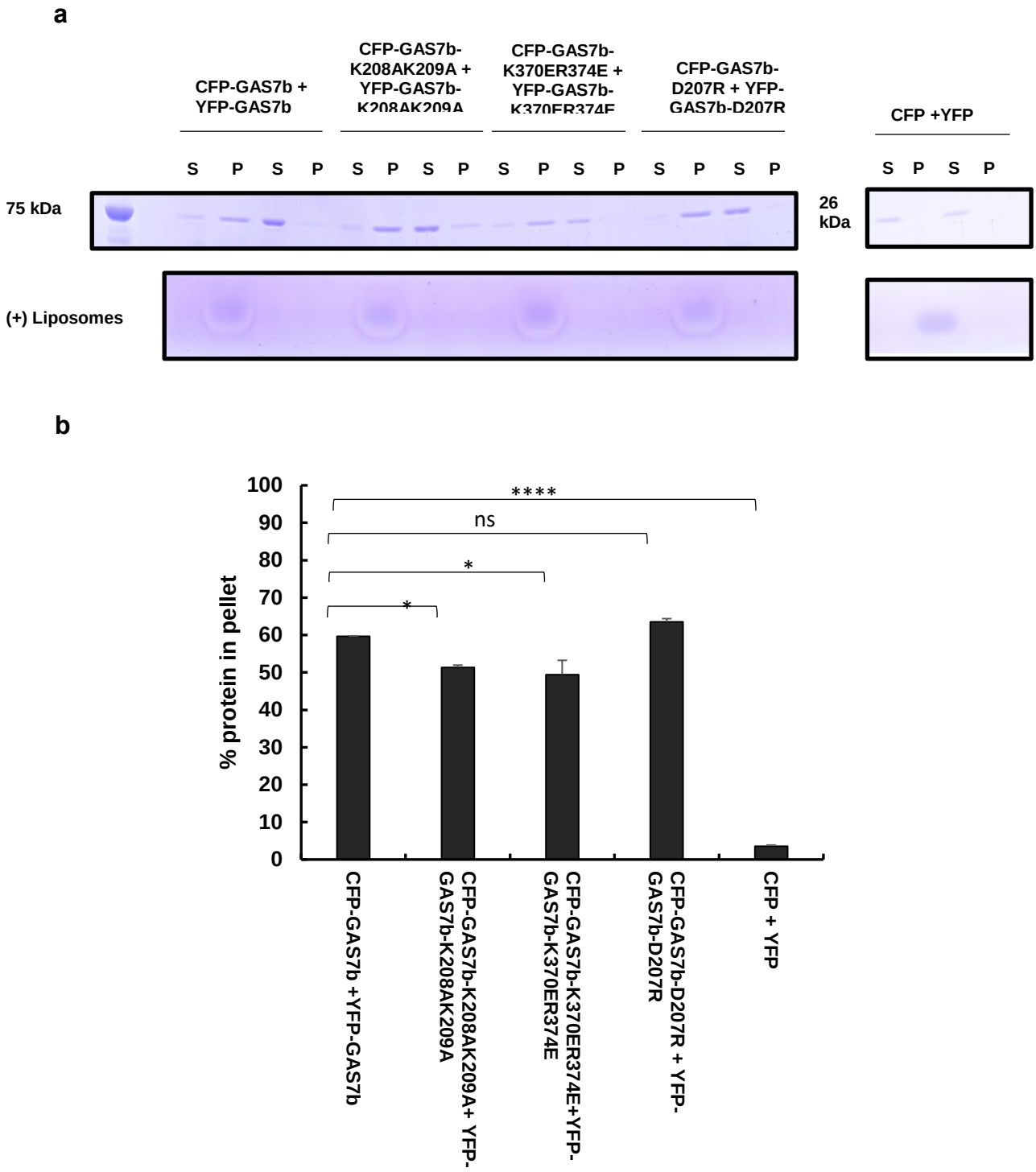

Figure 13: Liposome co-sedimentation assay for CFP or YFP tagged GAS7b. a) The SDS–PAGE of liposome co-sedimentation assay. b) Quantification of liposome co-sedimentation result presented in a. The concentration of tagged GAS7b, tagged GAS7b-D207R and tagged GAS7b-K208AK209A are 0.5 µM. The liposomes concentration is 0.5 mg/ml. Error bars: SD. The P-values were obtained by two-tailed Student's t-test. Two mutation are significant, $p<0.05$, against the positive control and D207R is not significant against the positive control. *$p<0.05$; ****$p<0.0001$, ns=not significant.

3.3 GAS7b on Giant Unilamellar Vesicle (GUV)

The Giant unilamellar vesicles were successfully produced by the natural swelling method using the buffer containing 300 mM sucrose, 10 mM Tris HCl pH 7.5, and 1 mM EDTA-Na pH 8.0, and the lipids composed of 20% POPC, 20% POPE, and 60% POPS. The swelling process was started with the hydration at 45°C for 10 minutes to develop giant unilamellar vesicle from a thin layer of lipid. By using fluorescence microscopy, the localization and binding of GAS7b on GUV can be observed. There was no fluorescence signal detected on GUV alone (Figure 14). In contrast, in the presence of CFP or YFP-GAS7b, the localization and binding of GAS7b with GUV can be detected on the surface of the GUV. This indicated that the binding between this GUV lipid membrane and GAS7b occurred. Hereafter, I have used all the GUV-liposomes in my experiments.

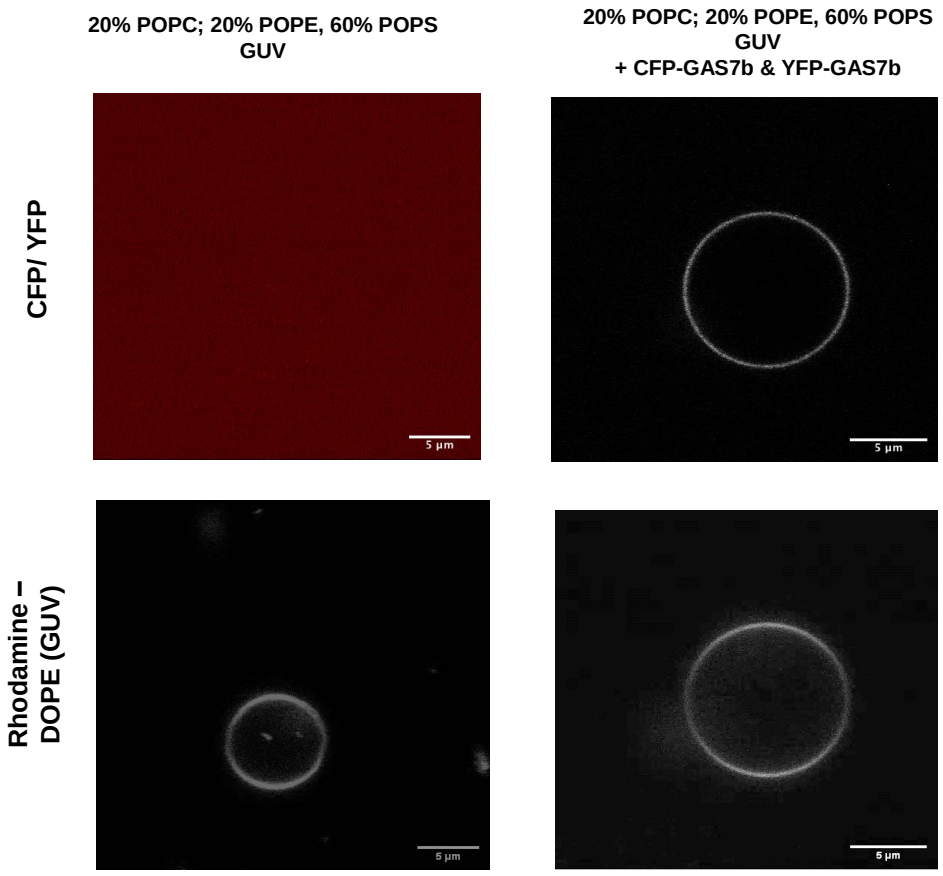

Figure 14: Giant unilamellar vesicles. This GUVs were incubated with 0.5 µM CFP-GAS7b + YFP-GAS7b and 20% POPC; 20% POPE; 60% POPS and rhodamine-DOPE. The liposomes concentration is 0.5 mg/ml. Scale bars = 5 µm.

3.4 Fluorescence resonance energy transfer (FRET)

FRET is a technique to detect the molecular interaction between proteins. In this analysis, several lipids concentrations have been used to determine the optimum FRET, which are the liposomes composed of 20% POPC, 20% POPE, and 60% POPS, having abundant POPS for the GAS7b binding. Besides, 45% POPC, 45% POPE, 10% POPS and 10% DGS-NTA, having the composition closer to the plasma membrane, with the NTA for anchoring the cytoplasmic region of the receptor, or the phosphoinositide-supplemented liposomes that are stated otherwise. All FRET experiments were conducted using a FP-6500 spectrofluorometer. Immediately prior to measurement in spectrofluorimetry, the proteins at the stated concentration was placed in micro quartz cuvettes. After 45 seconds of measurement, the GUV with 0.5 mg/ml or stated concentrations were injected using a glass syringe.

3.5 The optimum lipid and GAS7b protein concentrations

I have plotted the highest average FRET ratio in Figure 15b from the data in Figure 15a. The liposomes at total 0.5 mg/ml gave the optimum FRET for the liposomes composed of 20% POPC, 20% POPE, and 60% POPS. Then, I further continued to examine the different GAS7b concentration in a range of 0.1-1 μM to find the concentration of the GAS7b for the FRET to occur. The absolute value of each concentration is shown on Figure 15c. The concentration CFP or YFP tagged-GAS7b was 0.4 μM when the FRET ratio was maximum at the 0.5 mg/ml liposomes (Figure 15d). In this kinetics approached, I also calculated the half-time of GAS7b to reach maximum assembly, by fitting the data in Solver (Excel). The half-time to the FRET saturation in (Figure 15f) by fitting the data from Figure 15e. The results showed that the half-time become faster as the concentration of GAS7b increased. At 1 μM GAS7b, the half-time was 1.4 seconds. Interestingly, all the concentrations showed the half-time less than 12 seconds.

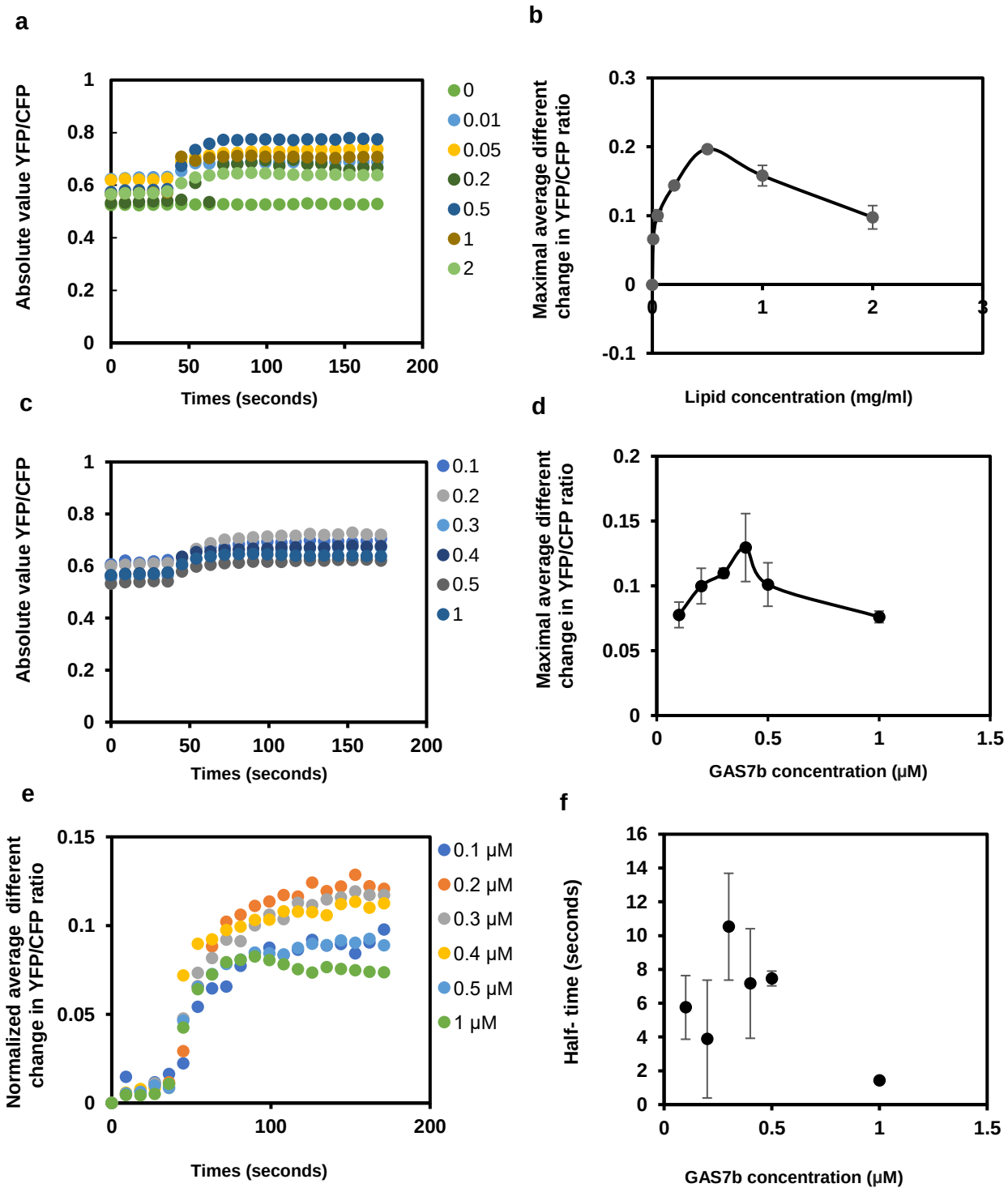

Figure 15: GAS7b binding affinity. a) The absolute value of highest average FRET ratio for b. b) FRET analysis of different concentration of PO lipids. c) Absolute value of YFP/CFP. d) The highest average FRET ratio that was minus with the first reading in absolute value c. e) The average FRET ratio of several concentration of GAS7b (0.1, 0.2, 0.3, 0.4, 0.5, 1 µM). f) Half-time of GAS7b based on the different concentration with 0.5 mg/ml PO lipids. From the curve fitting, the half-time show that 0.1 µM =5.7 s, 0.2 µM =3.8 s, 0.3 µM =10.5 s, 0.4 µM =7.1 s, 0.5 µM =7.4 s and 1 µM =1.4 s. The liposomes concentration is 0.5 mg/ml. Error bars: SD.

3.6 The FRET by mutant GAS7b proteins

I have also examined the FRET analysis of the GAS7b-mutants. The protein and lipid were used in this analysis were at 0.5 μM protein with 0.5 mg/ml of 20% POPC 20% POPE 60% POPS lipids. The FRET ratio for WT was rapidly increased when the liposomes were added. For both the mutants GAS7b-K208AK209A and GAS7b-K370ER374E, the normalized average of the FRET was reduced. This result clarifies that both of these point mutations involved in the interactions within dimers and interactions with the membrane affected the FRET, i.e., the protein assembly of the GAS7b.

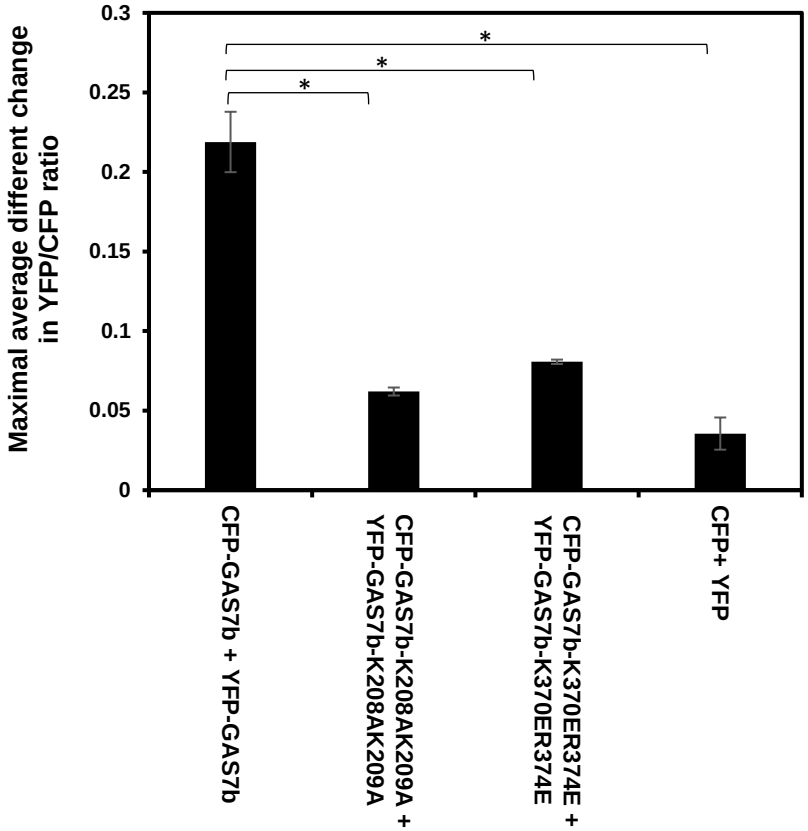

Figure 16: FRET analysis. a) Maximal average different change in YFP/CFP ratio of tagged-GAS7b and mutants upon membrane stimulation. For each trial, the fluorescence emission spectrum was acquired first at 433 nm excitation (450–550 nm emission). Additional controls were also conducted to measure CFP and YFP, n=2. The concentration of tagged GAS7b, tagged GAS7b-GAS7b-K208AK209A, tagged K370ER374E and CFP+YFP are 0.5 μM. The liposomes concentration is 0.5 mg/ml.Error bars: SD. The P-values were obtained by two-tailed Student's t-test. Two mutation are significant, $p<0.05$, against the positive control. *$p<0.05$.

3.7 The FRET dependently on the lipid binding

In order to mimic the PS composition in the plasma membrane, I tested the liposomes with a reduced percentage of POPS. Here, I used the liposome compositions, where the percentages of PS were 60% and 0%. Remarkably, the FRET analysis and liposome co-sedimentation assay is correlated (Fig 17a and b). The 10% PS liposomes exhibited the intermediate binding between 60% and 0% PS (Figure 17b and c). Even though 60% is the highest binding of PS with GAS7b, I had further my experiments with 10% PS to keep the PS percentage similar in the cells.

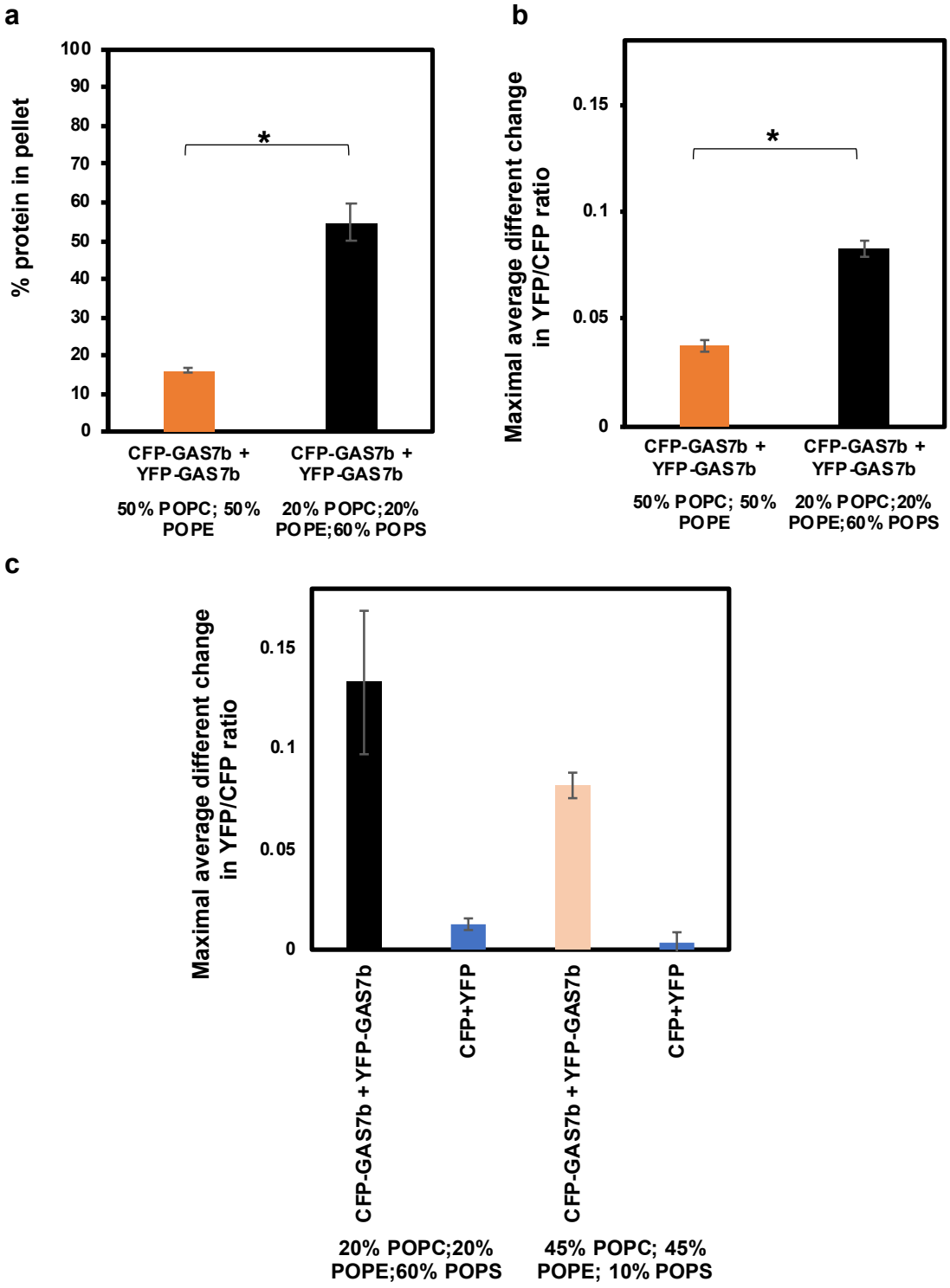

Figure 17: Phosphatidylserine affects the GAS7b binding. a) Liposome co sedimentation assay of percentage protein in pellet by 0.5 µM. CFP or YFP-GAS7b with 0% PS and 60% PS liposomes. b) FRET analysis of 0.5 µM CFP or YFP-GAS7b with 0% PS and 60% PS liposomes. c) FRET analysis of 60% PS and 10% PS liposomes. The liposomes concentration is 0.5 mg/ml. Error bars: SD. The P-values were obtained by two-tailed Student's t-test. *p<0.05

3.8 Optimum CFP to YFP ratio for the FRET of GAS7b

The ratio of CFP and YFP also was thought to affect FRET efficiency. Hence, the 1:1 to 1:10 ratios between CFP-GAS7b and YFP-GAS7b in 60% PS and 10% PS were examined (Figure 18). The results have shown 1:4 or 1:6 of CFP-GAS7b: YFP-GAS7b ratio was the best for 60% PS. However, as I will keep the 10% PS in my reconstituted liposome, I have compared the ratio of 1 CFP-GAS7b: 6 YFP-GAS7b in the presence of the 60% PS and 10% PS (Figure 18c). The results showed that in 10% PS, the 1:6 ratio seems to be similar trends in 60% PS. Hence, 1:6 of CFP-GAS7b: YFP-GAS7b ratio in 10% PS was used hereafter in the FRET analysis of the effect of the binding proteins of GAS7b on the FRET. Considering the plausible configuration of GAS7b in Figure 9a adapted from Figure 4a, in Hanawa Suetsugu et al (42), the ratio of 1:6 would maximize the FRET efficiency between CFP-GAS7b to YFP-GAS7b.

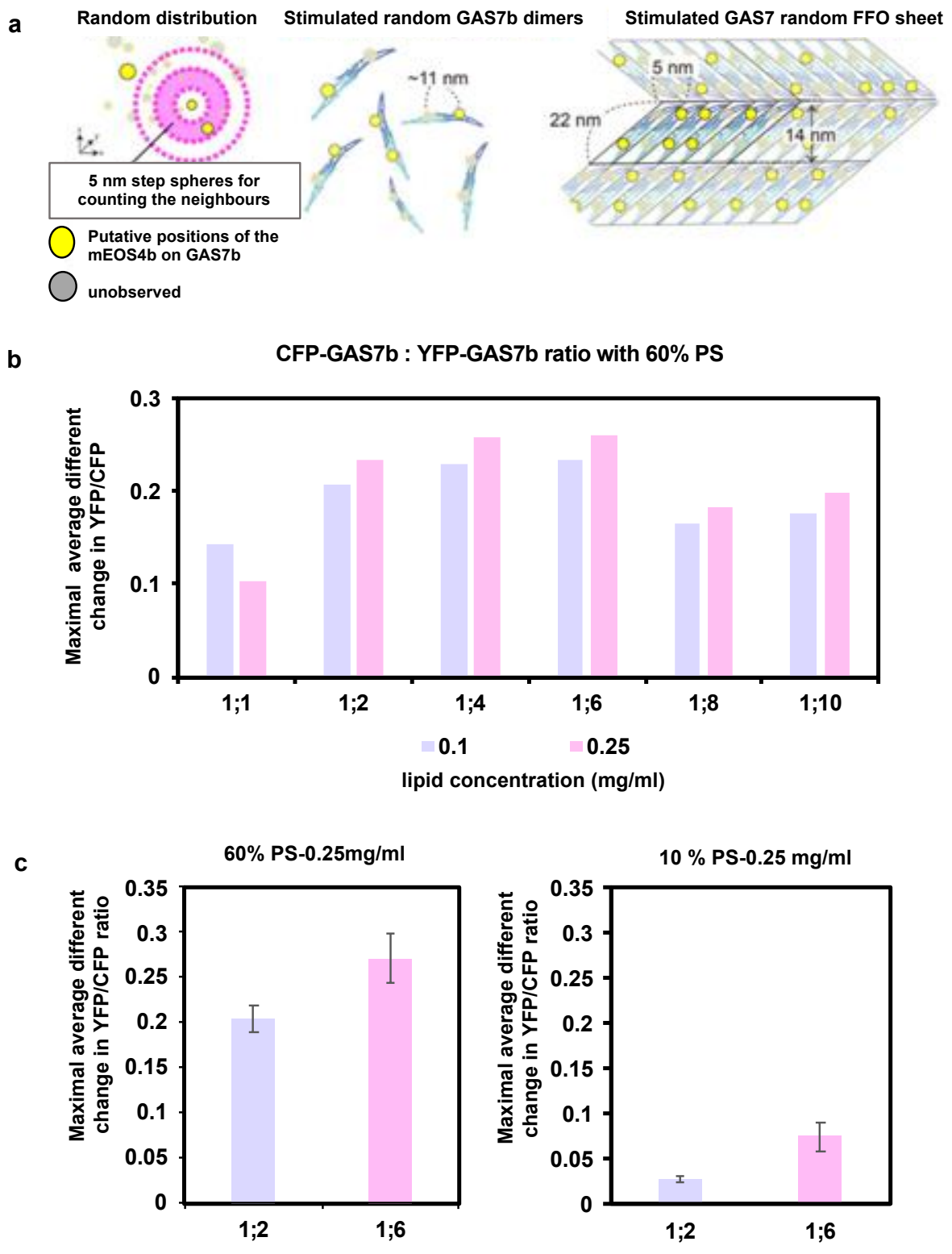

Figure 18: 1: 6 is suitable ratio for CFP-GAS7b: YFP-GAS7b in vitro. a) Illustration of the possible spatial distribution of GAS7 adapted from Figure 4a, Hanawa Suetsugu et al (42). b) Maximal average different change in YFP/CFP ratio of 0.1 mg/ml and 0.25 mg/ml in range 1;1 to 1;10 of CFP-GAS7b: YFP-GAS7b ratio. 1:8 and 1:10 is consider as saturated binding. c) The different between 60% PS and 10% PS for 1;2 and 1:6 ratio. Final concentration of CFP-GAS7b+YFP-GAS7b is 1 µM.

3.9 Multivalent interaction by N-WASP, Nck, and WISH increased the FRET

As for this analysis, the first question arises whether the GAS7b is engaged together or not with GAS7 binding proteins. The previous study reported the actin binding protein, especially, N-WASP involved in regulated phagocytosis cascade (31). This interaction might be the possible multivalent interaction since GAS7b also essential in mediated phagocytosis cascade and bind to N-WASP. To ascertain if the GAS7b can interact with other adaptors proteins, I have further evaluated GAS7b interaction in multivalent interaction contexts. I have introduced other potential proteins in this experimental design, including Nck, Grb2, and WISH, because these proteins can bind to N-WASP and potentially link GAS7 to the receptor mediated signaling cascades.

Here, I try to resolve the GAS7b interaction with N-WASP and adaptor protein, Nck. In the presence of either N-WASP or Nck, GAS7b seems to recruit the N-WASP and Nck to the membrane, because the maximum FRET was decreased in the presence of N-WASP and Nck (Figure 19b and c), as compared with CFP-GAS7b and YFP-GAS7b alone. In the presence of both proteins, Nck and N-WASP showed the reduction in FRET ratios (Figure 19d). The results might suggest that there is a missing protein that can help the GAS7b protein assembly.

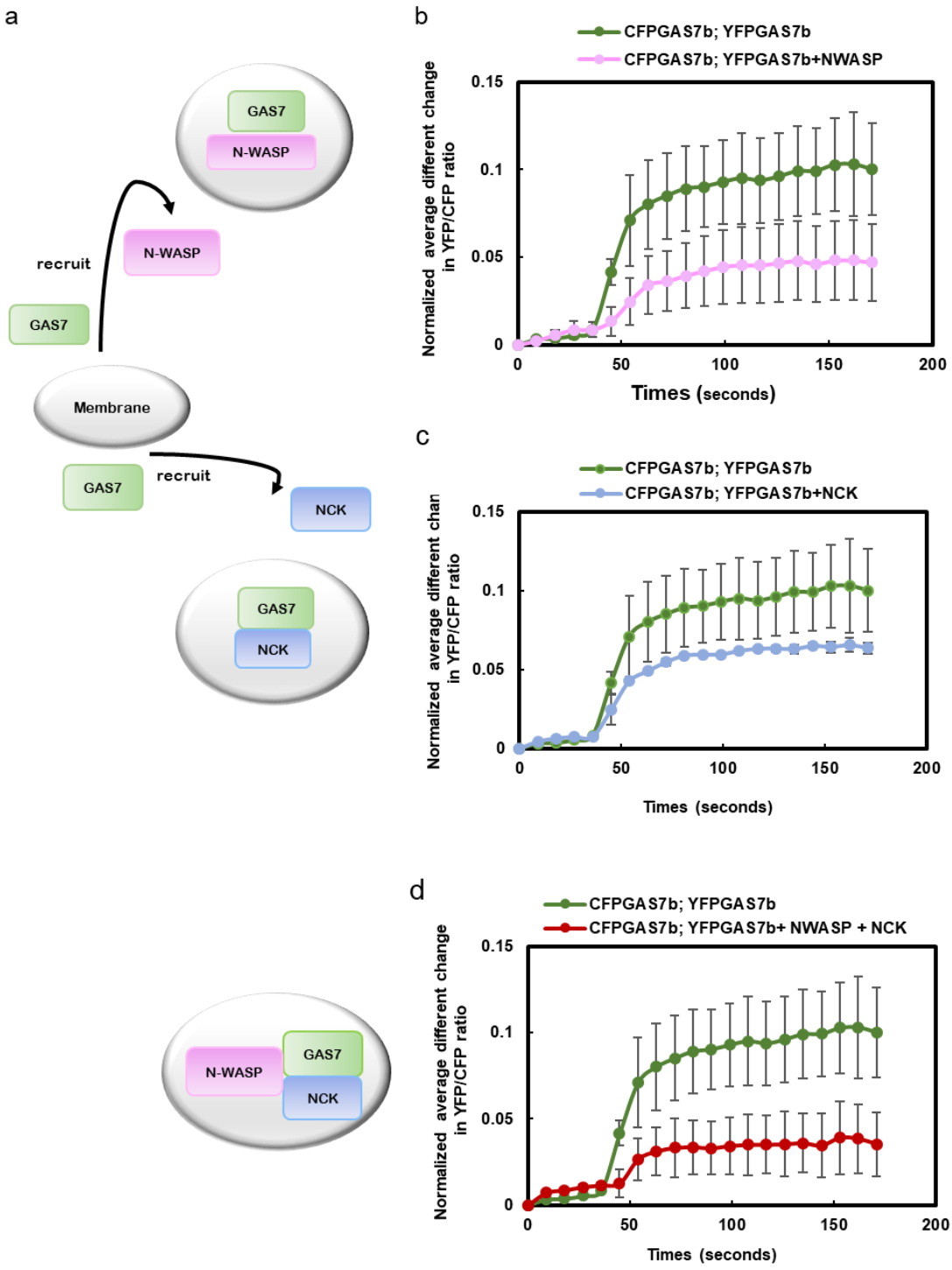

Figure 19: GAS7b assembly reduce in the present of N-WASP and Nck. a) Illustration how the GAS7b recruited N-WASP and Nck proteins. b) The graph of the recruitment of N-WASP to the membrane by GAS7b. c) The graph of the recruitment of Nck to the membrane by GAS7b. d) The reduction in normalized average FRET ratio in the presence of both N-WASP and Nck. The concentration of the proteins used here are 1 µM CFP-GAS7b + YFP-GAS7b, 0.5 µM N-WASP, 0.5 µM Nck. The liposomes concentration is 0.25 mg/ml.Error bars: SD.

With this missing link, the analysis in the human reference protein interactome mapping project (HuRI; http://www.interactome-atlas.org/) shows that GAS7 may also bind to WISH/NCKIPSD/DIP/SPIN90 protein. WISH contains the SH3 domain and interacts with N-WASP and Nck (19,89). Besides WISH, GAS7 also may interact with WDYHV1, YIF1A, CDC37, LSM4, and MCRS1 predicted in the HuRI (Figure 20a). WDYHV1 is a protein that mediates the protein degradation and lung cancer (90). Besides, YIF1A is a protein involved in the ER, Golgi, and the plasma membrane trafficking (91). The CDC37 is a molecular chaperon in complex with HSP90 and the kinases that controls the cell cycle control (92). In addition, LSM4 is a member of the LSm family of RNA-binding protein (93). MCRS1 is reported to be involved in FAS-independent death signaling in the nucleus (94). Hence, with this knowledge GAS7 is suggested to bind WISH in complex with N-WASP and Nck. With this regards, I introduced WISH protein in the FRET systems (Figure 20). Interestingly, FRET analysis revealed that WISH protein further enhanced the FRET. This fascinating result suggested that, the assembly of protein to become more stable and can function properly as the multivalent interaction is complete.

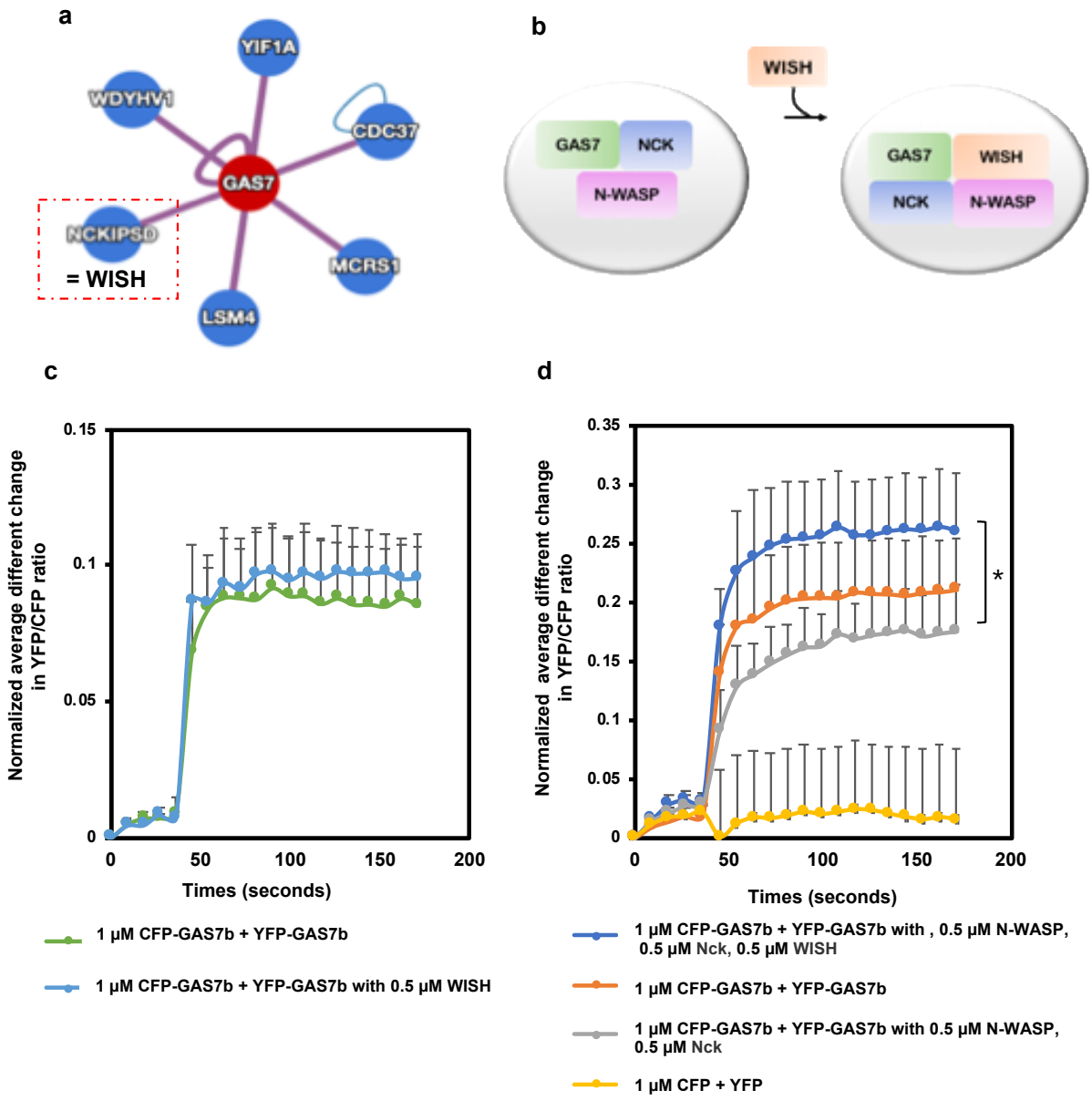

Figure 20: WISH protein linked all the protein assembly. a) Prediction of the GAS7 protein interaction with others protein predicted by HuRI website (http://www.interactome-atlas.org/search/GAS7#). b) Illustration of WISH can be the link for protein assembly.c) The CFP-GAS7b + YFP-GAS7b with WISH protein only. d) Maximum assembly of multicomplex protein was increase in the presence of 0.5 µM WISH protein. The protein concentration used here are 1 µM CFP-GAS7b + YFP-GAS7b, 0.5 µM N-WASP, 0.5 µM Nck and 0.5 µM WISH. The liposomes concentration is 0.25 mg/ml. Error bars: SD. The P-values were obtained by two-tailed Student's t-test. All the significant value is, $p<0.05$, against the positive control. *$p<0.05$.

3.10 Nck served as hub in this multicomplex interaction

There is an interpretive question in which adaptors protein that works together with GAS7b-N-WASP-WISH. Grb2/Ash is another major adaptor protein that interacts with N-WASP (95). Grb2 did not induce the FRET as high as Nck did (Figure 21b). This result might suggest that three SH3 domain is required for this multicomplex assembly. As WISH and N-WASP are known to bind to overlapping but distinct SH3 domains of Nck (89), this result indicates that each protein has different dynamics properties in recognizing the binding site for multivalent assembly.

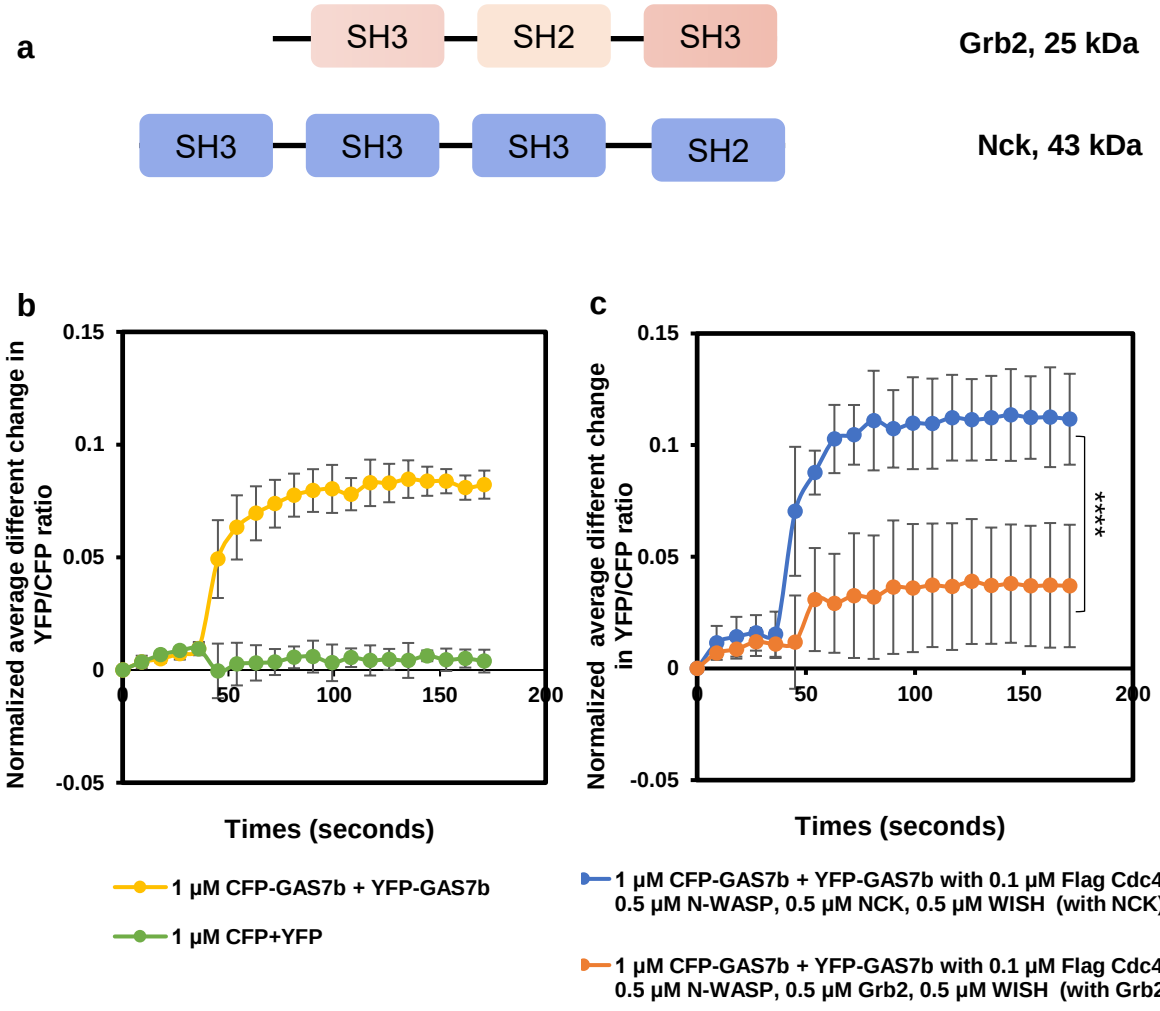

Figure 21: Nck, not Grb2 served as hub in this multicomplex interaction. a) Schematics domain of Grb2 and Nck. b) The 1 μM CFP-GAS7b + YFP-GAS7b alone without others protein. c) The comparison of Grb2 (orange line) or Nck (blue line) in normalized average different change in YFP/CFP ratio in present of 0.5 μM N-WASP, 0.5 μM WISH. The liposomes concentration is 0.25 mg/ml. Error bars: SD. The P-values were obtained by two-tailed Student's t-test. All the significant value is, $p<0.05$, against the positive control. **** $p<0.0001$.

3.11 The active form of Cdc42 increased the FRET

Cdc42 is known as a key regulator in actin dynamics and binds to N-WASP (20). Thus, I have continued my analysis in FRET by incorporating the Cdc42 purified from HEK 293 cell. After 2 days of transfection, the proteins were collected, purified using FLAG agarose beads and included in the FRET analysis. The presence of the active form of Cdc42, significantly enhanced the FRET (Figure 22a). The GDP-Cdc42 (the inactive form of Cdc42) is the negative control for this measurement (orange line).

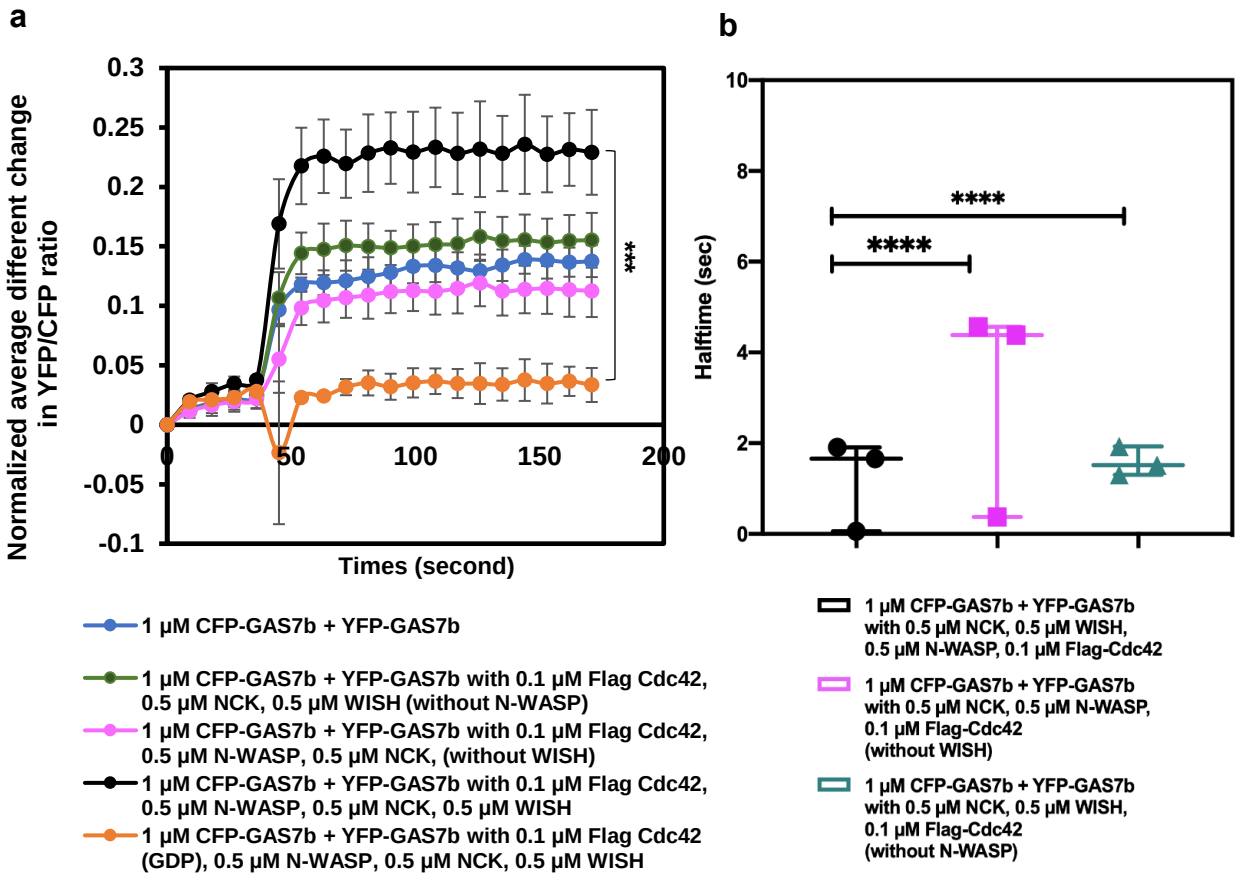

Figure 22: Cdc42 regulate the protein-protein assemble at membrane. a) FRET of 1 µM CFP-GAS7b+YFP-GAS7b with 0.5 µM Nck, 0.5 µM N-WASP, 0.5 µM WISH, and 0.1 µM Cdc42(GTPγS) have increase the normalized average different change in YFP/CFP ratio. b) Half-time of 1 µM CFP-GAS7b+YFP-GAS7b with 0.5 µM Nck, 0.5 µM N-WASP, 0.5 µM WISH, and 0.1 µM Cdc42 (GTPγS). The liposomes concentration is 0.25 mg/ml. Error bars: SD. The P-values were obtained by two-tailed Student's t-test. All the significant value is, $p<0.05$, against the positive control. ***$p<0.001$, **** $p<0.0001$.

The roles of Cdc42 as a key regulator in this multicomplex assembly is showed as the FRET ratio is the highest (Figure 22b-black line) compared with in presence of GDP-Cdc42 (inactive form), owing to the previous report that Cdc42 essentials in lipidation process. The half-time also showed that in the presence of GAS7b with active form of Cdc42, together with multicomplex proteins, the half-time is 1.209 seconds.

3.12 The membrane anchored phosphorylated receptor further increased the FRET in comparison with mutants and phosphoinositides

I next sought to investigate whether this assembly is not only related with Cdc42, but also correlated with the phosphorylation effect from ITAM peptide, by referring the signaling cascade in the phagocytosis. Therefore, I have extended my experiments with the analysis related with the Src kinase and ITAM peptide (FcγRIIa) with His-tag for the tethering into the liposomes containing NI-Nitrilotriacetic acid (NTA). In this experimental design, the liposomes compositions are 45% POPC; 45% POPE; 10% POPS and 10% DGS-NTA. In this composition, the His-tagged protein is expected to bind to DGS-NTA liposome. As a result, I have observed that the half-time to reach maximum assembly was faster with Src kinase and FcγRIIa signalling, indicating that the protein-protein assembly has been further increased. The maximums intensity of FRET analysis increased in the presence of the molecular scaffolds, including N-WASP, Nck, and WISH, and it was further enhanced by the presence of an active form of Cdc42. Moreover, Src and FcγRIIa mediated more assembly, reaching approximately 50% FRET efficiency (Figure 23a; green line). The half-time of the protein-protein assembly quantitatively showed the fastest of the assembly rate by the presence of these N-WASP, Nck, WISH, Cdc42, Src, and FcγRIIa (Figure 23b; green line).

In contrast, in the presence of Src and FcγRIIa, all the mutants with multicomplex proteins, including the membrane-binding deficient mutant of GAS7b such as CFP or YFP tagged lys208AK209Arg, CFP or YFP tagged Lys370GluArg374Glu, CFP or YFP tagged WW Tyr65Cys GAS7b, as well as the SH3 domain mutant of WISH, WISH Tyr52Ala have a reduction in FRET ratio when compared with WT with multicomplex proteins (Fig 23b). The half-time also show the slower to reach maximum assembly compared with WT (Fig 23b). Therefore, this suggesting the defect in this multicomplex assembly. However, the mechanism behind this assembly remains unclear, to date.

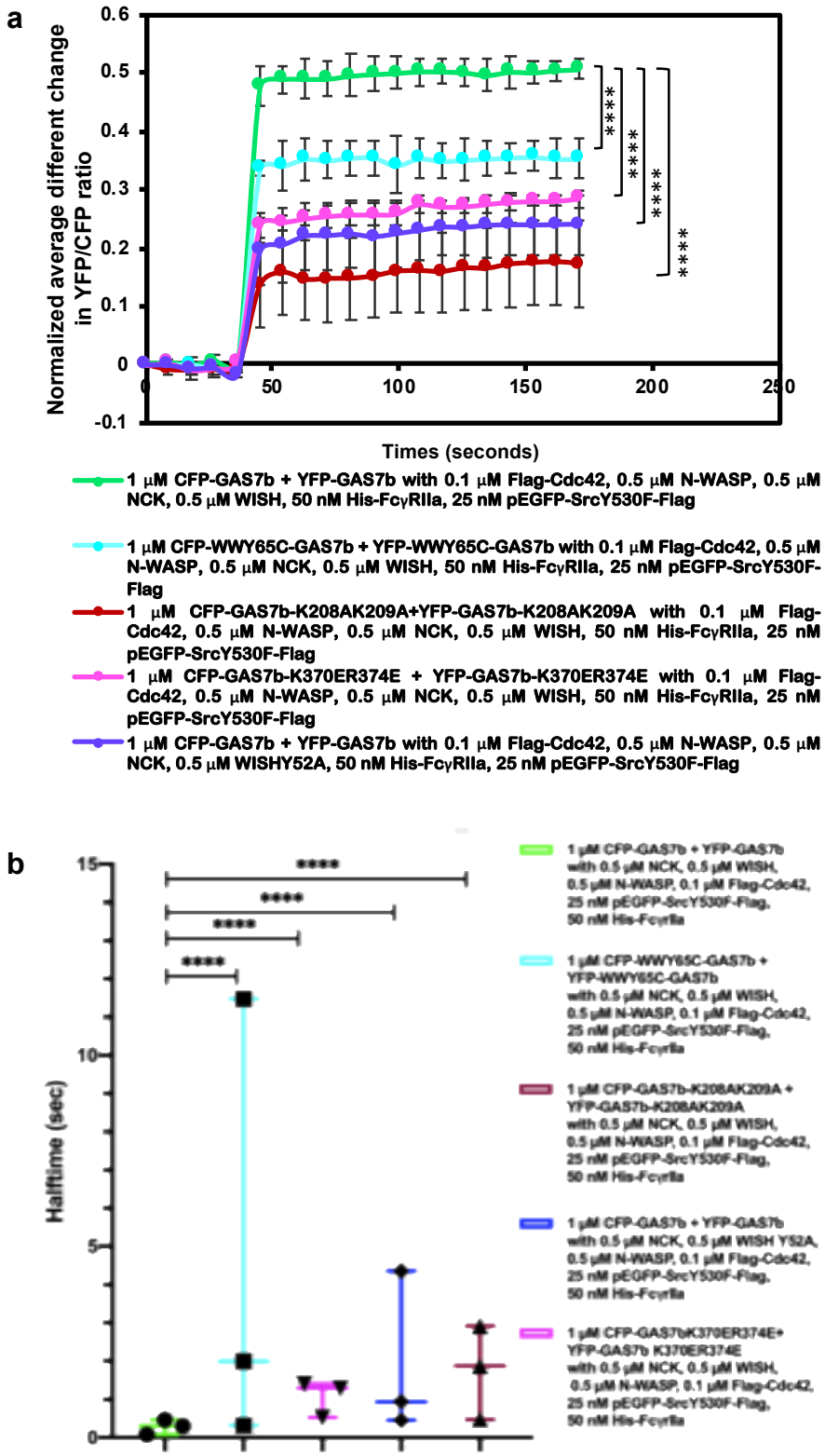

Figure 23: Src and FcγRII escalate the protein complex assembly. a) Normalized average different change in YFP/CFP ratio of Src and FcγRIIa with all multicomplex protein. b) Half-time of 1 µM CFP-GAS7b+YFP-GAS7b with 0.5 µM Nck, 0.5 µM N-WASP, 0.5 µM WISH, 0.1 µM Cdc42 (GTPγS), 25 nM pEGFP-SrcY530F-Flag, 50 nM His-FcγRIIa. The liposomes concentration is 0.25 mg/ml. Error bars: SD. The P-values were obtained by two-tailed Student's t-test. All the significant value is, $p<0.05$, against the positive control. ****$p<0.0001$

Following, I have also studied about the phosphorylation of Src kinase and ITAM peptide (FcγRIIa) with the presence of 1 mM ATP and 1 mM ADP. In the presence of ATP, pEGFP-SrcY530F-Flag showed to phosphorylate His-FcγRIIa (Figure 24b).

In addition, phosphoinositide has been speculated to contribute in this multicomplex proteins assembly at membrane. Thus, I have extended my experiments to examine the FRET ratio of GAS7b and multicomplex proteins with the presence of the pEGFP-SrcY530F-Flag and the His-FcγRIIa with a different lipid composition. Here, I have compared the lipid composition between 5% PIP_2, 5% PIP_3 and 10% POPS. The results show that, multicomplex proteins with 5% PIP_2 have the highest FRET ratio in comparison to 5% PIP_3 and 10% PS. This outcome clarifies that PIP_2 signaling is essential to mediate the phagocytosis cascade. Nevertheless, there was also a significant increase between PIP_2 lipids when I compared the result between PIP_3 and PS lipids (Figure 24c).

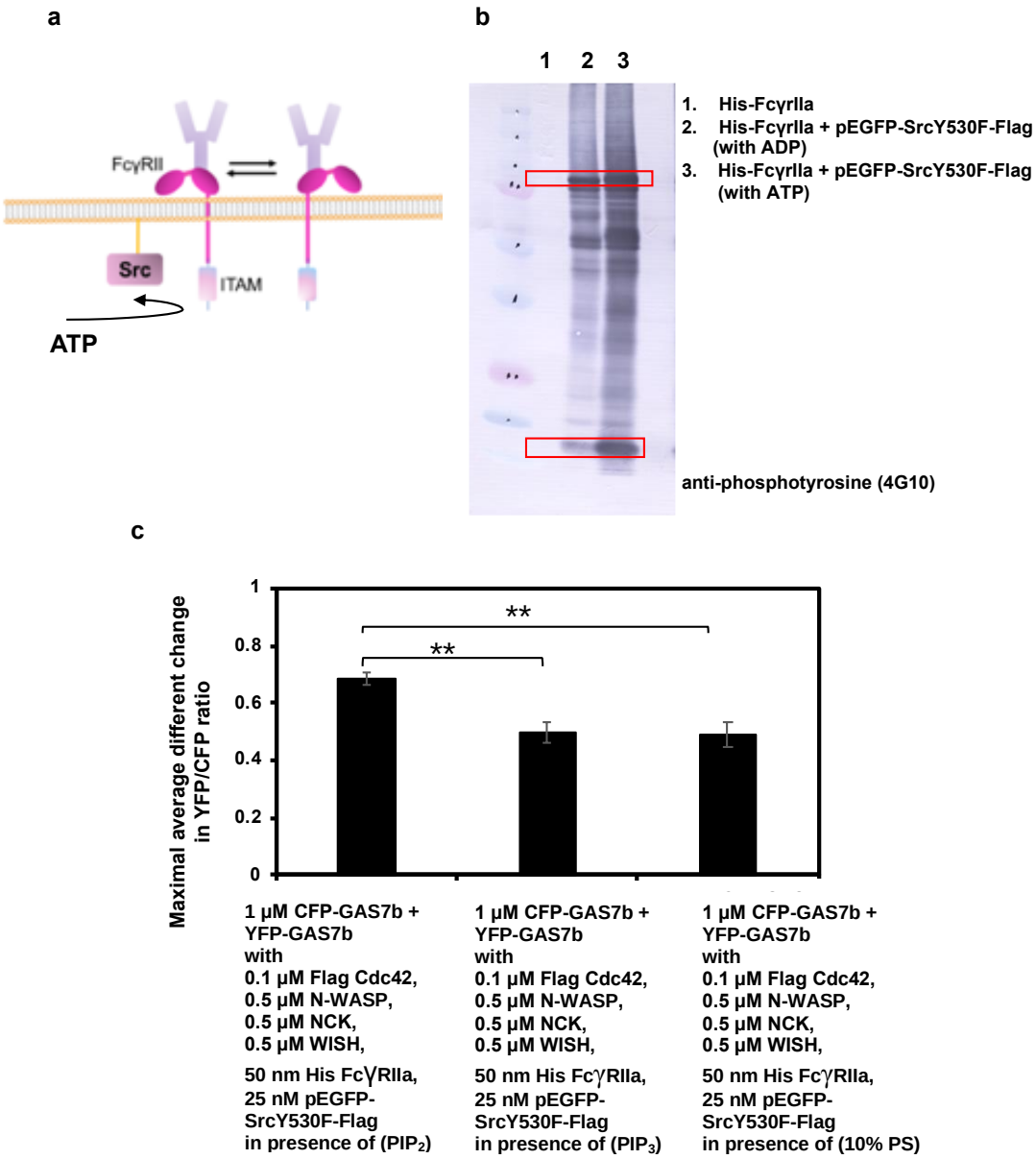

Figure 24: Phosphoinositides have different affinity of the GAS7b assembly. a) Illustration on Src kinase in the presence of ATP. b) Phosphorylation of 50 nM pEGFP-SrcY530F-Flag and 25 nM His-FcγRIIa in the presence of 1 mM ATP and 1 mM ADP. Red square represents molecular weight of pEGFP-SrcY530F-Flag (60kDa) and His-FcγRIIa (11 kDa) c) The effects of 5% PIP_2, 5% PIP_3 and 10% PS in the presence of ATP with multicomplex protein assembly at membrane, n=3. The liposomes concentration is 0.25 mg/ml. The P-values were obtained by two-tailed Student's t-test. **p<0.01.

3.13 Cdc42 and Src-dependent FRET of GAS7b in the cell

Finally, coupled with my in vitro results, I have intensified my hypothesis about whether these multicomplex proteins are cooperatively working together in the cellular experiments. In this cellular FRET experiments, RAW264.7 GAS7b-knockout cells expressing CFP-GAS7b and YFP-GAS7b-IRES-CFP-GAS7b were used for FLIM analysis. For the analysis, I have used the phasor program to examine a GAS7 lifetime (Figure 25). The phasor plot is a graphical analysis generated from FLIM intensity data. In phasor analysis, the software can generate the lifetime (ns) in each pixel in FLIM map to one dot at a universal circle. The fluorescence lifetime is referred to the average time between absorption and emission of light in excitation state, will become shorter if the molecules are closer to each other. The shorter lifetime will indicate that FRET has occurred.

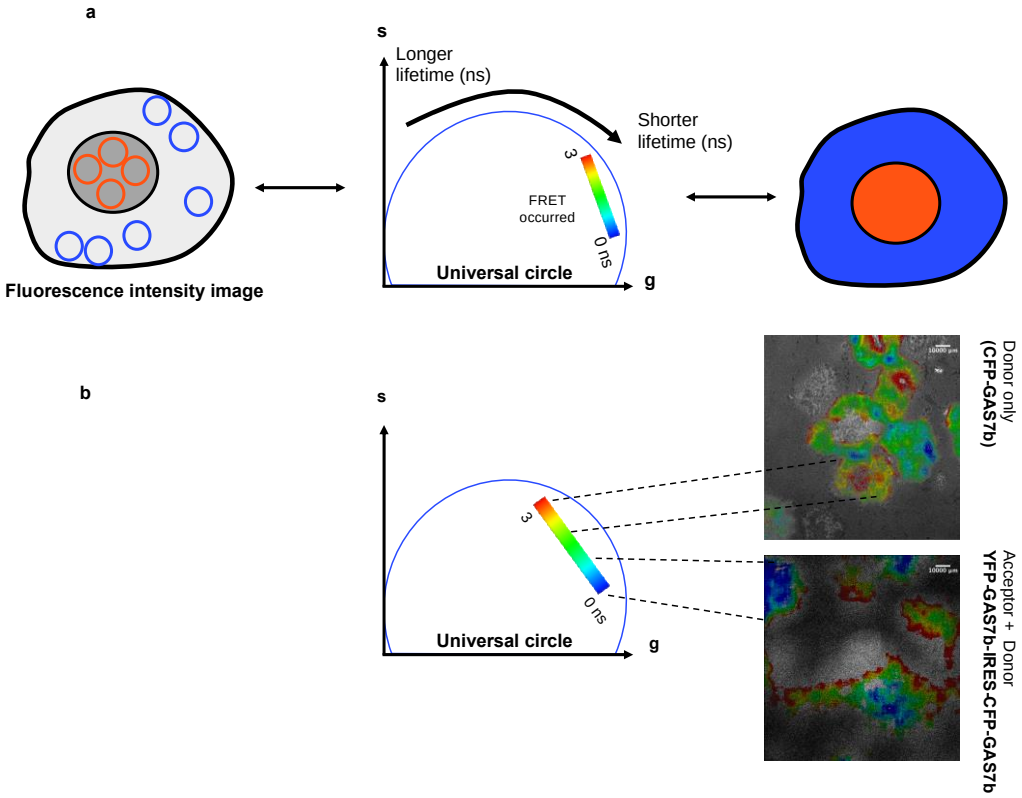

Figure 25: Illustration of phasor plot analysis. a) The phasor analysis will convert the fluorescence lifetime information from fluorescence intensity image to a phasor plot presented in the universal circle. The intensity image will then map into different place at a universal circle based on lifetime (ns) on phasor coordinates (g,s). Lastly, from the phasor's calculated lifetime, the phasor color mapped FLIM image can automatically be generated. The lifetimes would be shorter if the FRET occurred as the fluorophores are closed together. (Adapted and reconstituted from (87)). b) Representative image of donor group only and acceptor and donor group image. The warm colors represent longer lifetimes and cool colors represent shorter lifetimes as per color scale provided. Scale bars; 10 µm. Schematics not drawn to scale.

The lifetimes of YFP-GAS7b-IRES-CFP-GAS7b was significantly longer with the presence of Cdc42 inhibitor (ML141) and the Src inhibitor PP2 as examined by the phasor analysis. However, for the control CFP-GAS7b, the lifetimes are not significantly different between the non-treated and treated group (Figure 26c).

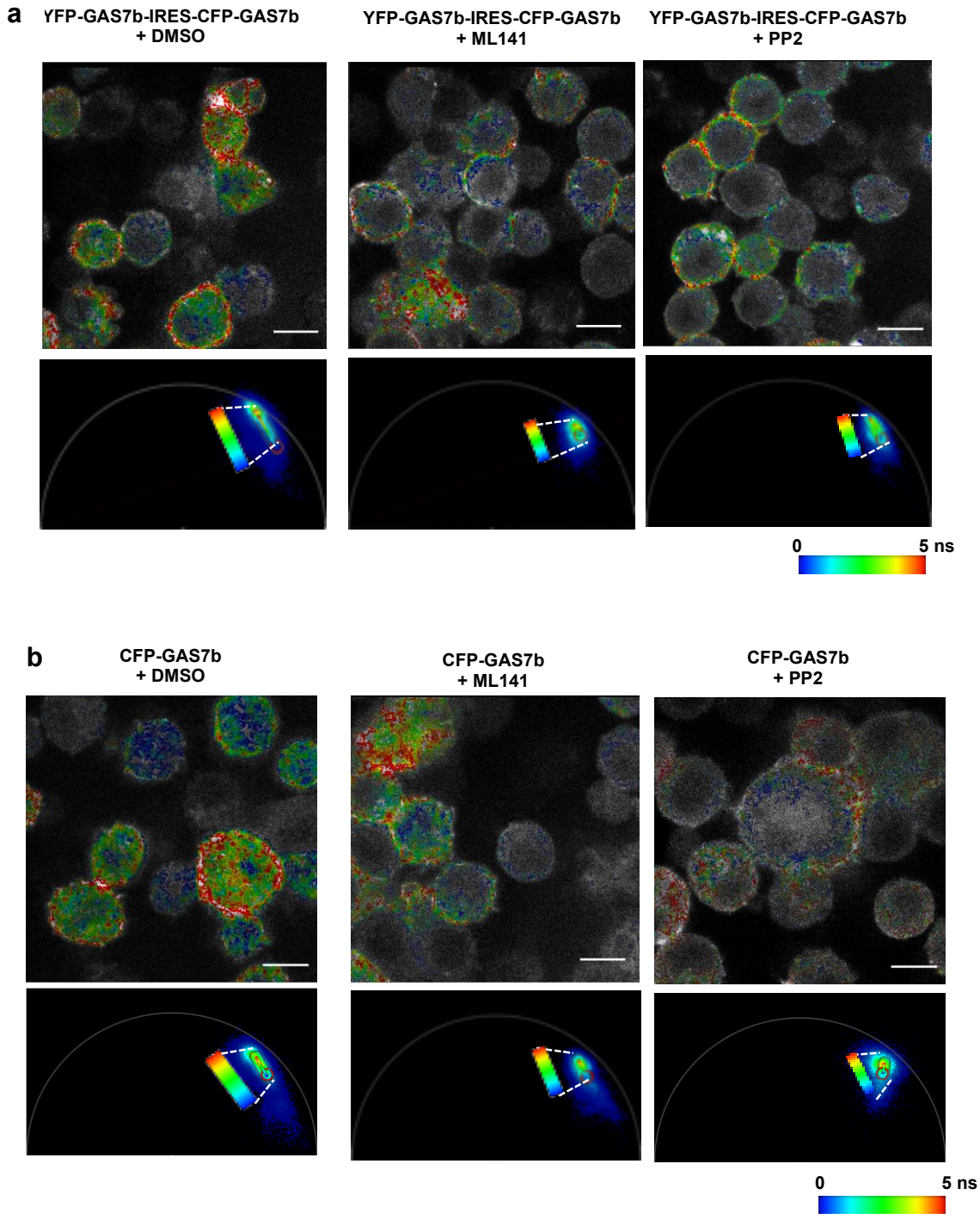

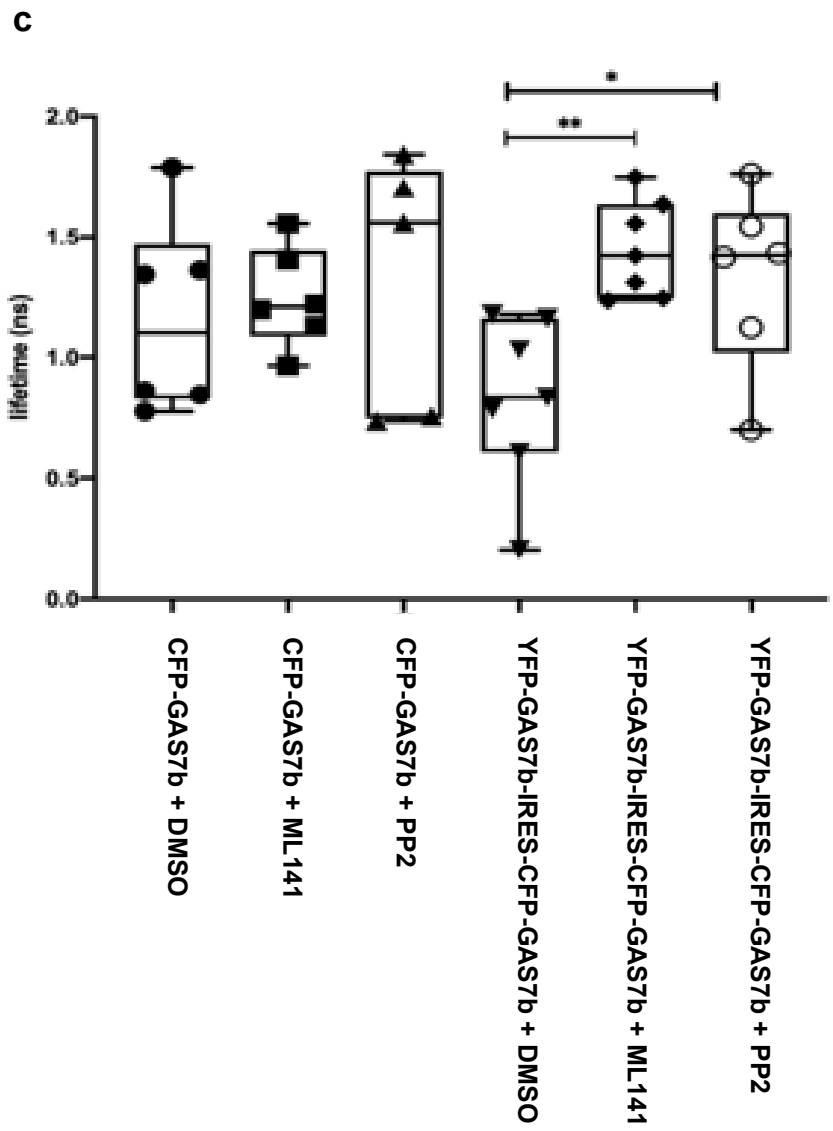

Figure 26: Phasor FLIM analysis of FRET in RAW 264.7. a) Upper; The representative intensity image of YFP-GAS7b-IRES-CFP-GAS7b treated with DMSO (control), 10 µM of ML141 (Cdc42 inhibitor) and 10 µM of PP2 (Src inhibitor). Lower; the universal circle that shows the lifetime in each group. b) Upper; The representative intensity image of CFP-GAS7b treated with DMSO (control), 10 µM of ML141 (Cdc42 inhibitor) and 10 µM of PP2 (Src inhibitor). Lower; the universal circle that shows the lifetime in each group. c) The quantification of the lifetime of CFP-GAS7b and YFP-GAS7b-IRES-CFP-GAS7b. The P-values were obtained by two-tailed Student's t-test. All the significant value is, $p<0.05$, against the positive control. Scale bars = 10 µm *$p<0.05$, **$p<0.01$.

4.0 Discussions

In this study, I focused on GAS7b that contains WW domain and F-BAR domain. Recently, we have revealed that GAS7b binds to the lipid membrane and also forms a sheet-like assembly on the crystals structure, reconstituted membrane, and mammalian cells (42). However, the kinetics and the regulation of GAS7b assembly into the tightly packed sheet on the lipid membrane is yet to be revealed. Thus, I have designed FRET based approaches to evaluate the time deployment of this interaction between GAS7b for its oligomeric assembly.

4.1 The liposome binding, the oligomerization, and the FRET

For the binding ability of these proteins, in vitro liposome co-sedimentation assays have been used to demonstrate the CFP or YFP-GAS7b and CFP or YFP-GAS7b mutants bind to liposomes. In this assay, the 0.5 μM proteins and 0.5 mg/ml liposomes were used. The binding of GAS7b with liposome was more than 50% for WT and 60% for Lys207Arg (Figure 11). Yet, there is no significant difference between Lys207Arg mutant and WT. The Lys207Arg mutation in the loops of GAS7b reduced the oligomer formation (42). I have also found that there is a significantly decrease in binding for mutation at another site of the loop, like Lys208AlaLys209Ala (Figure 11d). The result show as reducing the negative charge of the amino acid site that contributed to the binding, the binding will be decreased. In comparison with mutants in the loops of GAS7, I, therefore introduced one more mutated the site at the end of F-BAR, Lys370GluArg374Glu, which was believed to contribute to the binding of the GAS7 with membrane. As expected, the liposome co-sedimentation assay also showed a reduction in binding for this tagged mutation (Figure 13b). In line with this, this mutant also had a reduction in FRET, suggesting that the binding and the FRET is in proportional relationships (Figure 13 and 16 respectively).

Phosphatidylserines (PS) is the lipids that accumulate at the plasma membrane that represent 10% of the phospholipids (37). Thus, 10% PS have been used in this study to mimic this cell percentage. Intriguingly, the binding ability of GAS7b also reduced when I reduce the negativity of liposome composition to 50% POPC: 50% POPE (= 0%PS) (Figure 17). Correlated with this result, by FRET analysis, in the 10% PS, the binding of GAS7b also reduced when compared with 60% PS (Figure 17). Though the binding reduced in 10% PS, this results enough to signifies that GAS7b bind to the membrane by electrostatic binding.

I have expected that the oligomer formation of GAS7b on the membrane can be observed by FRET, resolving the kinetics for the oligomeric assembly of GAS7b on the membrane. In FRET analysis, the detection of YFP fluorescence emission upon CFP excitation indicates that FRET occurs between the CFP and YFP. This result from their distance of interaction that has proximity (<10 nm). By using FRET analysis, I have revealed that have 1:6 ratio of CFP-GAS7b: YFP-GAS7b is the best ratio to evaluate kinetics of GAS7b (Figure 18) and multivalent protein interaction study. Furthermore, the 1:6 ratio of CFP-GAS7b: YFP-GAS7b looks to be compatible with the sheet model of the GAS7 assembly in introduction section on Figure 8c and d. This ratio also reflected the probability of random orientation of CFP and YFP in solution which correlates spatial orientation of GAS7 reported in Figure 4a in Hanawa Suetsugu et al. (42), which adapted to my (Figure 18a).

4.2 The rapid kinetics of FRET indicative of very rapid GAS7b assembly

With the increased of the concentration of GAS7b, high order oligomerization starts to decrease (Figure 15d). Couple with this, GAS7b shows an increase in the assembly when in contact with liposomes in different concentration; from 0.1 to 1 μM (Figure 15e). I have speculated that this sharp increase might result from how fast the GAS7b can contact the membrane. These behaviors suggested the GAS7b concentration was too high to interact with the membrane above 0.5 μM at 0.5 mg/ml lipid liposomes, which contained ~500 μM lipid molecules. Because 5×10^6 lipid molecules in a 1 μm^2 and the GAS7b protein area on the membrane per a dimer is ~5 nm × 20 nm = 0.1 μm^2 (illustration about size of GAS7 on Figure 18a). The results have explained by the saturation of the binding have been occurred. There appeared to be no lag time or no critical concentrations for the FRET to occur at the concentrations I examined, which would be reasonable because the Kd between GAS7b and these liposomes was 0.02 μM (Figure 12). Subsequently, I also calculated the Kd of tagged GAS7b in several concentrations; from 0.1 to 0.5 μM (Figure 27), to compare with non-tagged Kd of GAS7b (Figure 12). Interestingly with this regard, the Kd for tagged GAS7b was 0.03 μM. The result likely to rationale my findings that the CFP and YFP tagged might not affect the binding of GAS7b to the liposomes, though it is still unclear how the CFP and YFP size might disrupt the GAS7b assembly. The maximum binding of tagged GAS7b seems to be lowered than non-tagged GAS7b because the CFP and YFP tagged have high solubility in solution. Besides, I also cannot rule out the binding ability of GAS7b to liposomes in the presence of phosphoinositide and different percentage of PS.

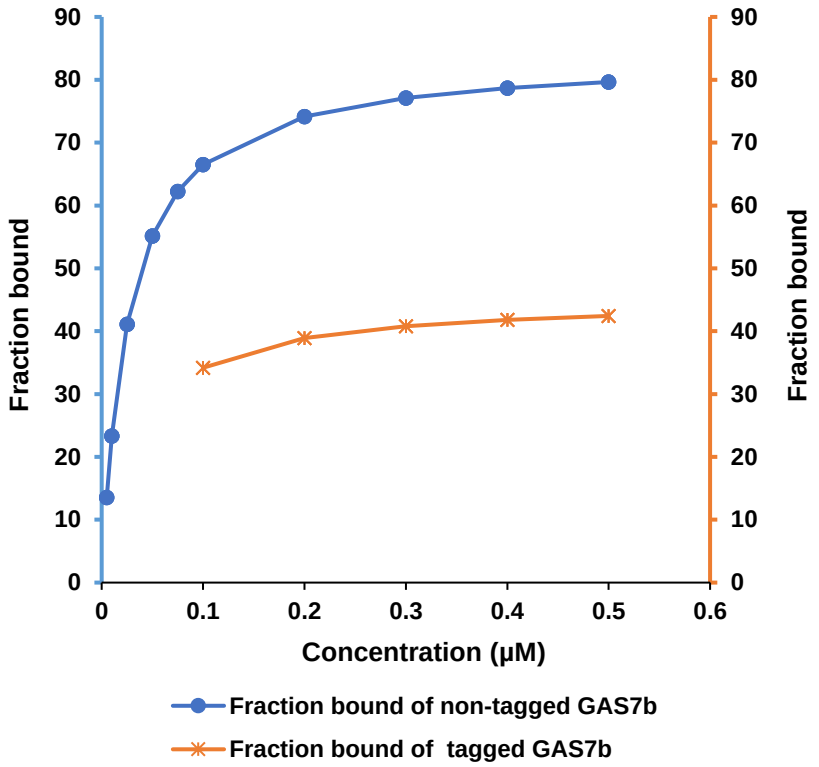

	non-tagged GAS7b	tagged GAS7b
Kd(μM)	0.02	0.03
Liposomes compositions	20% POPC: 20% POPE: 60% POPS	45% POPC: 45% POPE: 10% POPS: 5% PIP_2

Figure 27: The Kd of the non-tagged GAS7b and the tagged GAS7b. For non-tagged GAS7b, the fraction bound was measured by liposome co-sedimentation assay with non-tagged GAS7b (n=3), while for tagged GAS7b, the fraction bound was measured by liposome co-sedimentation assay with CFP-GAS7b+YFP-GAS7b (n=3). Both analyses were fitting in the Excel, by solver software to calculate the Kd.

As rudimentary as it may seem, the oligomerization of CFP-GAS7b and YFP-GAS7b can reach maximum assembly in less than 200 seconds in FRET analysis (Figure 15e). This reflects how fast the signal comes from the receptor to downstream component to act cooperatively against foreign pathogens. This is also reported by (96) in the mechanism of phagocytosis, the engulfment of pathogens, or movement of the cell to protect from foreign particles begins at 10 seconds and is completely engulfed by 46 seconds in theirs model. Concomitant with this, my result also shows a rapid increase in oligomerization formation as from the introduction of the lipid membrane to GAS7b with the increase of time. This reaction was taken in 50 seconds and started to flatten the graph. Along these lines, I truly believed that GAS7b moves around 50 seconds and assembly with other essentials proteins at the membrane for the invagination process of phagocytosis with the lipid protein ratio is 1:1.

4.3 The comparison with other F-BARs

With the rapid formation of oligomerization that occurred when liposome was added (Figure 15e and Figure 16) even at different percentage of PS (Figure 17b and c), this rationalized that the oligomerization of GAS7b forms on the membrane. As GAS7b is more unlikely to have binding by the insertion of the loops, but prefers to interact with the nearest dimer of the F-BAR domain, in that event, I speculated that GAS7b can assemble or oligomerize first without deforming the membrane. With a shallow concave structure, this probably explain why GAS7b have recognize the flat membrane rather than shaping the membrane (42). This also happened with the mammalian FCHSD2 proteins, that has shallow proteins curvature, localized also at flat membrane during endocytosis (75). Together with this, I speculated that the modes of oligomerization are also depended on protein structure. As most F-BAR superfamily proteins involved in invagination of the membrane, McDonald and Gould has also discussed that membrane shaping do not depend on the oligomerization of protein (85). Correspondingly, there is a similar evidence from the previous report that revealed the tetramer formation of the BAR domain in SNX-BAR is not compulsory in the lipid binding and membrane deformation (97). In such a way, concurrent with this evidence, the oligomer state of GAS7 (like dimer, tetramer and oligomer) are not considered as a prerequisite phase before the binding to lipid, but more to dimer-dimer interaction would occur on the 2D membrane surface, where the chance of the protein interactions apparently abundant than in the 3D solution. However, in order to prove this oligomerization state changing, EM study like Sun and his groups did (97), should be conducted to clarify more about this oligomerization phase.

4.4 The role of signaling proteins in the GAS7 assembly

In the presence of GAS7b-N-WASP-Nck in the FRET systems, FRET ratio seems reduced (Figure 19c), suggesting that other proteins might be the potential link in this oligomer assembly. This result was supported by analysis in the HuRI, which showed GAS7 can also bind with WISH protein (Figure 20a). Remarkably, as expected, by introducing WISH protein in the FRET system, the maximum assembly was increase (Figure 20c). WISH protein also consists of PPXY motif that located on SH3 domain that previous reported to bind with WW domain. To test this hypothesis, I have mutated Y52A in WISH protein (in PPXY motif), to inhibit the binding to WW domain of GAS7. From this experiment, I have observed that, the normalized average different change in FRET ratio is reduced. The slightly reduction in FRET shows that the protein-protein interaction still can be occurred. These results suggested that

GAS7b would have strong multivalent interaction with WISH protein (Figure 28c). Coupled with this, pull-down assay between WISH and GAS7b also showing that WISH also can bind to F-BAR domain of GAS7 (unpublished data). As, this results consistence between FRET analysis and pull-down assay, I cannot rule out the facts that there are multiple binding sites between this interaction. Hence, there might be others mutation site should be introduced to totally inhibit the binding.

To further demarcate the interaction of this complex with GAS7b, I have also mutated the WW domain of GAS7b. Predominantly, GAS7b is thought to interact with N-WASP and WISH via its WW domain. Tyr65Cys have been mutate to evaluate the binding ability of WW domain. This activity may be more prominent function of the WW domain of GAS7b, raising the possibility that the WW domain could have weak interaction with N-WASP as well as with WISH protein. Interestingly, the FRET result showed the reduction in maximum assembly (Figure 28b). Accordingly, this result clarify that WW are in a position to serve as connector of GAS7b with N-WASP and WISH protein. Together, this result was supported from previous study, where GAS7b can localized with N-WASP (42). However, I cannot ignore the mechanism behind, where the specific domain in WISH and N-WASP that involved with this interact with WW domain of GAS7. With this regard, I proposed that the pull-down assay experiment with each domain mutation in WISH and N-WASP protein. This experiments design might be revealed a complete mechanism behind this multivalent interaction.

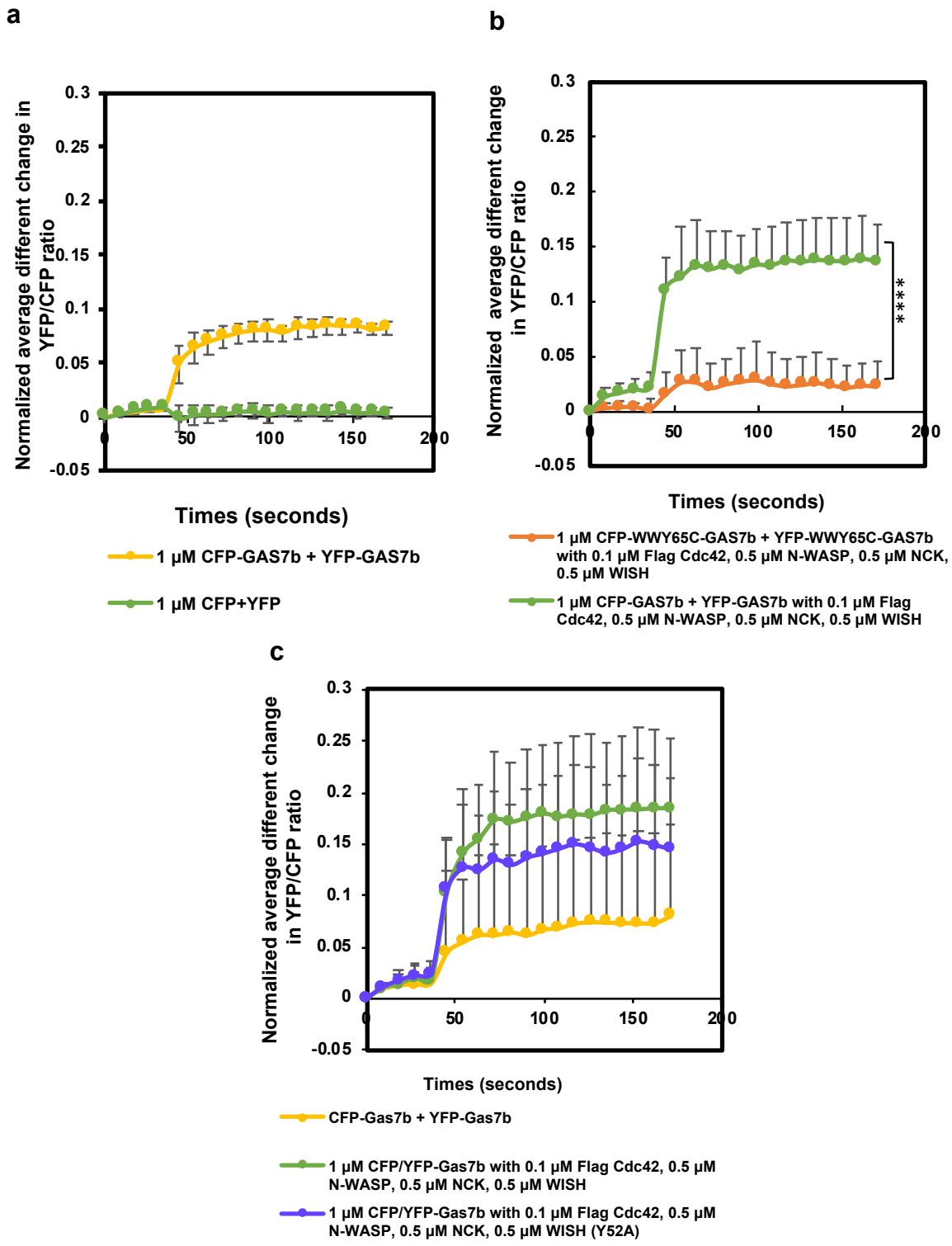

Figure 28: Mutagenesis analysis with FRET. a) The 1 µM of CFP-GAS7b+YFP-GAS7b alone without others protein. b) FRET ratio was reduced in comparison of 1 µM CFP-GAS7b + YFP-GAS7b with 1 µM CFP-WWY65C-GAS7b + YFP-WWY65C-GAS7b with 0.5 µM Nck, 0.5 µM N-WASP, 0.5 µM WISH, 0.1 µM Cdc42 (GTPγS). c) FRET ratio was reduced in comparison of 1 µM CFP-GAS7b + YFP-GAS7b and mutation on WISH SH3 (Y52A) with 0.5 µM Nck, 0.5 µM N-WASP, 0.5 µM WISH, 0.1 µM Cdc42 (GTPγS). The liposomes concentration is 0.25 mg/ml. Error bars: SD. The P-values were obtained by two-tailed Student's t-test. All the significant value is, $p<0.05$, against the positive control. **** $p<0.0001$.

To shed more light on the role of Nck that is an adaptor in regulating actin dynamics, I was curious to know whether removing one of the adaptor proteins such as, Nck itself will disrupt the FRET ratio. Nck is known to serve as a bridge of activated receptors to several signaling pathways (31). In this study, I have observed that, in the presence of Nck compared with Grb2, the normalized average different change in YFP/CFP ratio is increased suggesting that Nck is actually crucial in phagocytosis cascade (Figure 21). According to the same authors, Nck is essential to initiate the recruitment of N-WASP to phagocytic cups. As this link between Nck and N-WASP is involved in regulating actin rearrangements, this might explain why Nck can serve as a hub in this multicomplex interaction. Moreover, Nck also showed to have strong interaction with WISH and N-WASP as removing Nck from FRET systems will inhibit the FRET ratio (Figure 19a). This correlates with the study by Lim and his colleagues, that reported WISH will bind to the first and last SH3 domain of Nck (89). However, Grb2 also have been reported to involve in the binding with N-WASP (95), even able to modulate Arp2/3 and plays a role as adaptors in linking the protein assembly via SHP-1 and activating Rac (32). Hence, in my study I have focused on the interaction with N-WASP and Cdc42, not Rac. This may partly explain why Grb2 is not cooperatively working together in my reconstituted liposomes for protein-protein assembly (Figure 22). But I cannot rule out the possibility of Grb2 in regulating the binding of this multicomplex proteins especially in pathways that are related to SHP-1 and Rac together.

Given the established role of N-WASP as nucleation promoting factor of actin polymerization, it seemed to be obvious that N-WASP is a protein that pave the ways in actin dynamics. Cdc42 is the key to regulating actin dynamics during FcγR-mediated phagocytosis (22,31). Because N-WASP binds to the activated Cdc42, I have tested whether GAS7b could act together with N-WASP-WISH-Nck and Cdc42, in order to achieve more robust assembly of oligomerization at membrane. This observed multicomplex assembly is depended on Cdc42. In the presence of GTPγS-Cdc42, the maximum assembly was increased to 0.25 of normalized FRET ratio, that suggesting Cdc42 will act as key regulators in this multicomplex assembly (Figure 22a). The results are also consistence with half-time also revealing, the Cdc42-N-WASP-WISH-Nck and GAS7b multicomplex (1.209 sec) is the faster compare with without WISH (3.107 sec) and without N-WASP (1.584 sec) (Figure 22b). Therefore, inputs from all proteins of the complex, Cdc42-N-WASP-WISH-Nck and GAS7b may congregate and stimulate significant assemble at the membrane. Furthermore, this suggesting that Cdc42 also might undergo lipidation process to pin N-WASP-WISH-Nck and GAS7b at the membrane

(Figure 30). Although, Cdc42 can release auto inhibition state of N-WASP by binding with the CRIB domain (20), additional works is required to further clarify the mechanism behind this in my reconstituted FRET systems.

The Cdc42 activation in phagocytosis relates to phagocytotic receptor FcγRIIa which are phosphorylated by Src, then supposed to recruit Nck and then N-WASP (31). It is noteworthy that both Src & Cdc42 could accommodate phagocytic efficiency may clarify why multiple adaptors protein needs to be interacted and why their effects are not redundant, but preferably cooperatively working together. Even if Cdc42 is inactivating, wherein in this experiment, I have using Cdc42-GDP, would be sufficient to inhibit the phagocytosis process (Figure 22-orange line). Thus, despite domain-domain interaction, a complete set of scaffolds of these proteins were interacted in a coordinated manner to initiate the phagocytosis process. The ITAM and Src kinase is essential in regulating phagocytosis cascade. In my study, the FRET analysis revealed that, in the presence of GAS7b with multicomplex protein, Src and FcγRIIa, the FRET ratio was increased to 50% (Figure 23a-green line). In contrast, all mutants showed the reduction with WT. This result suggesting that the Src and FcγRIIa also importance in regulating this pathway. Interestingly, the half-time of the assembly quantitatively showed the enhancement of the assembly rate by the presence of these N-WASP, Nck, WISH, Cdc42, Src, and FcγRIIa (Figure 23b). In the presence of all multicomplex proteins, half-time is the fastest (0.2841 sec) compared with mutant in WISH proteins, WISH-Y52A (1.917 sec), mutant on WW domain of GAS7b, WW-Y65C-GAS7b mutations (4.5968 sec), membrane-binding deficient mutant of GAS7b like K208AK209A (1.755 sec) and K370ER374E (1.0728 sec) suggesting the defect or dysfunction in this multicomplex assembly. The illustration on how possibility of assembly between GAS7b-Nck-N-WASP-WISH-Cdc42, that cooperatively working with the signaling effects from Src kinase and FcγRIIa at the membrane was illustrated in (Figure 29).

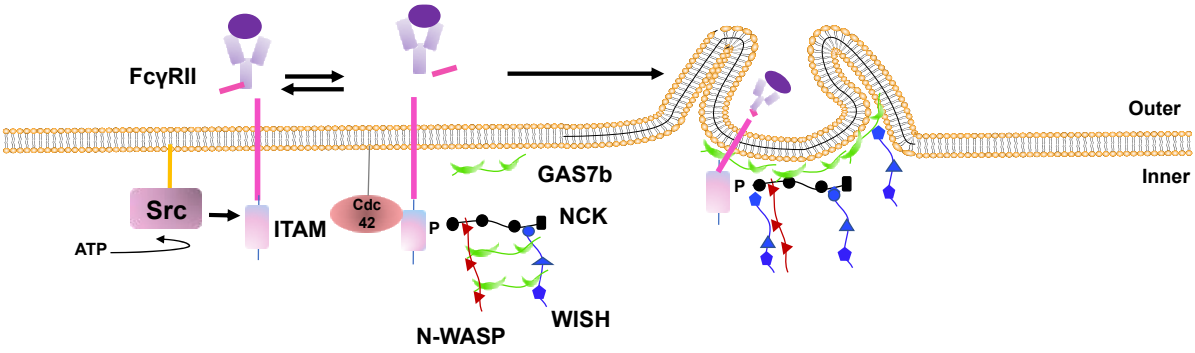

Figure 29: Illustration of the GAS7b and multicomplex protein adaptors (Nck-N-WASP-WISH-Cdc42). The multicomplex suggested all the proteins cooperatively engaged with the signaling effects from Src kinase and FcγRIIa at the membrane.

Given the importance of signaling from phosphoinositides in phagocytosis (4), I have also extended my analysis in the present of PIP_2 and PIP_3 phospholipids. This cascade is clearly involving the phosphoinositides, as FcγRIIa is located at extracellular of the membrane and at the intracellular, where the Src kinase are anchored. Consequently, phosphoinositides will be a platform to connect between Src and FcγRs. Following this signaling process, the residing of Src at ITAM could activated the FcγRIIa in the outer leaflet. From this, I have found that, PIP_2 will have higher maximum FRET ratio (Figure 24c). This result showed that, PIP_2 signaling is essential in activating downstream effectors for actin polymerization. There is also study by Mu and their group, phagocytosis is mediated by lipid sorting of PIP_2 (98). Of note, upon engagement of ITAM-containing FcγRs, Nck will bind phosphorylated ITAMs to recruit N-WASP/WASP (31). N-WASP will also be activated by and PIP_2 (17,99). Furthermore, PIP_2 and PIP_3 might involve in different pathway of lipid mediated phagocytosis. PIP_3 is reported to activate Rac protein and also WAVE complex. This pathway of activation might partly explain why in the present of PIP_3 and only 10% PS, the results showed significantly difference with presence of PIP_2 in my FRET conditions. F-BAR also prefer to bind with PIP_2 in comparison with PIP_3 and PS (100). Thus, more experiments about lipid-mediated phagocytosis should be done to clarify this difference.

Taking all this into account, Src and Cdc42 is key regulator of this multicomplex assembly. Thus, I want to further clarify whether the effects of Src and Cdc42 inhibitor will cause impeded to phagocytosis cascades. To answer this question, I have performed FLIM FRET in RAW246.7 cells. To complement the phagocytosis cascade onto my cellular FRET

experiments, I have observed that the FRET based on the frustrated phagocytosis events in the RAW264.7 that expressing the YFP-GAS7b-IRES-CFP-GAS7b (Figure 26a) This frustrated phagocytosis is occurred when macrophages cells seeded on IgG opsonized surface, spread their cell membrane as trying to engulf the pathogen. In this experiment, dimethylsulphoxide (DMSO), non-competitive inhibitor of Cdc42 (ML414) and the Src inhibitor (PP2), have been used. Surprisingly, I have observed a significant longer in the lifetime in the present of ML141 (lifetimes=1.5 ns) compared with YFP-GAS7b-IRES-CFP-GAS7b treated with DMSO (lifetimes=0.8 ns) suggesting that loss of signal in the cells for the phagocytosis process (Figure 26c). Besides, ML141 also have disrupted the function of Cdc42 in coordinating the multicomplex protein assembly which resulting in longer lifetimes. This also explained that the lipidation process by Cdc42 also be interrupted, resulting in hinder of the protein-protein assembly at membrane. The similar effect also was observed on PP2 treated cells (lifetimes=1.3 ns) (Figure 26c). PP2 seems to block the phosphorylation process of Src, which consequently inhibited the Cdc42-N-WASP-WISH-Nck and GAS7b multicomplex assemble in the cells. However, more experiments to support this protein-protein interaction should be conducted.

These observations agree with my FRET in spectrofluorometer experiments in which in the presence of Src and peptide attached on membrane, the FRET ratio was increased rapidly. Meanwhile, in RAW264.7 the lifetime became longer in the presence of the inhibitor. Both experimental designs speculating that the Src and Cdc42 is the key to regulate protein-protein interaction in mediated phagocytosis cascades. However, I still do not know about any specific domain that might been phosphorylated by Src. With this regard, I, therefore, suggest more phosphorylation study of Src kinase with each proteins complex should be tested as Src is one of the modulators in phagocytosis cascade. Intriguingly, the FRET system that have been established in this study would pave a fast and reliable method to any related protein-protein assembly experiments for future study.

5.0 Conclusions

Phagocytosis is a process that relates to actin rearrangements. This process is governed by multicomplex proteins. GAS7b is known to assemble at phagocytotic cups. Furthermore, GAS7b can bind with N-WASP and WISH through WW domain. How the GAS7b regulate this phagocytosis cascade with other signaling processes remain poorly understood. In order to gain insight about this, I designed this FRET experiment with CFP or YFP tagged in presence of actin binding proteins like N-WASP and adaptor protein, Nck. Then, I used this model to further evaluate and understand how this multicomplex proteins cooperatively interact together, before assembling at the membrane. I have also found that the WISH protein is also involved in this cascade.

My findings also have illustrated how a molecular signaling works together to cognate binding motifs and further link protein-protein interaction. This cascade is initiated with a signaling events from ITAM receptors of FcγRIIa and Src kinase, which further activates the Cdc42, PIP_2. Then, coordinates the protein-protein assembly at the membrane as well as clarify the essential of GAS7b in phagocytosis process. Hence in this study, I have revealed that, this multicomplex of GAS7b-Nck-N-WASP-WISH-Cdc42, cooperatively works with the signaling effects from Src kinase and FcγRIIa might contribute to new potential pathways in regulating phagocytosis cascade.

Overall, this multicomplex protein that have fast half-time, <0.3 sec with FRET by spectroflurometer and shorter lifetime, <0.8 ns in cellular FRET by FLIM. In contrast, with the presence of Cdc42 and Src inhibitor, the results showed longer lifetime in cellular FRET experiment, further supporting my findings. The model of the multicomplex protein assembly that mediated phagocytosis process is proposed as in the figure below (Figure 30).

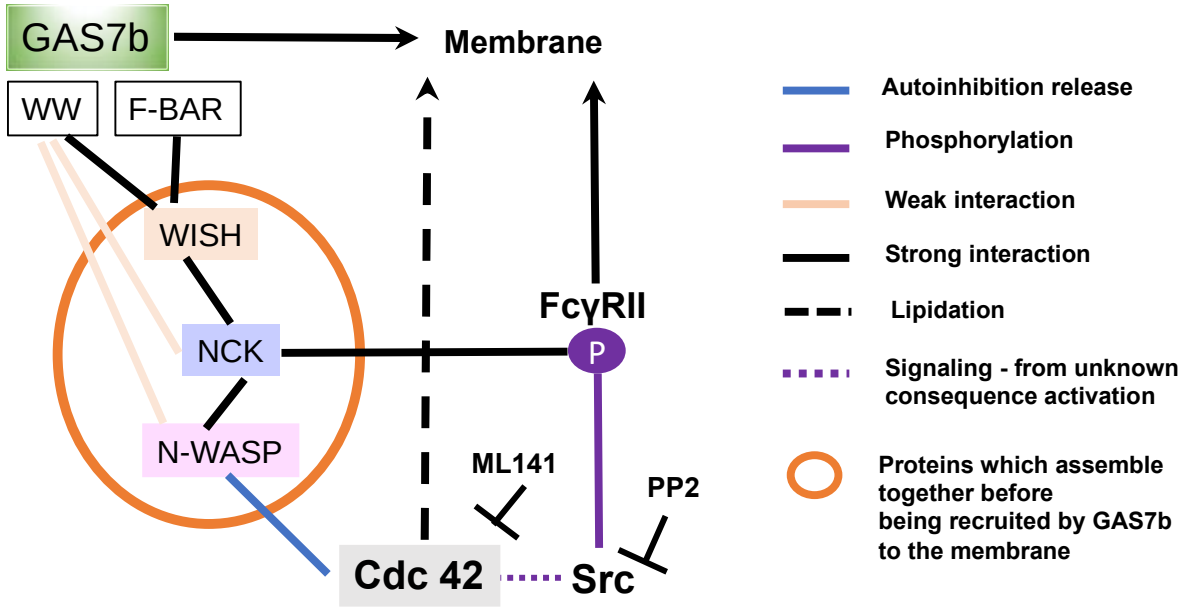

Figure 30: Model for multicomplex interaction in mediated phagocytosis cascade by GAS7b-Nck-N-WASP-WISH-Cdc42. The Cdc42 will unmask the auto inhibition state of N-WASP, thus exposing the VCA region for actin arrangements. The activation of this cascade initiated by signaling from FcγRIIa and Src family kinase, further promote the assembly of all the proteins complex at the membrane. The proteins in orange circle will interact together, then recruited by GAS7b before lipidation by Cdc42 on membrane. Src also might have different signaling effects to Cdc42 (pink dotted line) in which the mechanisms behind is unknown. ML141 and PP2 inhibitor may hinder the multicomplex interaction, as well as phagocytosis cascade.

Anyhow, I cannot rule out there is also other proteins and signaling activators such as Rac, WAVE complex that also may cooperatively work together with GAS7b-Nck-N-WASP-WISH-Cdc42 pathways to mediate phagocytosis cascade. My works that I presented here have interesting information and consequences to molecular biology, especially related with actin binding proteins and phagocytosis cascade. The results clearly show how apparently simple method, revealing about selective protein-protein interactions can direct signaling to orchestrate a particular cellular scaffold at the membrane. Lastly, by knowing the complete interaction of protein-protein in phagocytosis cascade, an interesting possibility, which could be test in the future, weather this GAS7b-Nck-N-WASP-WISH-Cdc42 pathway can compensated the disease that have failure in the engulfment of the pathogens, like WAS diseases. Thus, compensated the WAS diseases by GAS7 protein might be the future direction of this study.

6.0 Acknowledgement

This doctoral thesis has been kept on track and been seen through to completion with the support and encouragement of numerous people, in which I therefore would like to offer my utmost sincere thanks to all of them.

At this moment of accomplishment of this doctoral thesis, first of all I would like to express my sincere gratitude to my supervisor, Prof Dr Shiro Suetsugu for his brilliant ideas, invaluable guidance, continuous encouragement and constant support in making this research possible. I appreciate his consistent progressive vision about my progress in my lab works, and for pushing me farther than I thought I could go. He also had taken a lot of efforts to meticulously go through my thesis and came up with helpful suggestions. Thank you very much, Sensei!

I am also extremely indebted to my assistant professor Dr Tamako Nishimura and Dr Takehiko Inaba for helping me throughout my study and conducting this research. Theirs cooperation indeed makes my work became easier and faster. I also sincerely thankful for my adviser, Prof Dr Bessho Yasumasa and Prof Dr Tomoya Tsukazaki, for all their suggestions, advices and comments during my doctoral studies.

Besides, I would like to extend my gratitude to all my labmates and member of the Molecular Medicine and Cell Biology Laboratory, for their kindness, friendships and in many ways throughout my doctoral study. Many special thanks go to Dr Satoko Maki in Bio-school for her excellent cooperation in supporting, encouraging and inspiring all international students during our stay in NAIST, Japan. Thank you very much also for NAIST International Scholarship for sponsoring my doctoral study in NAIST.

I would like to express my heartfelt gratitude to my beloved parents, Wan Mohamad Noor, Ruhani Yusoff and my family, for their love, dream and sacrifice throughout my life. I cannot find the appropriate words that could properly describe my appreciation for their devotion, support and faith in my ability to attain my goals.

Finally, thank you everyone for simply being there, at the moment I needed the most.

7.0 References

1. Anania, J. C., Chenoweth, A. M., Wines, B. D., and Hogarth, P. M. (2019) The Human Fc gamma RII (CD32) Family of Leukocyte FcR in Health and Disease. *Front. Immunol.* **10**, 17
2. Suzuki, T., Kono, H., Hirose, N., Okada, M., Yamamoto, T., Yamamoto, K., and Honda, Z. (2000) Differential involvement of Src family kinases in Fc gamma receptor-mediated phagocytosis. *J.Immun.* **165**, 473-482
3. Uribe-Querol, E., and Rosales, C. (2020) Phagocytosis: Our Current Understanding of a Universal Biological Process. *Front. Immunol.* **11**, 13
4. Botelho, R. J., Scott, C. C., and Grinstein, S. (2004) Phosphoinositide involvement in phagocytosis and phagosome maturation. *Curr.Top.Microbiol.Immunol.* **282**, 1-30
5. Kwiatkowska, K., Frey, J., and Sobota, A. (2003) Phosphorylation of Fc gamma RIIA is required for the receptor-induced actin rearrangement and capping: the role of membrane rafts. *J. Cell Sci.* **116**, 537-550
6. Czech, M. P. (2000) PIP2 and PIP3: Complex roles at the cell surface. *Cell* **100**, 603-606
7. Kwiatkowska, K., and Sobota, A. (1999) Signaling pathways in phagocytosis. *Bioessays* **21**, 422-431
8. Rohatgi, R., Ma, L., Miki, H., Lopez, M., Kirchhausen, T., Takenawa, T., and Kirschner, M. W. (1999) The interaction between N-WASP and the Arp2/3 complex links Cdc42-dependent signals to actin assembly. *Cell* **97**, 221-231
9. Ridley, A. J. (2001) Rho proteins: Linking signaling with membrane trafficking. *Traffic* **2**, 303-310
10. Aspenstrom, P. (2019) BAR Domain Proteins Regulate Rho GTPase Signaling. *Protein Reviews - Purinergic Receptors, Vol 20* **1111**, 33-53
11. Sinha, S., and Yang, W. (2008) Cellular signaling for activation of Rho GTPase Cdc42. *Cell. Signal.* **20**, 1927-1934
12. Torres, E., and Rosen, M. K. (2006) Protein-tyrosine kinase and GTPase signals cooperate to phosphorylate and activate Wiskott-Aldrich syndrome protein (WASP)/neuronal WASP. *J. Biol. Chem.* **281**, 3513-3520
13. Imai, K., Nonoyama, S., and Ochs, H. D. (2003) WASP (Wiskott-Aldrich syndrome protein) gene mutations and phenotype. *Curr Opin Allergy Clin Immunol* **3**, 427-436
14. Ochs, H. D., and Thrasher, A. J. (2006) The Wiskott-Aldrich syndrome. *J. Allergy Clinl Immunol* **117**, 725-738
15. Tsuboi, S., and Meerloo, J. (2007) Wiskott-Aldrich syndrome protein is a key regulator of the phagocytic cup formation in macrophages. *J. Biol. Chem.* **282**, 34194-34203
16. Miki, H., Miura, K., and Takenawa, T. (1996) N-WASP, a novel actin-depolymerizing protein, regulates the cortical cytoskeletal rearrangement in a PIP2-dependent manner downstream of tyrosine kinases. *EMBO J.* **15**, 5326-5335
17. Suetsugu, S., Hattori, M., Miki, H., Tezuka, T., Yamamoto, T., Mikoshiba, K., and Takenawa, T. (2002) Sustained activation of N-WASP through phosphorylation is essential for neurite extension. *Dev. Cell* **3**, 645-658
18. Yamaguchi, H., Miki, H., Suetsugu, S., Ma, L., Kirschner, M. W., and Takenawa, T. (2000) Two tandem verprolin homology domains are necessary for a strong activation of Arp2/3 complex-induced actin polymerization and induction of microspike formation by N-WASP. *Proc. Natl. Acad. Sci. U.S.A.* **97**, 12631-12636

19. Fukuoka, M., Suetsugu, S., Miki, H., Fukami, K., Endo, T., and Takenawa, T. (2001) A novel neural Wiskott-Aldrich syndrome protein (N-WASP) binding protein, WISH, induces Arp2/3 complex activation independent of Cdc42. *J. Cell Biol* **152**, 471-482
20. Rohatgi, R., Ho, H. Y. H., and Kirschner, M. W. (2000) Mechanism of N-WASP activation by CDC42 and phosphatidylinositol 4,5-bisphosphate. *J. Cell Biol* **150**, 1299-1309
21. Nayak, R. C., Chang, K. H., Vaitinadin, N. S., and Cancelas, J. A. (2013) Rho GTPases control specific cytoskeleton-dependent functions of hematopoietic stem cells. *Immunol. Rev.* **256**, 255-268
22. Park, H., and Cox, D. (2009) Cdc42 Regulates Fc(gamma) Receptor-mediated Phagocytosis through the Activation and Phosphorylation of Wiskott-Aldrich Syndrome Protein (WASP) and Neural-WASP. *Mol. Biol. Cell* **20**, 4500-4508
23. Takenawa, T., and Suetsugu, S. (2007) The WASP-WAVE protein network: connecting the membrane to the cytoskeleton. *Nat. Rev. Mol. Cell Biol.* **8**, 37-48
24. Teodorof, C., Il Bae, J., Kim, S. M., Oh, H. J., Kang, Y. S., Choi, J., Chun, J. S., and Song, W. K. (2009) SPIN90-IRSp53 complex participates in Rac-induced membrane ruffling. *Exp. Cell Res.* **315**, 2410-2419
25. Kim, Y., Kim, S., Lee, S., Kim, S. H., Park, Z. Y., Song, W. K., and Chang, S. (2005) Interaction of SPIN90 with dynamin I and its participation in synaptic vesicle endocytosis. *J. Neurosci.* **25**, 9515-9523
26. Luan, Q., Liu, S. L., Helgeson, L. A., and Nolen, B. J. (2018) Structure of the nucleation-promoting factor SPIN90 bound to the actin filament nucleator Arp2/3 complex. *EMBO J.* **37**
27. Kim, D. J., Kim, S. H., Lim, C. S., Choi, K. Y., Park, C. S., Sung, B. H., Yeo, M. G., Chang, S. H., Kim, J. K., and Song, W. K. (2006) Interaction of SPIN90 with the Arp2/3 complex mediates lamellipodia and actin comet tail formation. *J. Biol. Chem.* **281**, 617-625
28. Meng, W. X., Numazaki, M., Takeuchi, K., Uchibori, Y., Ando-Akatsuka, Y., Tominaga, M., and Tominaga, T. (2004) DIP (mDia interacting protein) is a key molecule regulating Rho and Rac in a Src-dependent manner. *EMBO J.* **23**, 760-771
29. Banjade, S., and Rosen, M. K. (2014) Phase Transitions of Multivalent Proteins Can Promote Clustering of Membrane Receptors. *Elife* **3**
30. Banjade, S., Wu, Q., Mittal, A., Peeples, W. B., Pappu, R. V., and Rosen, M. K. (2015) Conserved interdomain linker promotes phase separation of the multivalent adaptor protein Nck. *Proc. Natl. Acad. Sci. U.S.A.* **112**, E6426-E6435
31. Dart, A. E., Donnelly, S. K., Holden, D. W., Way, M., and Caron, E. (2012) Nck and Cdc42 co-operate to recruit N-WASP to promote Fc gamma R-mediated phagocytosis. *J. Cell Sci.* **125**, 2825-2830
32. Rajaram, M. V. S., Arnett, E., Azad, A. K., Guirado, E., Ni, B., Gerberick, A. D., He, L.-Z., Keler, T., Thomas, L. J., Lafuse, W. P., and Schlesinger, L. S. (2017) M. tuberculosis-Initiated Human Mannose Receptor Signaling Regulates Macrophage Recognition and Vesicle Trafficking by FcR gamma-Chain, Grb2, and SHP-1. *Cell Rep.* **21**, 126-140
33. Case, L. B., Zhang, X., Ditlev, J. A., and Rosen, M. K. (2019) Stoichiometry controls activity of phase-separated clusters of actin signaling proteins. *Science* **363**, 1093-+
34. Ponimaskin, E., Voyno-Yasenetskaya, T., Richter, D. W., Schachner, M., and Dityatev, A. (2007) Morphogenic signaling in neurons via neurotransmitter receptors and small GTPases. *Mol. Neurobiol.* **35**, 278-287
35. Harayama, T., and Riezman, H. (2018) Understanding the diversity of membrane lipid composition. *Nat. Rev. Mol. Cell Biol.* **19**, 281-296

36. Bigay, J., and Antonny, B. (2012) Curvature, Lipid Packing, and Electrostatics of Membrane Organelles: Defining Cellular Territories in Determining Specificity. *Dev. Cell* **23**, 886-895
37. van Meer, G., and de Kroon, A. (2011) Lipid map of the mammalian cell. *J. Cell Sci.* **124**, 5-8
38. Baptista, D., Teixeira, L., van Blitterswijk, C., Giselbrecht, S., and Truckenmuller, R. (2019) Overlooked? Underestimated? Effects of Substrate Curvature on Cell Behavior. *Trends Biotechnol.* **37**, 838-854
39. Kitamata, M., Inaba, T., and Suetsugu, S. (2020) The roles of the diversity of amphipathic lipids in shaping membranes by membrane-shaping proteins. *Biochem. Soc. Trans.* **48**, 837-851
40. Itoh, T., Erdmann, K. S., Roux, A., Habermann, B., Werner, H., and De Camilli, P. (2005) Dynamin and the actin cytoskeleton cooperatively regulate plasma membrane invagination by BAR and F-BAR proteins. *Dev. Cell* **9**, 791-804
41. Blue, R. E., Curry, E. G., Engels, N. M., Lee, E. Y., and Giudice, J. (2018) How alternative splicing affects membrane-trafficking dynamics. *J. Cell Sci.* **131**
42. Hanawa-Suetsugu, K., Itoh, Y., Ab Fatah, M., Nishimura, T., Takemura, K., Takeshita, K., Kubota, S., Miyazaki, N., Noor, W., Inaba, T., Nguyen, N. T. H., Hamada-Nakahara, S., Oono-Yakura, K., Tachikawa, M., Iwasaki, K., Kohda, D., Yamamoto, M., Kitacy, A., Shimada, A., and Suetsugu, S. (2019) Phagocytosis is mediated by two-dimensional assemblies of the F-BAR protein GAS7. *Nat. Commun.* **10**, 13
43. Tan, R., Foster, P. J., Needleman, D. J., and McKenney, R. J. (2018) Cooperative Accumulation of Dynein-Dynactin at Microtubule Minus-Ends Drives Microtubule Network Reorganization. *Dev. Cell* **44**, 233-+
44. Birge, R. B., Boeltz, S., Kumar, S., Carlson, J., Wanderley, J., Calianese, D., Barcinski, M., Brekken, R. A., Huang, X., Hutchins, J. T., Freimark, B., Empig, C., Mercer, J., Schroit, A. J., Schett, G., and Herrmann, M. (2016) Phosphatidylserine is a global immunosuppressive signal in efferocytosis, infectious disease, and cancer. *Cell Death Differ.* **23**, 962-978
45. Suetsugu, S. (2016) Higher-order assemblies of BAR domain proteins for shaping membranes. *Microscopy* **65**, 201-210
46. Suetsugu, S., Kurisu, S., and Takenawa, T. (2014) Dynamic shaping of cellular membranes by phospholipids and membrane-deforming proteins. *Physiol. Rev.* **94**, 1219-1248
47. Shimada, A., Niwa, H., Tsujita, K., Suetsugu, S., Nitta, K., Hanawa-Suetsugu, K., Akasaka, R., Nishino, Y., Toyama, M., Chen, L., Liu, Z.-J., Wang, B.-C., Yamamoto, M., Terada, T., Miyazawa, A., Tanaka, A., Sugano, S., Shirouzu, M., Nagayama, K., Takenawa, T., and Yokoyama, S. (2007) Curved EFC/F-BAR-domain dimers are joined end to end into a filament for membrane invagination in endocytosis. *Cell* **129**, 761-772
48. Nishimura, T., Morone, N., and Suetsugu, S. (2018) Membrane re-modelling by BAR domain superfamily proteins via molecular and non-molecular factors. *Biochem. Soc. Trans.* **46**, 379-389
49. Stanishneva-Konovalova, T. B., Derkacheva, N. I., Polevova, S. V., and Sokolova, O. S. (2016) The Role of BAR Domain Proteins in the Regulation of Membrane Dynamics. *Acta Naturae* **8**, 60-69
50. Drager, N. M., Nachman, E., Winterhoff, M., Bruhmann, S., Shah, P., Katsinelos, T., Boulant, S., Teleman, A. A., Faix, J., and Jahn, T. R. (2017) Bin1 directly remodels actin dynamics through its BAR domain. *EMBO Rep.* **18**, 2051-2066

51. Senju, Y., Itoh, Y., Takano, K., Hamada, S., and Suetsugu, S. (2011) Essential role of PACSIN2/syndapin-II in caveolae membrane sculpting. *J. Cell Sci.* **124**, 2032-2040
52. Zobel, T., Brinkmann, K., Koch, N., Schneider, K., Seemann, E., Fleige, A., Qualmann, B., Kessels, M. M., and Bogdan, S. (2015) Cooperative functions of the two F-BAR proteins Cip4 and Nostrin in the regulation of E-cadherin in epithelial morphogenesis (vol 128, pg 499, 2015). *J. Cell Sci.* **128**, 1453-1453
53. Wang, Q., Navarro, M. V. A. S., Peng, G., Molinelli, E., Goh, S. L., Judson, B. L., Rajashankar, K. R., and Sondermann, H. (2009) Molecular mechanism of membrane constriction and tubulation mediated by the F-BAR protein Pacsin/Syndapin. *Proc. Natl. Acad. Sci. U.S.A.* **106**, 12700-12705
54. Tsuboi, S., Takada, H., Hara, T., Mochizuki, N., Funyu, T., Saitoh, H., Terayama, Y., Yamaya, K., Ohyama, C., Nonoyama, S., and Ochs, H. D. (2009) FBP17 Mediates a Common Molecular Step in the Formation of Podosomes and Phagocytic Cups in Macrophages. *J. Biol. Chem.* **284**, 8548-8556
55. Takano, K., Toyooka, K., and Suetsugu, S. (2008) EFC/F-BAR proteins and the N-WASP-WIP complex induce membrane curvature-dependent actin polymerization. *EMBO J.* **27**, 2817-2828
56. Shimizu, T., Hirose, K., Uchida, C., and Uchida, T. (2020) Growth arrest specific protein 7 inhibits tau fibrillogenesis. *Biochem. Biophys. Res. Commun.* **526**, 281-286
57. Saengsawang, W., Mitok, K., Viesselmann, C., Pietila, L., Lumbard, D. C., Corey, S. J., and Dent, E. W. (2012) The F-BAR Protein CIP4 Inhibits Neurite Formation by Producing Lamellipodial Protrusions. *Curr. Biol.* **22**, 494-501
58. Peter, B. J., Kent, H. M., Mills, I. G., Vallis, Y., Butler, P. J. G., Evans, P. R., and McMahon, H. T. (2004) BAR domains as sensors of membrane curvature: The amphiphysin BAR structure. *Science* **303**, 495-499
59. Suetsugu, S., and Gautreau, A. (2012) Synergistic BAR-NPF interactions in actin-driven membrane remodeling. *Trends in Cell Biol.* **22**, 141-150
60. Simunovic, M., Voth, G. A., Callan-Jones, A., and Bassereau, P. (2015) When Physics Takes Over: BAR Proteins and Membrane Curvature. *Trends in Cell Biol.* **25**, 780-792
61. Tarricone, C., Xiao, B., Justin, N., Walker, P. A., Rittinger, K., Gamblin, S. J., and Smerdon, S. J. (2001) The structural basis of Arfaptin-mediated cross-talk between Rac and Arf signalling pathways. *Nature* **411**, 215-219
62. de Curtis, I., and Meldolesi, J. (2012) Cell surface dynamics - how Rho GTPases orchestrate the interplay between the plasma membrane and the cortical cytoskeleton. *J. Cell Sci.* **125**, 4435-4444
63. Kamioka, Y., Fukuhara, S., Masuda, M., Sawa, H., Nagashima, K., Matsuda, M., and Mochizuki, N. (2004) A novel dynamin-associating molecule, formin-binding protein 17, induces tubular membrane invaginations and participates in endocytosis. *Mol. Biol. Cell* **15**, 79A-79A
64. Gallop, J. L., and McMahon, H. T. (2005) BAR domains and membrane curvature: bringing your curves to the BAR. *Lipids, Rafts and Traffic* **72**, 223-231
65. Masuda, M., Takeda, S., Sone, M., Ohki, T., Mori, H., Kamioka, Y., and Mochizuki, N. (2006) Endophilin BAR domain drives membrane curvature by two newly identified structure-based mechanisms. *EMBO J* **25**, 2889-2897
66. Saarikangas, J., Zhao, H., Pykalainen, A., Laurinmaki, P., Mattila, P. K., Kinnunen, P. K. J., Butcher, S. J., and Lappalainen, P. (2009) Molecular Mechanisms of Membrane Deformation by I-BAR Domain Proteins. *Curr. Biol.* **19**, 95-107
67. Renard, H. F., Simunovic, M., Lemiere, J., Boucrot, E., Garcia-Castillo, M. D., Arumugam, S., Chambon, V., Lamaze, C., Wunder, C., Kenworthy, A. K., Schmidt,

A. A., McMahon, H. T., Sykes, C., Bassereau, P., and Johannes, L. (2015) Endophilin-A2 functions in membrane scission in clathrin-independent endocytosis. *Nature* **517**, 493-+
68. Zhao, H. X., Pykalainen, A., and Lappalainen, P. (2011) I-BAR domain proteins: linking actin and plasma membrane dynamics. *Curr. Opin. Cell Biol.* **23**, 14-21
69. Ahmed, S., Goh, W. I., and Bu, W. Y. (2010) I-BAR domains, IRSp53 and filopodium formation. *Semin. Cell Dev. Biol.* **21**, 350-356
70. Scita, G., Confalonieri, S., Lappalainen, P., and Suetsugu, S. (2008) IRSp53: crossing the road of membrane and actin dynamics in the formation of membrane protrusions. *Trends in Cell Biol.* **18**, 52-60
71. Suetsugu, S., Murayama, K., Sakamoto, A., Hanawa-Suetsugu, K., Seto, A., Oikawa, T., Mishima, C., Shirouzu, M., Takenawa, T., and Yokoyama, S. (2006) The RAC binding domain/IRSp53-MIM homology domain of IRSp53 induces RAC-dependent membrane deformation. *J. Biol. Chem.* **281**, 35347-35358
72. Mattila, P. K., Pykalainen, A., Saarikangas, J., Paavilainen, V. O., Vihinen, H., Jokitalo, E., and Lappalainen, P. (2007) Missing-in-metastasis and IRSp53 deform PI(4,5)P-2-rich membranes by an inverse BAR domain-like mechanism. *J. Cell Biol.* **176**, 953-964
73. Liu, S. X., Xiong, X. Y., Zhao, X. X., Yang, X. F., and Wang, H. (2015) F-BAR family proteins, emerging regulators for cell membrane dynamic changes-from structure to human diseases. *J. Hematol. Oncol.* **8**
74. Guerrier, S., Coutinho-Budd, J., Sassa, T., Gresset, A., Jordan, N. V., Chen, K., Jin, W. L., Frost, A., and Polleux, F. (2009) The F-BAR Domain of srGAP2 Induces Membrane Protrusions Required for Neuronal Migration and Morphogenesis. *Cell* **138**, 990-1004
75. Almeida-Souza, L., Frank, R. A. W., Garcia-Nafria, J., Colussi, A., Gunawardana, N., Johnson, C. M., Yu, M. M., Howard, G., Andrews, B., Vallis, Y., and McMahon, H. T. (2018) A Flat BAR Protein Promotes Actin Polymerization at the Base of Clathrin-Coated Pits. *Cell* **174**, 325-+
76. Chao, C. C. K., Chang, P. Y., and Lu, H. H. P. (2005) Human gas7 isoforms homologous to mouse transcripts differentially induce neurite outgrowth. *J. Neurosci. Res.* **81**, 153-162
77. You, J.-J., and Lin-Chao, S. (2010) Gas7 Functions with N-WASP to Regulate the Neurite Outgrowth of Hippocampal Neurons. *J. Biol. Chem.* **285**, 11652-11666
78. Bhupana, J. N., Huang, B. T., Chang, Y. L., and Chao, S. L. (2019) Gas7 regulates mitochondrial morphology and physiology. *FASEB J.* **33**
79. Tseng, R.-C., Chang, J.-W., Mao, J.-S., Tsai, C.-D., Wu, P.-C., Lin, C.-J., Lu, Y.-L., Liao, S.-Y., Cheng, H.-C., Hsu, H.-S., and Wang, Y.-C. (2015) Growth-arrest-specific 7C protein inhibits tumor metastasis via the N-WASP/FAK/F-actin and hnRNP U/beta-TrCP/beta-catenin pathways in lung cancer. *Oncotarget* **6**, 44207-44221
80. Chang, J. W., Kuo, W. H., Lin, C. M., Chen, W. L., Chan, S. H., Chiu, M. F., Chang, I. S., Jiang, S. S., Tsai, F. Y., Chen, C. H., Huang, P. H., Chang, K. J., Lin, K. T., Lin, S. C., Wang, M. Y., Uen, Y. H., Tu, C. W., Hou, M. F., Tsai, S. F., Shen, C. Y., Tung, S. L., and Wang, L. H. (2018) Wild-type p53 upregulates an early onset breast cancer-associated gene GAS7 to suppress metastasis via GAS7-CYFIP1-mediated signaling pathway. *Oncogene* **37**, 4137-4150
81. Lazakovitch, E. M., She, B. R., Lien, C. L., Woo, W. M., Ju, Y. T., and Sue, L. C. (1999) The Gas7 gene encodes two protein isoforms differentially expressed within the brain. *Genomics* **61**, 298-306

82. Becalska, A. N., Kelley, C. F., Berciu, C., Stanishneva-Konovalova, T. B., Fu, X. F., Wang, S. Y., Sokolova, O. S., Nicastro, D., and Rodal, A. A. (2013) Formation of membrane ridges and scallops by the F-BAR protein Nervous Wreck. *Mol. Biol. Cell* **24**, 2406-2418
83. McDonald, N. A., Kooi, C. W. V., Ohi, M. D., and Gould, K. L. (2015) Oligomerization but Not Membrane Bending Underlies the Function of Certain F-BAR Proteins in Cell Motility and Cytokinesis. *Dev. Cell* **35**, 725-736
84. McDonald, N. A., Lind, A. L., Smith, S. E., Li, R., and Gould, K. L. (2017) Nanoscale architecture of the Schizosaccharomyces pombe contractile ring. *eLife* **6**, 23
85. McDonald, N. A., and Gould, K. L. (2016) Linking up at the BAR: Oligomerization and F-BAR protein function. *Cell Cycle* **15**, 1977-1985
86. Ho, H. Y. H., Rohatgi, R., Lebensohn, A. M., Ma, L., Li, J. X., Gygi, S. P., and Kirschner, M. W. (2004) Toca-1 mediates Cdc42-dependent actin nucleation by activating the N-WASP-WIP complex. *Cell* **118**, 203-216
87. Ranjit, S., Malacrida, L., Jameson, D. M., and Grafton, E. (2018) Fit-free analysis of fluorescence lifetime imaging data using the phasor approach. *Nat. Protoc* **13**
88. Digman, M. A., Caiolfa, V. R., Zamai, M., and Gratton, E. (2008) The phasor approach to fluorescence lifetime imaging analysis. *Biophys. J.* **94**, L14-L16
89. Lim, C. S., Park, E. S., Kim, D. J., Song, Y. H., Eom, S. H., Chun, J. S., Kim, J. H., Kim, J. K., Park, D., and Song, W. K. (2001) SPIN90 (SH3 protein interacting with Nck, 90 kDa), an adaptor protein that is developmentally regulated during cardiac myocyte differentiation. *J. Biol. Chem.* **276**, 12871-12878
90. Liu, M. X., Zhou, K. C., and Cao, Y. (2014) MCRS1 overexpression, which is specifically inhibited by miR-129*, promotes the epithelial-mesenchymal transition and metastasis in non-small cell lung cancer. *Mol. Cancer* **13**
91. Yoshida, Y., Suzuki, K., Yamamoto, A., Sakai, N., Bando, M., Tanimoto, K., Yamaguchi, Y., Sakaguchi, T., Akhter, H., Fujii, G., Yoshimura, S., Ogata, S., Sohda, M., Misumi, Y., and Nakamura, N. (2008) YIPF5 and YIF1A recycle between the ER and the Golgi apparatus and are involved in the maintenance of the Golgi structure. *Exp. Cell Res.* **314**, 3427-3443
92. Pearl, L. H. (2005) Hsp90 and Cdc37 - a chaperone cancer conspiracy. *Curr. Opin. Genet. Dev* **15**, 55-61
93. Wilusz, C. J., and Wilusz, J. (2005) Eukaryotic Lsm proteins: lessons from bacteria. *Nat. Struct. Mol. Biol.* **12**, 1031-1036
94. Ren, Y., Busch, R. K., Perlaky, L., and Busch, H. (1998) The 58-kDa microspherule protein (MSP58), a nucleolar protein, interacts with nucleolar protein p120. *Eur. J. Biochem.* **253**, 734-742
95. Carlier, M. F., Nioche, P., Broutin-L'Hermite, I., Boujemaa, R., Le Clainche, C., Egile, C., Garbay, C., Ducruix, A., Sansonetti, P., and Pantaloni, D. (2000) GRB2 links signaling to actin assembly by enhancing interaction of neural Wiskott-Aldrich syndrome protein (N-WASp) with actin-related protein (ARP2/3) complex. *J. Biol. Chem.* **275**, 21946-21952
96. Richards, D. M., and Endres, R. G. (2014) The Mechanism of Phagocytosis: Two Stages of Engulfment. *Biophys. J.* **107**, 1542-1553
97. Sun, D. P., Varlakhanova, N. V., Tornabene, B. A., Ramachandran, R., Zhang, P. J., and Ford, M. G. J. (2020) The cryo-EM structure of the SNX-BAR Mvp1 tetramer. *Nat. Commun.* **11**
98. Mu, L. B., Tu, Z. Y., Miao, L., Ruan, H. F., Kang, N., Hei, Y. Z., Chen, J. H., Wei, W., Gong, F. L., Wang, B. J., Du, Y. N., Ma, G. H., Amerein, M. W., Xia, T., and

Shi, Y. (2018) A phosphatidylinositol 4,5-bisphosphate redistribution-based sensing mechanism initiates a phagocytosis programing. *Nat. Commun.* **9**

99. Higgs, H. N., and Pollard, T. D. (2000) Activation by Cdc42 and PIP2 of Wiskott-Aldrich Syndrome protein (WASp) stimulates actin nucleation by Arp2/3 complex. *Mol. Biol. Cell* **11**, 178A-178A

100. Tsujita, K., Suetsugu, S., Sasaki, N., Furutani, M., Oikawa, T., and Takenawa, T. (2006) Coordination between the actin cytoskeleton and membrane deformation by a novel membrane tubulation domain of PCH proteins is involved in endocytosis. *J. Cell Biol.* **172**, 269-279